Exploring Novel Aspects of Cardiac Mechanics Using Exercise CMR

Edlund, Jonathan

2025

Document Version:
Publisher's PDF, also known as Version of record

Exploring Novel Aspects of Cardiac Mechanics Using Exercise CMR

JONATHAN EDLUND
DEPARTMENT OF CLINICAL PHYSIOLOGY | FACULTY OF MEDICINE | LUND UNIVERSITY

Exploring Novel Aspects of Cardiac Mechanics Using Exercise CMR

Exploring Novel Aspects of Cardiac Mechanics Using Exercise CMR

Jonathan Edlund

LUND
UNIVERSITY

Thesis for the degree of Doctor of Philosophy
Thesis advisors: Dr. Katarina Steding-Ehrenborg, Prof. Håkan Arheden
Faculty opponent: Prof. Aaron Baggish

To be presented for public critique in the Lecture hall 1 (Föreläsningssal 1) at SUS Lund on Friday, 28th of November 2025 at 09:00.

Organization: LUND UNIVERSITY **Date of issue:** November 28th 2025

Author: Jonathan Edlund

Title: Exploring Novel Aspects of Cardiac Mechanics Using Exercise CMR

Abstract: Heart failure is a global health concern whose burden is increasing as our population ages. Early diagnosis and accurate prognosis are critical for improving outcomes, highlighting the need for novel methods that can better identify and elucidate the pathophysiology of heart failure. The cardinal symptom of heart failure is exercise intolerance, yet most cardiac imaging is performed at rest, potentially overlooking abnormalities that manifest only during exertion. This thesis aimed to advance the noninvasive assessment of cardiac function at rest and during exercise by exploring novel cardiac mechanics using cardiovascular magnetic resonance (CMR).

Four studies were conducted. Study I validated a method that greatly accelerates the analysis of noninvasive, CMR-derived pressure-volume (PV) loops. This method was then applied across healthy volunteers, individuals with subclinical diastolic dysfunction, and heart failure subtypes, and it showed results comparable to those obtained using invasive methods. Study II developed an algorithm that enables analysis of free-breathing, non-ECG-gated, real-time CMR images acquired during exercise. This was validated against conventional gated cine imaging for left ventricular mass and volumes at rest and during exercise.

Using these tools, Study III assessed hydraulic forces, a novel mechanism of diastolic function, by measuring the atrioventricular area difference (AVAD) in athletes and sedentary controls using exercise CMR. End-diastolic AVAD increased from rest to moderate exercise in both groups, indicating that the net hydraulic force augments diastolic filling during exertion. In contrast, Study IV showed that in heart failure, end-diastolic AVAD decreased with exercise, suggesting a diminished hydraulic contribution to filling.

Collectively, these findings further our understanding of the role of diastolic hydraulic forces during exercise in both the healthy and the failing heart and advance the methods for CMR-derived, noninvasive PV loop analysis as well as exercise CMR.

Key words: cardiovascular magnetic resonance imaging; heart failure; pressure-volume loops; exercise imaging; exercise physiology; hydraulic forces; atrioventricular area difference

Language: English **Number of pages:** 132

ISSN: 1652-8220

ISBN: 978-91-8021-781-1

Signature_____ Lund 2025-10-21

Exploring Novel Aspects of Cardiac Mechanics Using Exercise CMR

Jonathan Edlund

LUND
UNIVERSITY

Faculty Opponent

Prof. Aaron Baggish
University of Lausanne
Vaud, Switzerland

Evaluation Committee

Prof. Magnus Dencker
Lund University
Lund, Sweden

Dr. Frida Dangardt
University of Gothenburg
Gothenburg, Sweden

Prof. Mats Börjesson
University of Gothenburg
Gothenburg, Sweden

Cover by Hanna Gyllander.

Faculty of Medicine, Department of Clinical Physiology, Lund Cardiac MR Group
ISSN: 1652-8220
ISBN: 978-91-8021-781-1
Lund University, Faculty of Medicine Doctoral Dissertation Series 2025:128

Printed in Sweden by Media-Tryck, Lund University, Lund 2025

Media-Tryck is a Nordic Swan Ecolabel certified provider of printed material. Read more about our environmental work at www.mediatryck.lu.se

MADE IN SWEDEN

Dedicated to my fluffy companions
Catullus, Jasnah, and Nimbus

Contents

List of Publications

This thesis is based on the following publications and manuscripts:

1 **Noninvasive assessment of left ventricular pressure-volume relations: inter-and intraobserver variability and assessment across heart failure subtypes**

J. Edlund, P.M. Arvidsson, A. Nelsson, J.G. Smith, M. Magnusson, E. Heiberg, K. Steding-Ehrenborg, H. Arheden
The American Journal of Cardiology, 184:48-55 (2022)

2 **Validation and quantification of left ventricular function during exercise and free breathing from real-time cardiac magnetic resonance images**

J. Edlund, K. Haris, E. Ostenfeld, M. Carlsson, E. Heiberg, S. Johansson, B. Östenson, N. Jin, A.H. Aletras, K. Steding-Ehrenborg
Scientific Reports, 12:1:5611 (2022)

3 **Exercise cardiovascular magnetic resonance shows improved diastolic filling by atrioventricular area difference in athletes and controls**

J. Edlund, B. Östenson, E. Heiberg, H. Arheden, K. Steding-Ehrenborg
Journal of Applied Physiology 137:6:1554-1562 (2024)

4 **Atrioventricular area difference assessed by exercise cardiovascular magnetic resonance shows impaired diastolic filling in heart failure patients**

J. Edlund, B. Östenson, J. Åkesson, E. Heiberg, H. Arheden, K. Steding-Ehrenborg
Manuscript

Popular Summary

Heart failure is a condition in which the heart is unable to pump enough blood to meet the body's needs. It increases the risk of early death and affects about 10% of people aged 70 years or older. Those living with heart failure often struggle most during exertion, when simply walking up stairs, carrying groceries, or biking to work can leave them breathless. Most medical scans of the heart are done while patients lie still, which means problems that only appear during exertion may be missed.

To better help those living with heart failure, we need to increase our understanding of how the failing heart pumps at rest and during exertion. This thesis uses and develops advanced cardiovascular magnetic resonance (CMR) techniques to examine newly described measures of how the heart pumps, both at rest and during ongoing exercise.

Four studies are included in this thesis. In the first, we used a newly developed method that investigates the relationship between pressure and volume inside the heart by using images from CMR and a standard arm blood pressure measurement. We also validated a method of greatly speeding up this analysis. The results showed that the new, accelerated method gives comparable results to old methods, and the analysis was successful across different types of heart failure.

The second study focused on developing and validating a method for using CMR during ongoing exercise inside the scanner, with a bicycle ergometer. The results showed that this method enabled accurate measurement of heart volumes and mass during exercise.

Using this method, the third and fourth studies examined the heart during exercise, first in healthy volunteers and athletes and then in patients with heart failure. We focused on hydraulic forces, a newly identified mechanism that helps the heart to fill with blood as it relaxes, measured at rest and during exercise. The results showed that hydraulic forces increased in healthy volunteers and athletes during exercise. In contrast, the hydraulic forces instead decreased in patients with heart failure.

Together, the findings from this thesis increase our understanding of how the heart fills with blood during exercise in both healthy and failing hearts. This thesis also advances CMR

methods for investigating the relationship between pressure and volume in the heart, and for using CMR to image the heart during ongoing exercise.

Populärvetenskaplig sammanfattning

Hjärtsvikt är ett tillstånd som innebär att hjärtat inte kan pumpa tillräckligt med blod för att fullständigt täcka kroppens behov. Tillståndet ökar risken för tidig död, och drabbar cirka 10% av personer över 70 år. Personer som lever med hjärtsvikt märker framför allt av sina problem först vid ansträngning. Att bara gå i trappor, bära matkassar eller cykla till jobbet kan ge onormal andfåddhet. De flesta medicinska undersökningar av hjärtat görs dock när patienten ligger stilla, vilket innebär att problem som bara uppträder vid ansträngning eventuellt missas.

För att bättre hjälpa personer med hjärtsvikt behöver vi öka vår förståelse av hur det sviktande hjärtat pumpar, både i vila och under fysisk ansträngning. Denna avhandling använder och vidareutvecklar metoder för magnetkameraundersökning av hjärtat, i syfte att undersöka nya mått på hjärtats pumpförmåga, både i vila och under pågående ansträngning.

Avhandlingen består av fyra studier. I den första använde vi en nyutvecklad metod för att undersöka sambandet mellan tryck och volym i hjärtat. Denna metod fungerar genom att kombinera mätningar från magnetkameraundersökningar av hjärtat med ett vanligt blodtryck från armen. Vi utvärderade även en metod som kraftigt påskyndade tiden det tog att genomföra dessa mätningar. Resultaten visade att den nya, accelererade metoden gav jämförbara resultat med äldre metoder, och kunde användas för olika typer av hjärtsvikt.

Den andra studien gick ut på att utveckla och validera en metod för att utföra magnetkameraundersökningar av hjärtat under pågående ansträngning med hjälp av en träningscykel, liggandes i själva magnetkameran. Resultaten visade att metoden fungerar för mätningar av hjärtats volymer och massa under fysisk ansträngning.

I den tredje och fjärde studien användes sedan denna nyutvecklade metod för att undersöka hjärtat under ansträngning, först hos friska frivilliga och idrottare, och sedan hos personer med hjärtsvikt. I studierna undersökte vi hydrauliska krafter i hjärtat, ett nyupptäckt mått kopplat till hur hjärtat fyller sig med blod när det slappnar av. Resultaten visade att dessa krafter ökade under ansträngning hos friska och idrottare och hjälpte hjärtat fyllas med blod, medan krafterna tvärt om minskade hos personer med hjärtsvikt.

Sammantaget bidrar resultaten från denna avhandling till att öka förståelsen för hur hjärtat fylls med blod under ansträngning, både i det friska och det sviktande hjärtat. Avhandlingen bidrar också till vidareutvecklingen av avancerade magnetkameraundersökningar, både för att undersöka sambandet mellan tryck och volym i hjärtat och för att möjliggöra bildtagning under pågående ansträngning.

Abbreviations

2ch	two-chamber
3ch	three-chamber
4ch	four-chamber
bSSFP	balanced steady-state free precession
CMR	cardiovascular magnetic resonance
CO	cardiac output
CT	computed tomography
ECG	electrocardiogram
ED	end-diastole
EDV	end-diastolic volume
EF	ejection fraction
ES	end-systole
ESV	end-systolic volume
HFmrEF	heart failure with mildly reduced ejection fraction
HFpEF	heart failure with preserved ejection fraction
HFrEF	heart failure with reduced ejection fraction
LA	left atrium
LV	left ventricle
LVM	left ventricular mass
MAP	mean arterial pressure
MRI	magnetic resonance imaging
NYHA	New York Heart Association
PV	pressure-volume
RAAS	renin–angiotensin–aldosterone system
RF	radiofrequency
SAX	short-axis
SPECT	single-photon emission computed tomography
TPR	total peripheral resistance

The cure for boredom is curiosity. There is no cure for curiosity.

— Dorothy Parker

Preface

I have always had a healthy dose of skepticism towards just accepting facts without explanation, sometimes to the detriment of my teachers and parents when I was growing up. For instance, my mother will happily recount that I, as a young child, didn't believe her when she told me that numbers are infinite. Naturally, for me to be convinced, I had her start counting from one up towards infinity each night before bed, starting each night where she left off the previous day.

Luckily, I outgrew this phase, and I now accept that numbers are, in fact, infinite (even though I still struggle with the concept of infinity in general, but that is neither here nor there). What I did not outgrow was my skepticism or my curiosity to find out how things work.

Stemming from this, I realized already during my school years that I probably wanted to get into research when I grew up. Doing research on what, and in what capacity, was not always clear. I knew that I wanted to do research that felt meaningful and would ultimately benefit people. For this, either biomedicine or medical technology seemed like the best choice for me. After some nudging from family and friends, I was convinced to take the biomedical route rather than the technological one. Instead, my interest in technology would have to be relegated to a hobby (for the time being).

Thus, I enrolled in the bachelor's program in biomedicine in Lund. However, towards the end of the program and after spending a good number of hours in various biology labs, I realized that I wanted to do research that was more directly related to people, maybe even in a clinical setting. In addition, my favorite course in the program was an introduction to physiology and pathophysiology, which made me more interested in understanding how the body works. To continue this newfound interest in physiology, the next logical step was for me to go to medical school, also in Lund.

Five years later, and approaching the end of medical school, it was time for me to find somewhere to do my master's thesis project. I had recently attended a lecture on pediatric radiology by Erik Hedström from the cardiac MR group in Lund, where he showed moving images acquired by cardiovascular magnetic resonance (CMR) of a living fetus still inside the womb, beating heart and all. This fascinated me. How can one, by using nothing but magnets and radio waves (grotesquely simplified), get videos of such high quality, depicting something as small as the beating heart of a fetus while still inside the womb?

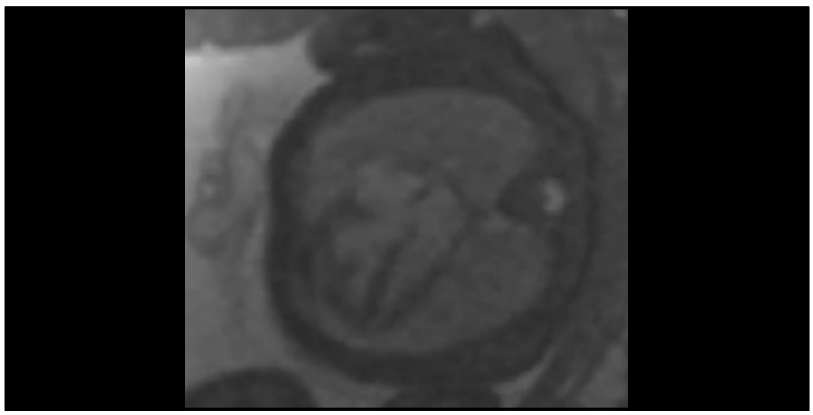

Magnetic resonance image of a fetus inside the womb, with the heart located in the center of the image. *Ryd et al., JAMA Network Open, 2021. Still image cropped from a video, licensed under an Open Access Creative Commons Attribution (CC BY) license.*

I contacted Erik after the lecture and asked if they had any projects available for a master's thesis in their research group. He replied that the best way for me to find out was to attend one of their weekly research meetings, held every Monday. So, the following week, I showed up at the meeting that would, unbeknownst to me at the time, ultimately start me on my journey towards this thesis being written.

The research meeting resulted in me having a one-on-one meeting with my to-be supervisor, Katarina Steding-Ehrenborg, to discuss the different research lines and projects in the group. Out of the ones listed, Katarina's own project line, which involves using CMR to investigate the heart during ongoing exercise, caught my attention. CMR seemed challenging enough while lying still. How would you go about doing this during exercise?

I ended up doing my master's thesis project in the group, enjoying my time enough to stay for another research project during the following summer on a stipend. Half a year later, a week after graduating from medical school, I started working as a junior physician at the Department of Clinical Physiology in Lund, home of the Cardiac MR group, with working hours split between clinical work and research. Finally, in April of 2020, I enrolled as a PhD student in the group, which finally brings us to today, and this thesis.

Context of This Thesis

This thesis was carried out within the Lund Cardiac MR Group at the Department of Clinical Physiology in Lund, Skåne University Hospital, under the supervision of Katarina Steding-Ehrenborg (main supervisor) and Håkan Arheden (co-supervisor).

The thesis was originally planned to include four studies, beginning with a validation of the exercise CMR method used in our research group. The following studies would then focus on data from a planned exercise intervention trial on heart failure, including data from both CMR and muscle biopsies.

Mere weeks before the planned start of the exercise trial, however, we were hit by the COVID-19 pandemic. Because of a central decision suspending all trials requiring at-risk participants to travel to the hospital, we had to postpone the study.

To adapt, we instead focused on the research we were still able to do. This involved research on already gathered data, or by including patients from the clinical workflow. When the pandemic started winding down, and after a new ethics application due to the old one lapsing during the pandemic, we could finally initiate the exercise intervention trial.

In April of 2022, recruitment of the first participants to the EXercise intervention in Patients with hEaRT failure with preserved and reduced ejection fraction In SwEden (EXPERTISE) trial started. The first examinations took place in August of 2023, and as of writing, the study is still ongoing.

Ultimately, this thesis ended up deviating slightly from the original plan largely due to the pandemic. It still includes a validation study of our exercise CMR methodology, but only one study on data from the EXPERTISE trial rather than the three planned ones. Instead, one study based on clinical patients, and one using already gathered exercise CMR data on healthy volunteers and athletes, were added.

The result is a thesis in which we explore and advance methods for measuring novel cardiac mechanics using advanced CMR techniques in the healthy, the trained, and the failing heart, both at rest and during ongoing exercise.

Part I

Research Context

Knowledge rooted in experience shapes what we value
and as a consequence how we know what we know
as well as how we use what we know.

— Bell Hooks

1. Introduction

The heart and blood have been recognized as vital to life already from the earliest written records of medicine, though the interpretations have varied across cultures. In ancient Egyptian medical papyri (circa 1600 BCE), the heart is described as the central regulator of all bodily fluids, directing their movement through a network of vessels [1]. Comparable heart-centered ideas appear across Mesopotamian, Ayurvedic, and Chinese medical traditions, linking the heart to pulse and channel systems, or as central for emotions [2]. Nonetheless, the lineage most directly shaping our modern anatomical models ran from Egypt through the Greek and Roman schools.

In ancient Greece, the Hippocratic tradition introduced the humoral theory of vital body fluids (blood, phlegm, yellow bile, and black bile), with the heart being mostly important for the blood humor [2, 3]. Aristotle offered a more cardiocentric view, where the heart was the primary organ of life and the seat of the soul, and supplied the blood with innate heat [4]. During the same era, Praxagoras first distinguished arteries from veins, and Erasistratus compared the heart to a pump, working as a blacksmith's bellows, although with the arteries normally filled with air and veins with blood [5, 6].

It was not until Claudius Galen, a practicing physician in the Roman Empire during the 2nd century, that it was discovered that both arteries and veins contained blood, derived from vivisecting animals and other experiments [5]. His theory of the cardiovascular system was still somewhat flawed, though, believing venous blood to originate from the liver, and for arterial and venous blood to mix through imperceptible pores between the left and right sides of the heart.

Galen's theories of the cardiovascular system were mostly held as truth for almost fifteen centuries. One correction was made in the 13th century by Ibn al-Nafis, an Arab physician who demonstrated for the first time that blood flowed from the right to the left side of the heart via the lungs rather than through imperceptible pores in the heart [7].

The one to truly elevate our understanding of the cardiovascular system as a closed loop was William Harvey, who in 1628 published his findings in *Exercitatio Anatomica de Motu Cordis et Sanguinis in Animalibus* [8]. By using ligatures and demonstrating that venous

valves permit flow only toward the heart, he showed that blood moves in a single direction. By estimating stroke volume and heart rate to calculate how much blood was leaving the heart every minute, he concluded that the same blood must circulate in the body, as the output from the heart greatly exceeded any reasonable production of new blood.

The final piece of the puzzle needed to finally close the cardiovascular loop was laid by Marcello Malpighi in 1661 in his work *De pulmonibus*. There, he described the structure of capillaries in the lung, and thus the first demonstrable link between arteries and veins outside of the actual heart [9].

Thus, we reach our modern understanding of the cardiovascular system as a closed loop, with the primary purpose of supplying blood carrying oxygen and nutrients to tissues of the body in exchange for carbon dioxide and other metabolic waste.

Today, cardiovascular research has evolved into a rich, multidisciplinary field, merging physiology, imaging, and advanced post-processing methods to study the heart, vessels, blood flow, and their interactions in ever greater detail.

1.1 The Cardiovascular System

The cardiovascular system can broadly be divided into two components, the systemic circulation and the pulmonary circulation, with the heart connecting the two and acting as a pump, forming a closed loop.

The systemic circulation originates from the left side of the heart and supplies the body with oxygenated blood. The pulmonary circulation stems from the right side of the heart and pumps oxygen-poor blood to the lungs, where the exchange of carbon dioxide and oxygen occurs.

Blood vessels are categorized as arteries, capillaries, and veins. Arteries are high-pressure vessels that carry blood away from the heart, with small arteries and arterioles regulating regional blood flow. Veins are low-pressure vessels that return blood to the heart and serve as capacitance vessels, buffering blood volume [10]. Capillaries are the smallest vessels, which link arteries and veins in the tissues of the body. The capillaries are permeable, which allows for the exchange of gases, nutrients, wastes, and other small molecules with surrounding tissues.

The cardiovascular system is highly dynamic, needing to adjust across states such as sleep, walking and running, to sustain high enough arterial pressure and flow to maintain perfusion (tissue blood flow), while minimizing the energy cost. The systemic circulation, supplying tissues and organs from head to toe, operates at relatively high resistance and pressure. The pulmonary circulation, which only carries blood to and from the lungs, operates at lower resistance and pressure.

Finally, we have the heart, the pump that maintains arterial pressure and blood flow to sustain the cardiovascular system throughout life. We begin with a brief overview of cardiac anatomy, then describe the cardiac cycle, pumping mechanisms, and other hemodynamic parameters in greater detail.

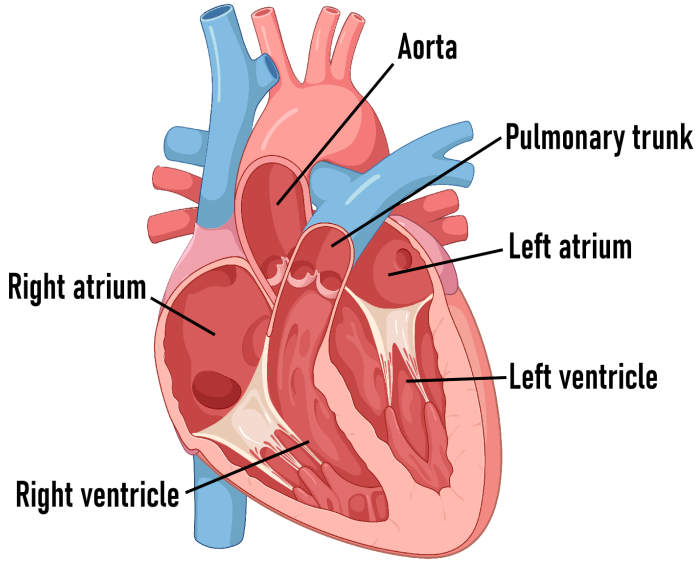

Figure 1.1: Cardiac anatomy. *Created in BioRender and modified in Inkscape. Edlund, J. (2025) https://BioRender.com/172yo5q*

1.1.1 Cardiac Anatomy

Situated within the mediastinum of the thoracic cavity is the central component of the cardiovascular system, the heart. While the heart mostly consists of muscle tissue, the organ is surrounded by a stiff, fibrous pericardial sac. The pericardial sac itself is attached to surrounding tissues, keeping the heart mostly stationary.

The heart has four chambers: two atria and two ventricles. These are split into the left and right sides by the interatrial and interventricular septa. The atria function as reservoirs and conduits for blood entering the heart, whereas the ventricles act like pumps, generating pressure for the blood to flow out of the heart into the circulatory system.

Following the path of the blood, starting on the right side, oxygen-poor blood from the systemic circulation deposits into the right atrium through the inferior and superior vena cava. The blood then passes through the tricuspid valve into the right ventricle, and is ejected by the ventricle across the pulmonary valve into the pulmonary trunk and circulation.

After passing through the lungs, now-oxygenated blood returns from the lungs via the pulmonary veins, depositing into the left atrium. It then flows through the mitral valve into the left ventricle, and is ejected across the aortic valve into the aorta to supply the systemic circulation.

1.1.2 Cardiac Pump Physiology

The heart acts as the central pump of the circulatory system, with the ventricles generating the pressure that drives blood through it. Resistance is higher in the systemic (left side) circulation than in the pulmonary (right side) circulation. This difference is reflected in the shape of the ventricles, where the left ventricle is more conical and has a thicker wall, enabling it to generate higher pressures than the right ventricle.

Historically, the left ventricle has been considered the more important of the two, residing in the spotlight in both research and diagnostics. This also holds true for the present thesis, in which all four included studies focus on the left ventricle. Nevertheless, the right ventricle plays a crucial and increasingly recognized role in cardiovascular physiology and disease [11]. A detailed assessment of its function, however, lies beyond the scope of this thesis.

The Cardiac Cycle and Wiggers Diagram

An intuitive way to start describing the pump physiology of the left ventricle is to go through what happens for one heartbeat, one cardiac cycle. The cardiac cycle consists of two repeating phases, diastole and systole. During diastole, the ventricles relax, filling with blood from the atrium. During systole, the ventricles contract, pumping blood out through the aorta and pulmonary artery.

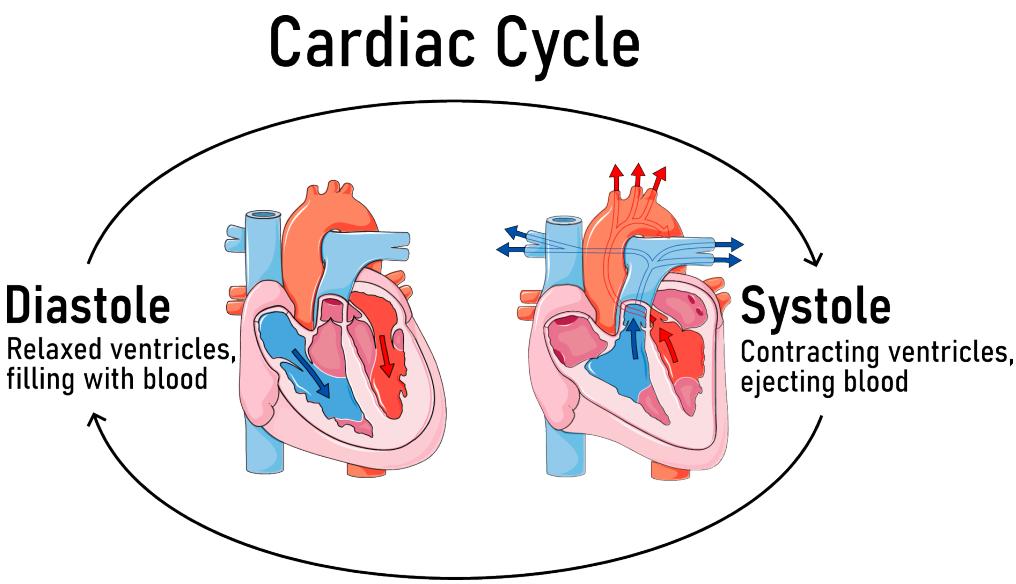

Figure 1.2: The cardiac cycle. *Figure modified by adding arrows and annotations to figures from Servier Medical Art by Servier. Licensed CC BY 4.0 (https://creativecommons.org/licenses/by/4.0/).*

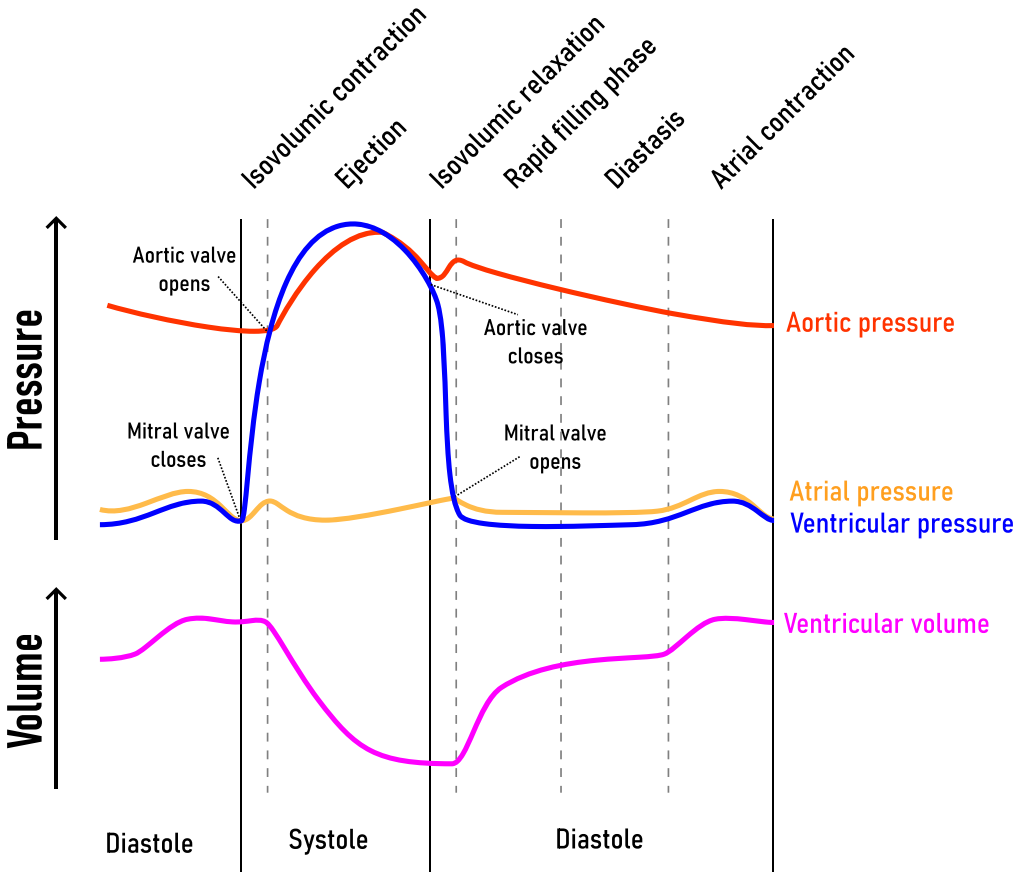

Figure 1.3: A modified Wiggers Diagram. *Adaptation from "Wiggers Diagram 2" from Wikimedia Commons. Licensed CC BY 4.0 (https://creativecommons.org/licenses/by/4.0/).*

The cardiac cycle can be visualized in greater detail in a modified Wiggers Diagram (Figure 1.3) where aortic, atrial and ventricular pressures as well as ventricular volume are plotted over the cardiac cycle [12, 13].

End-diastole, the point at which the ventricle is at its largest volume, occurs just before the ventricle starts contracting. When systole starts and the ventricle contracts, the pressure in the ventricle eventually exceeds that of the atrium, closing the mitral valve. For a short period of time both the mitral and aortic valves are closed while the ventricle is still contracting, called the isovolumetric contraction.

When ventricular pressure finally exceeds that of the aorta, the aortic valve opens and blood is ejected into the aorta. As the ventricle begins to relax, we enter diastole. Ventricular pressure falls rapidly, briefly reversing flow and causing the aortic valve to close. As during

contraction, there is again a short period when both valves are closed, this time during the isovolumetric relaxation.

When the pressure in the ventricle falls below that of the atrium, we enter the early rapid filling phase, where the mitral valve opens and blood is rapidly sucked into the ventricle from the atrium. This is followed by the diastasis, a period where the ventricle and atrium are at an equilibrium with no significant inflow of blood to the ventricle. Finally, towards the end of diastole, the atrium contracts, depositing the last volume of blood into the ventricle, which brings us back to end-diastole.

Cardiac Volumes

Having gone through the cardiac cycle, we can now define several key variables that are important when discussing and evaluating cardiac physiology and function. Among these is the end-diastolic volume (EDV), which is the volume of the ventricle when at its largest. Similarly, end-systolic volume (ESV) is the volume at the very end of systole, when the ventricle is at its smallest. From these, the volume of blood ejected by the ventricle for one cardiac cycle, the stroke volume, can be calculated by subtracting ESV from EDV:

$$stroke\,volume = EDV - ESV$$

The stroke volume can then be used to calculate the ejection fraction, a ratio showing how much of the blood from diastole is ejected during systole:

$$Ejection\,fraction = \frac{stroke\,volume}{EDV}$$

Finally, cardiac output (CO) is a measure of how much blood the heart supplies to the systemic circulation, measured as l/min:

$$CO = SV \times heart\,rate$$

Next, we will discuss some of the mechanisms that determine these volumes.

Preload and Afterload

Two major concepts that affect cardiac volumes are preload and afterload. In short, preload encapsulates factors that increase the filling of the ventricle during diastole, caused for example by an increase in venous return of blood to the heart or an increased blood volume. Afterload represents the load the ventricle pumps against on the arterial side, thus closely linked to arterial pressure [14].

Generally, an increase in preload leads to an increase in stroke volume. This is primarily through the Frank-Starling mechanism, an intrinsic trait of myocytes (the muscle cells of the heart) to more strongly contract the further they are stretched [15–17]. Thus, increased filling in diastole leads to further stretched myocytes, which increases the potential of the myocytes to contract. This allows the ventricle to increase in EDV while largely maintaining ESV, resulting in a higher stroke volume.

In contrast, an increase in afterload usually leads to a decrease in stroke volume because it increases the resistance opposing ejection through the aortic valve. This leads to the valve closing earlier, as the ventricle cannot sustain pressure above aortic pressure for as long, shortening the ejection phase and leading to a higher ESV.

Total Peripheral Resistance and Blood Pressure

As mentioned, afterload represents the load which the left ventricle pumps against. This can be summarized as the total peripheral resistance (TPR), which is the net opposition to blood flow in the systemic circulation. TPR is largely determined by arterial tone and represents a central hemodynamic parameter. Further, it closely relates to the mean arterial pressure (MAP), which is the time-averaged pressure in the arteries over one cardiac cycle.

The TPR can be calculated using the same principles as for resistance calculated in fluid hydraulics:

$$Resistance = \frac{pressure\ gradient}{flow}$$

If we exchange the parameters for those used in the context of the cardiovascular system, we get:

$$TPR = \frac{MAP}{CO}$$

While this is a somewhat simplified formula that disregards the central venous pressure (which, under normal circumstances, is low enough to be negligible), it provides a fast way of relating TPR, MAP and CO to each other.

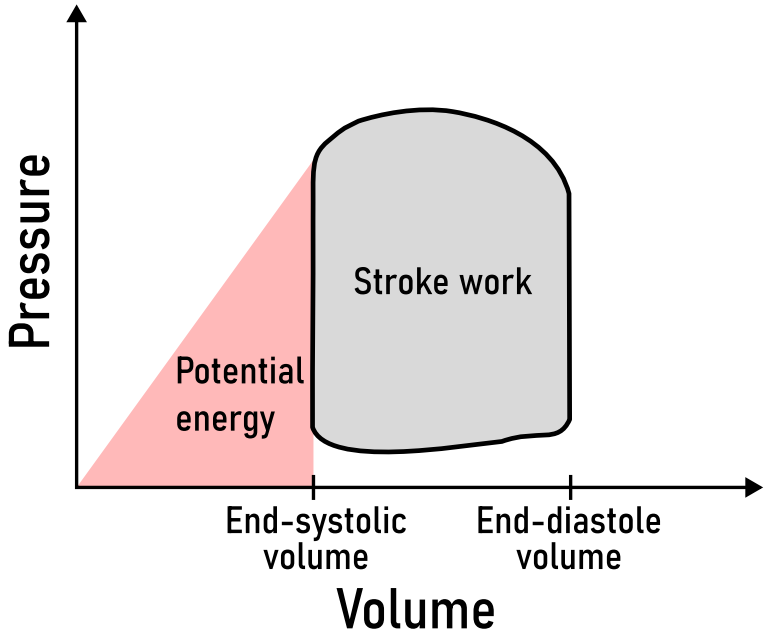

Figure 1.4: Schematic illustration of a left ventricular pressure-volume loop. Indicated in the figure are stroke work and potential energy, two components of cardiac energetics. Combined, these correlate to total myocardial oxygen consumption.

The Left Ventricular Pressure-Volume Relations

A way to visualize both the cardiac cycle and the components of preload and afterload is by analyzing the pressure-volume (PV) relationship of the ventricle. By plotting the ventricular volumes on the x-axis and pressure on the y-axis, the relationship forms a loop (a so-called PV loop) consisting of one cardiac cycle.

The groundwork for PV relations was laid by Otto Frank in the 1890s using isolated frog hearts [18]. Further work in the 20th century by Suga, Sunagawa, Sagawa and colleagues, performing experiments using the canine heart under different loading conditions, established the utility of PV analysis [19–21]. Their research showed the potential to measure load-independent hemodynamic parameters such as contractility, and measures of cardiac energetics like stroke work, ventricular efficiency, and potential energy. They also demonstrated that the total PV area (stroke work + potential energy) has a linear relation to myocardial oxygen consumption.

Pressure-volume analysis began to see clinical use in the 1980s with the development and implementation of the conductance catheter, an invasive technique that measures left ventricular pressure and estimates beat-to-beat volume from inside the ventricle [22]. Finally, modern techniques utilizing cardiovascular magnetic resonance (CMR) imaging for measuring volumes, together with a standard brachial cuff blood pressure measurements, can

generate PV loops noninvasively [23–25]. This method, together with a more detailed explanation of the different hemodynamic parameters that can be measured from PV analysis, is described in greater detail in the Methods section.

Pressure-volume loop analysis has also become a staple of teaching cardiovascular physiology, as it makes it easy to visualize how afterload and preload affect cardiac volumes and energetics. In the loop, end-diastole is represented in the lower right corner, where the pressure is low and volume is at its highest. Similarly, end-systole is represented in the upper left corner, where pressure is high and volume at its lowest. The roof of the loop represents the ejection phase, while the vertical lines on the right and left sides correspond to the isovolumetric contraction and relaxation, respectively.

Misconceptions of cardiac pumping mechanisms

Introductory figures in textbooks (this thesis is no exception, see the earlier figure showing the cardiac cycle) often show pumping as mainly a radial "squeezing" motion of the entire heart. Indeed, the Wikipedia page for "Heart" contains an animation of the cardiac cycle that shows this very phenomenon. In vivo CMR, however, tells a different story. Instead, the variation in total heart volume (defined as the total volume contained inside the pericardial sac) throughout the cardiac cycle has been measured to no more than 5–11% [26, 27].

This misconception is illustrated in Figure 1.5, where end-diastole and end-systole from the aforementioned Wikipedia animation and CMR images of a healthy heart are shown side by side. Note how much both the walls and apex (the bottom tip) of the heart move in the Wikipedia animation, compared to the largely stationary outer contours seen in the CMR images. In reality, the apex sits firmly within the fibrous pericardium, and the atria are anchored by the pulmonary veins at the base of the heart, thereby limiting movement of the outer walls. This brings us to the next topic, longitudinal pumping, which is the mechanism that actually contributes the most to generating stroke volume [28–30].

Longitudinal Pumping

Longitudinal pumping can be defined as the movement of the atrioventricular plane up and down in the base-to-apex, or longitudinal, direction during the cardiac cycle. Measured by CMR as the atrioventricular plane displacement, this motion is estimated to account for about 80% of the stroke volume in the right ventricle and 60% in the left [28–30].

The mechanism of longitudinal pumping in the heart resembles that of a piston, similar to a bicycle pump. The atrioventricular plane is pulled down toward the apex during systole by the contracting ventricle, and recoils toward the base during diastole. This mechanism shifts blood efficiently between atria and ventricles, as it preserves the shape of the cavity more effectively compared to a hypothetical purely radial deformation. Nevertheless, it

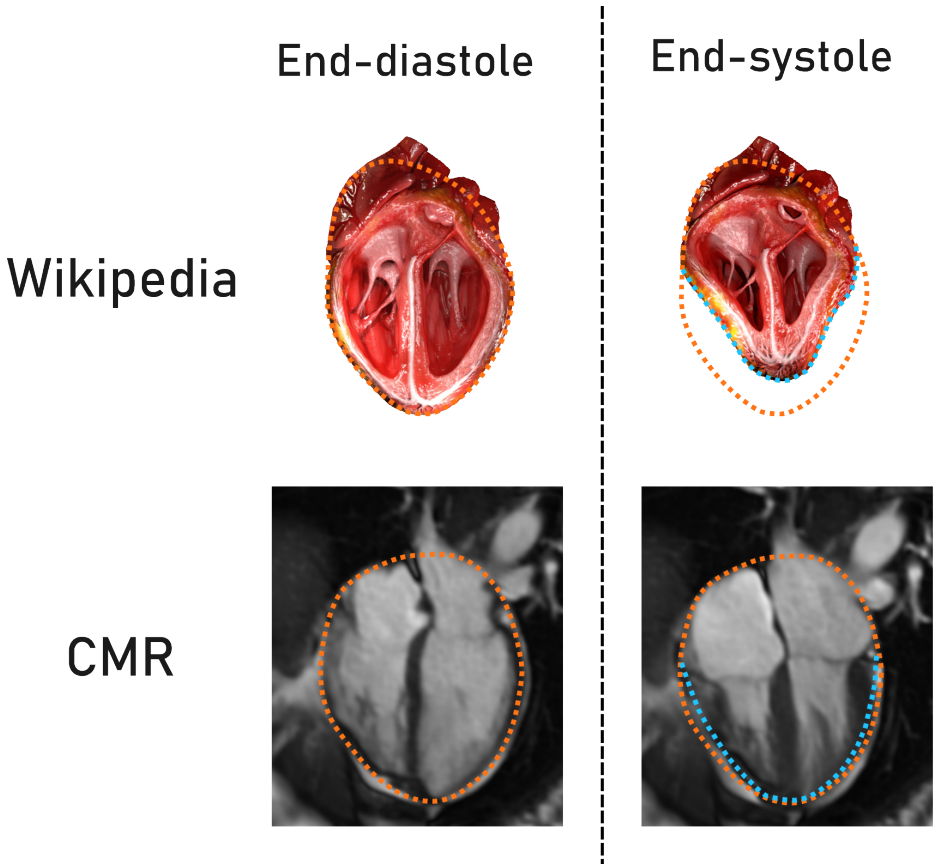

Figure 1.5: A common misconception is that the heart pumps blood mainly by "squeezing" the entire heart using the outer walls. In reality, pumping is primarily performed by longitudinal (base-to-apex) internal shortening. The top row shows images from Wikipedia, and the bottom row from cardiovascular magnetic resonance imaging. The orange dotted line shows the outer contour of the heart in end-diastole, the blue dotted line in end-systole. *The rendered images of the heart are from the Wikipedia article "Heart". Licensed CC BY 4.0 (https://creativecommons.org/licenses/by/4.0/).*

should be noted that radial pumping is still crucial for pressure generation, particularly in the left ventricle.

While the focus thus far has been on the systolic part of the cardiac cycle, for the ventricles to pump effectively, they also need to fill efficiently. This brings us to the next topic, diastolic function.

Diastolic Function

Diastolic function is as essential to cardiac pumping as systolic function. In brief, diastolic function encompasses both how quickly and how completely the ventricle can fill with blood between contractions. The different phases of diastole are visualized in Figure 1.6 along the ventricular volume curve. Additionally, diastole has both active and passive components [31, 32].

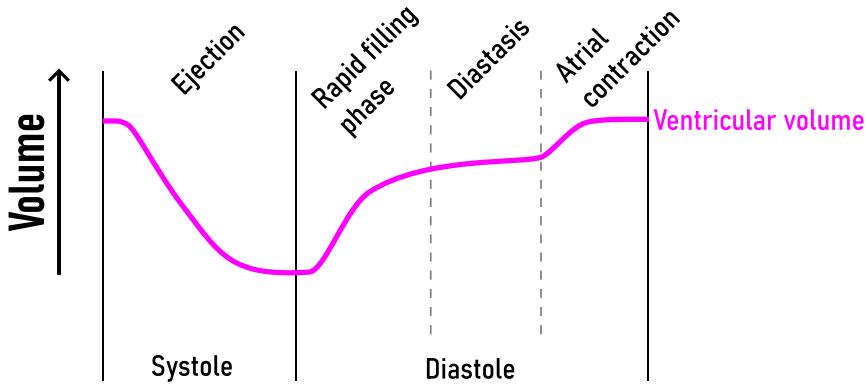

Figure 1.6: A diagram of left ventricular volume over the cardiac cycle, with the different phases of diastole denoted above the curve. *Adaptation from "Wiggers Diagram 2" from Wikimedia Commons. Licensed CC BY 4.0 (https://creativecommons.org/licenses/by/4.0/).*

The active component reflects how quickly the myocytes of the ventricle can relax. This is an energy-dependent cellular process that can be affected by factors such as sympathetic stimulation (which quickens relaxation) or acute ischemia (which slows relaxation). The passive components include ventricular stiffness (elastance, the inverse of compliance), with a stiff ventricle unable to fill as much. For example, a damaged ventricle with areas of stiff, fibrous tissue is not as distensible as a healthy one.

Another passive component is the ventricular recoil, the ability of the ventricle to spring back after contraction. Here, titin, a large spring-like protein, plays a central role. These store elastic energy when the ventricle contracts during systole, ready to recoil when the muscles relax, helping the ventricle return toward its resting shape. Other components of this restorative force are the extracellular matrix (with its networks of collagen and elastin) and the visceral pericardium [33, 34].

These mechanisms synergize to quickly drop ventricular pressure during the rapid filling phase of diastole, causing blood to be sucked into the ventricle from the atrium. The majority of filling occurs during this rapid filling phase, with the final boost being supplied by the atrial contraction toward the end of diastole.

Between the rapid filling phase and the atrial contraction lies the diastasis, a period with minimal or no blood flow between atrium and ventricle. Yet, diastolic forces remain active during this phase, maintaining the equilibrium between atrium and ventricle. Here, another aspect of diastolic function plays a role, hydraulic force.

Hydraulic Forces

Hydraulic force is a novel mechanism of diastolic function. The role of hydraulic forces acting inside the heart was previously theorized but was proven for the first time to be important for ventricular filling by Maksuti et al. in 2017 [35–38]. Since then, hydraulic forces have been shown to aid in left ventricular filling in the healthy heart, but also to hinder filling in certain patient groups [38–42].

The concept of hydraulic force is nothing new, and was described by Pascal during the 17th century by what is now known as Pascal's principle [43]. In short, Pascal's principle states that in a fluid within a closed container, any change in pressure applied at one point is transmitted equally throughout the fluid and to the walls of the container. This has everyday mechanical applications, such as in a hydraulic lift system used in car jacks.

This is illustrated in Figure 1.7, where a small input force applied to a narrow piston raises the pressure throughout the fluid. That same pressure then acts on a wider piston to generate a greater output force. The force applied to each piston can be calculated as the fluid pressure multiplied by the piston's area.

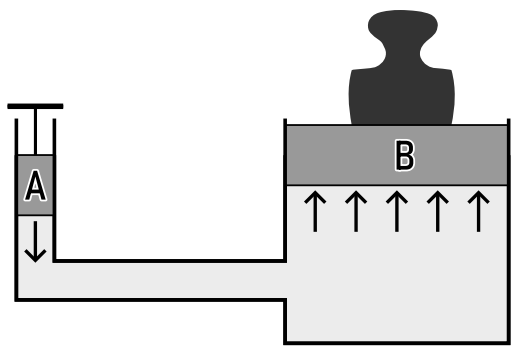

Figure 1.7: Schematic of a hydraulic lift. A force on the small piston (A) creates pressure in the fluid, transmitted undiminished to the large piston (B), producing a greater force due to its larger area.

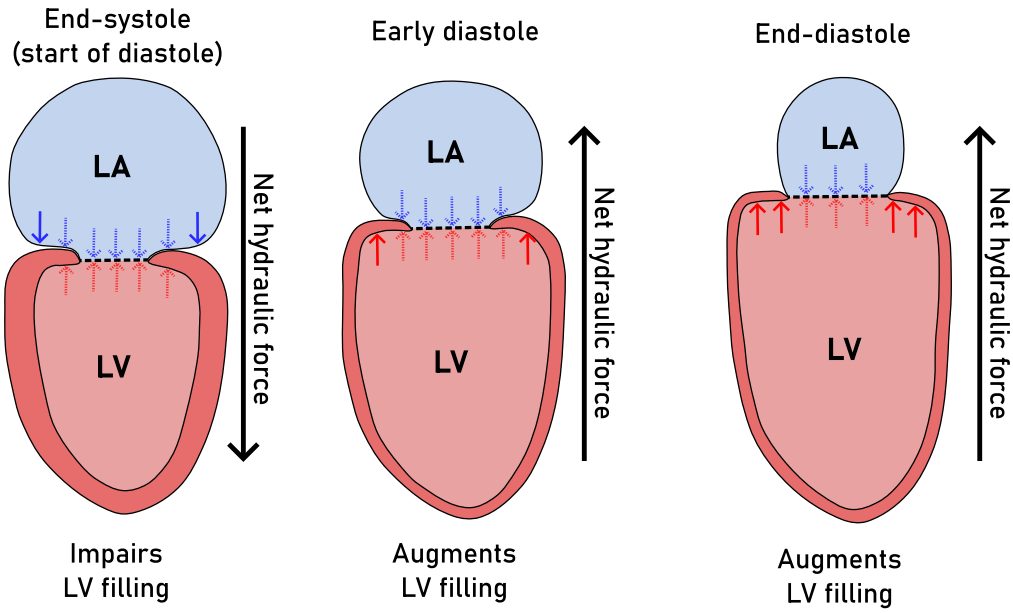

Figure 1.8: Schematic illustration of the left atrium (LA) and left ventricle (LV), indicating the net direction of the hydraulic force at the start, early, and end of diastole in a healthy heart.

In the context of the left side of the heart, the blood represents the fluid, and the endocardial surfaces of the ventricle and atrium define the walls of the container. The atrioventricular plane can be conceptualized as a hollow piston connecting the atrium and ventricle, with the radial walls unable to expand due to the pericardial sac. Thus, only the atrioventricular plane can be moved by an applied force.

As the mitral valve is open during diastole, the difference in pressure between atrium and ventricle is small enough to be considered negligible. Thus, the net hydraulic force across the atrioventricular plane is set by the difference in their areas, where a larger area generates a greater force.

Figure 1.8 is a schematic illustration of the left atrium and ventricle, divided by the atrioventricular plane, at three different points in diastole. The red and blue arrows show the hydraulic force pushing on the atrioventricular plane from either direction, with dashed arrows indicating where they cancel out. The ventricular area is larger than the atrial for the majority of diastole, resulting in the net hydraulic force pushing on the atrioventricular plane in the basal direction, aiding in the longitudinal filling of the ventricle.

1.2 Exercise Physiology

As mentioned, the cardiovascular system must be dynamic to meet the varying metabolic demands of the body. This section begins with a brief overview of the key mechanisms regulating the cardiovascular system that are important in the context of physical exercise.

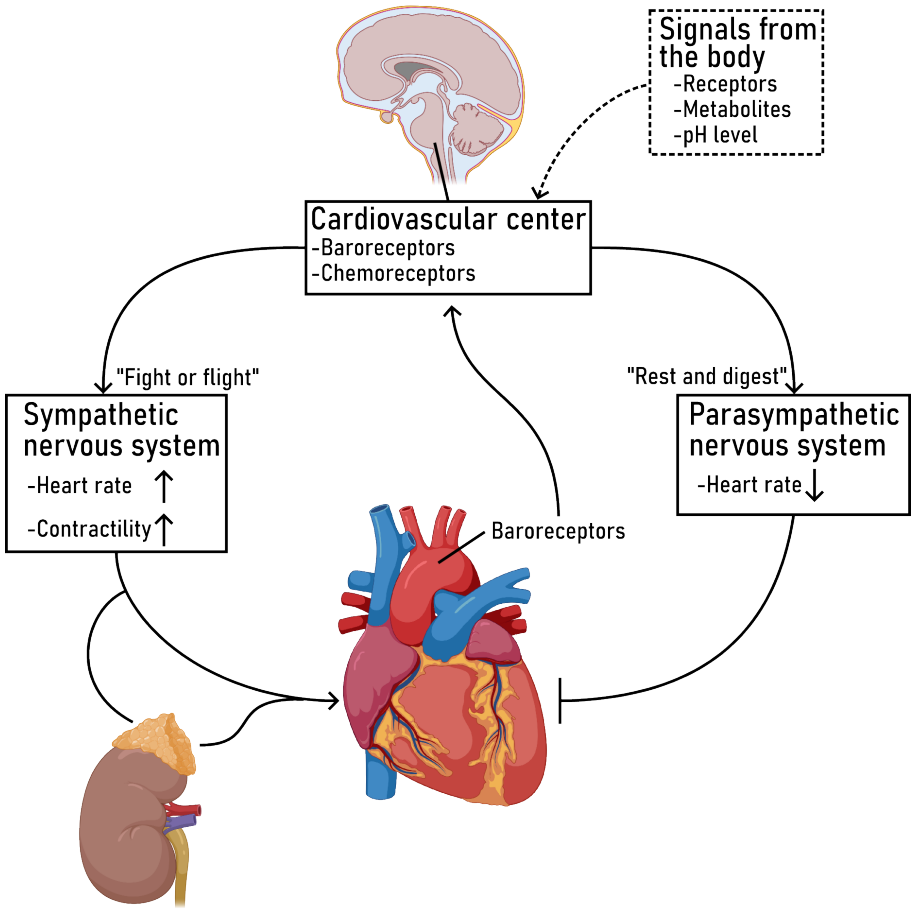

Figure 1.9: Overview of cardiac regulation via the autonomic nervous system. *Created in BioRender and further modified in Inkscape. Edlund, J. (2025) https://BioRender.com/0lwza6o*

1.2.1 Autonomic Regulation of Cardiac Function

Central to cardiovascular regulation is the autonomic nervous system. This neurohormonal system is active throughout the body and regulates a wide range of functions, including respiration, body temperature, and fluid balance [44]. Among its many functions, one of the most important is the regulation of the cardiovascular system. This includes the cardiovascular center, located in the brain stem, which affects the heart both directly through

innervation and indirectly through the release of adrenal hormones such as epinephrine from the adrenal glands [45].

The two most important components of the autonomic nervous system in this context are the sympathetic and the parasympathetic nervous branches. Sympathetic activation ("fight or flight") leads to an increase in heart rate and contractility. It also constricts vessels supplying the kidneys, liver, stomach, and intestines, while dilating vessels supplying large muscle groups, effectively redirecting blood flow from less essential organs to the muscles. In contrast, parasympathetic activation ("rest and digest") mainly leads to a reduction in heart rate mediated through the vagus nerve, also referred to as an increase in vagal tone.

Coupled to the autonomic nervous system are baroreceptors located in the carotid sinus and aortic arch, which are large arteries close to the heart [46]. These receptors are sensitive to the vessel wall being stretched, where increased stretch raises baroreceptor firing, augmenting vagal tone and inhibiting sympathetic activation. Thus, a sudden increase in blood pressure, which stretches the baroreceptors, rapidly decreases the heart rate. Conversely, a sudden fall in arterial pressure reduces baroreceptor firing, decreasing the vagal tone and increasing the heart rate.

Central receptors connected to the cardiovascular center also modulate the autonomic nervous system. These include baroreceptors in addition to those previously mentioned, as well as chemoreceptors sensitive to metabolites in, or acidity of, the blood. Further, the exercise pressor reflex is a mechanism involving receptors within skeletal muscles that signal for increased sympathetic activation during muscle activity [47].

Lastly, the autonomic nervous system affects cardiac function indirectly by regulating vascular tone and fluid balance. For example, sympathetic activation engages the renin–angiotensin–aldosterone system (RAAS), a hormonal cascade largely regulated by the kidneys [48]. This cascade leads to renal fluid retention and venous vasoconstriction, increasing preload. At the same time, RAAS activation causes arteriolar constriction, raising arterial pressure and afterload. These neurohormonal adjustments evolve over minutes to days, in contrast to the almost instantaneous effects of sympathetic and parasympathetic activity on heart rate and contractility.

1.2.2 Immediate Effects of Exercise

[hb] As mentioned, physical exercise greatly increases metabolic demand, which requires the cardiovascular system to increase CO. This serves to increase oxygen supply to working tissues and to enhance oxygen exchange in the lungs, and maximum oxygen consumption scales linearly with CO [49, 50]. Indeed, already in anticipation of planned physical exercise, the body shows signs of increased sympathetic activation [51–53].

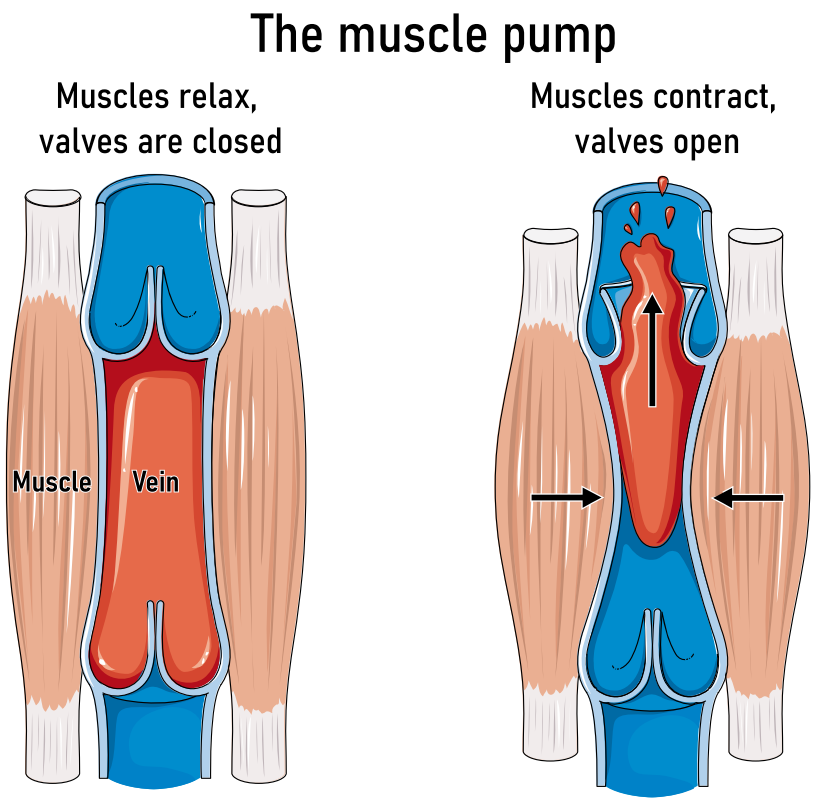

Figure 1.10: The muscle pump. *Figure modified by adding arrows and text to figures from Servier Medical Art by Servier. Licensed CC BY 4.0 (https://creativecommons.org/licenses/by/4.0/).*

Starting at the local level, exercise increases metabolic activity in contracting muscle cells, producing metabolites that signal nearby arterioles to dilate [54]. This reduces vascular resistance and redirects blood flow to the active muscle groups, but mean arterial pressure is quickly compensated through baroreceptors and other sympathetic pathways [47]. As exercise continues, metabolites and increased blood acidity stimulate central receptors, while the exercise pressor reflex further increases sympathetic activity.

Additionally, venous return is increased by the muscle pump during physical exercise, as illustrated in Figure 1.10 [55]. Larger veins have semilunar valves at regular intervals, oriented in such a way as to prevent backflow of blood [56]. Veins surrounded by large muscle groups, such as in the legs, receive a boost to blood flow as surrounding muscles contract and compress the veins. As an example, when running, the rhythmic alternation between contraction and relaxation of the muscles fills the veins and propels blood forward toward the heart, increasing venous return.

Together, these factors increase CO through a combination of elevated heart rate, enhanced stroke volume, and redistribution of blood flow to the exercising muscles.

1.2.3 Cardiac Output at Rest and Exercise

At rest, the typical CO of a healthy, untrained individual typically ranges between 4–6 l/min [14]. During vigorous exercise, this increases to 10-15 l/min, depending on age and sex [57, 58]. The increase in CO is mainly driven by an increase in heart rate and an initial increase in stroke volume [59–61]. While increased sympathetic activity somewhat shortens contraction (systole), it is primarily the time between contractions (diastole) that decreases as heart rate rises [62–64].

At a moderately elevated heart rate, preload may remain sufficient for diastolic filling to not become a limiting factor. That said, when approaching high heart rates during exercise, stroke volume can start to plateau or even decrease, limiting the potential maximum CO [65–67]. The exact response is somewhat debated, though, as studies vary in exercise modality (for example, supine versus upright exercise), in how they define exercise intensity, and in their methodological approaches to measuring stroke volume [61, 68].

In endurance athletes, CO can reach upwards of 40 l/min, significantly higher than that of untrained individuals [69]. However, maximum heart rate is largely determined by age, and thus not significantly higher in athletes [70]. Therefore, the difference in CO must be driven by an increased stroke volume compared with sedentary controls, maintained even at higher heart rates [71, 72].

1.2.4 Long-term Cardiovascular Adaptations to Exercise

Several mechanisms allow trained individuals to maintain stroke volume even at elevated heart rates. The fastest acting mechanism is an increase in total blood volume, which increases preload. Blood plasma volume can expand by up to 10% within one to four days of starting an exercise regimen, continuing to increase and then plateauing after a couple of weeks [73–75]. Although the contribution to total blood volume is comparatively small relative to plasma expansion, red blood cell count also increases after weeks to months, primarily enhancing the oxygen-carrying capacity of the blood [73].

In the long term, exercise at a sufficient level leads to an increase in cardiac volumes through cardiac remodeling, as reflected by larger atrial and ventricular volumes or greater total heart volume [76–78]. In elite athletes, this cardiac remodeling can be more pronounced and is sometimes referred to as ”athlete’s heart”, a physiological remodeling with proportional increases in both cavity size and wall thickness [79]. Although not necessarily related to structural remodeling, athletes also demonstrate improved diastolic function compared with healthy controls at rest [76, 80, 81].

This increase in cardiac volumes raises stroke volume which, in the absence of compensatory mechanisms, would elevate CO even at rest. Consistent with the body generally preferring to conserve energy, endurance training is associated with an increased vagal tone

and reduced sympathetic drive, lowering heart rate at rest [82, 83]. As a result, CO at rest is maintained at appropriate levels despite the increased stroke volume.

Nonetheless, there may be limits beyond which exercise becomes excessive. While the increased cardiac dimensions are beneficial to performance, elite levels of life-long endurance training may lead to increased risk of atrial fibrillation, cardiac fibrosis, and coronary atherosclerosis [84–89].

1.2.5 Long-term Benefits of Exercise

In general, it is worth noting that the benefits of exercise are numerous and well established. With regard to physical performance, these benefits include increased diffusion capacity in the lungs, improved endothelial function of arteries, and enhanced mitochondrial function in the skeletal muscles [90–93]. Looking beyond the cardiovascular system, these benefits include a decrease in all-cause mortality, better mental health, and increased quality of life [77, 94–96].

Overall, while excessive exercise at the elite level may carry certain long-term risks, the overwhelming body of evidence demonstrates that regular physical exercise confers substantial benefits not only to the cardiovascular system, but also to the body and mind as a whole.

1.3 Heart Failure

Having described the normal heart and the supra-normal athlete's heart, we now turn to the diseased heart, specifically, heart failure. Heart failure is a complex clinical syndrome that can be considered a common final pathway of many chronic cardiac conditions. In simplified terms, heart failure is the inability of the heart to pump enough blood to meet the metabolic demands of the body, or to do so only at the cost of elevated intracardiac pressures [97, 98].

Heart failure is associated with substantial morbidity and mortality, with a prevalence of approximately 1–2% in Europe [99, 100]. Additionally, prevalence rises steeply with age, with over 10% of adults aged ≥70 years diagnosed with heart failure [101]. Heart failure therefore represents a substantial global disease burden, expected to increase in parallel with our aging population [102].

While heart failure can be caused by a wide range of underlying conditions, these share several hallmark symptoms. These include increased breathlessness, ankle swelling, and fatigue. The cardinal symptom, however, is exercise intolerance [103].

This section provides a brief overview of pathophysiology, classification, and diagnosis of heart failure, concluding with a more in-depth examination of exercise intolerance.

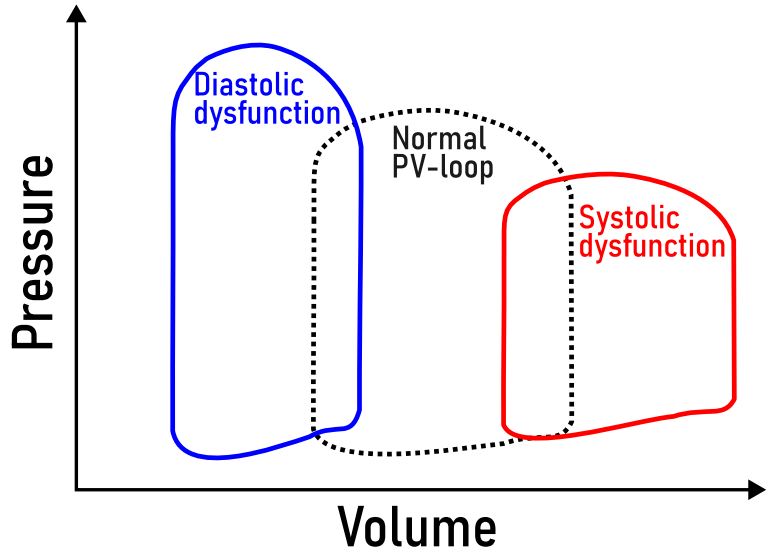

Figure 1.11: Exaggerated examples of how the pressure-volume loop may shift in diastolic and systolic heart failure compared to the normal loop. In diastolic dysfunction, increased myocardial stiffness shifts the loop upward and leftward, leading to higher diastolic pressure at a given volume and often a lower end-diastolic volume and stroke volume. In systolic dysfunction, reduced contractility shifts the loop rightward with increased end-systolic volume, often increased end-diastolic volume due to remodeling, lower peak systolic pressure, and reduced stroke volume.

Pathophysiology

Heart failure is fundamentally a disorder of cardiac pump mechanics, commonly divided into two often overlapping, categories: systolic and diastolic failure [97].

Systolic heart failure or dysfunction reflects impaired ventricular contractility, leading to reduced stroke volume and ejection fraction, and higher filling pressures [104]. Using PV analysis to illustrate, this corresponds to a rightward and downward shift of the entire PV loop, with increased ESV and sometimes also EDV [105]. This results in decreased ventricular efficiency and increased total oxygen consumption.

The pathophysiological mechanisms underlying systolic heart failure include loss of contractile myocardium and myocyte dysfunction. The most common causes include ischemic heart disease (loss of functional myocytes), long-standing hypertension (afterload-induced remodeling), and non-ischemic dilated cardiomyopathy of varying etiologies (myocarditis, excessive alcohol consumption or other toxins) [97, 98, 106, 107].

Diastolic failure or dysfunction, on the other hand, reflects impaired ventricular filling, leading to increased filling pressures while sometimes preserving ventricular volumes and ejection fraction [108, 109]. This results from impaired ventricular relaxation or increased passive stiffness, which physically restricts the ventricle's ability to expand [110].

Using PV analysis again to illustrate, this appears as a leftward and upward shift of the PV loop with a steeper rise in pressure per volume increase, leading to a higher ventricular filling pressure for any given volume.

In contrast to systolic heart failure, the causes of diastolic dysfunction are more varied. Still, the most common causes are those of systolic failure which include ischemic heart disease, long-standing hypertension, and remodeling caused by toxins [97, 98]. Where it differs, however, is in the higher prevalence of comorbidities, which may further accelerate the progression of myocardial dysfunction [111]. These include atrial fibrillation, obesity, and chronic kidney disease [112, 113]. While not a comorbidity, it is worth noting that diastolic failure is also more common in women and older individuals compared to systolic failure [114].

Maladaptation of the Autonomic Nervous System

Regardless of the underlying cause of heart failure, abnormally high sympathetic and reduced parasympathetic nervous activity are key clinical features of the syndrome [115–117]. Although sympathetic activation increases CO in the healthy heart, its benefits are limited in the failing heart and can become maladaptive. Raising preload in a stiff, noncompliant ventricle often fails to increase stroke volume and can be detrimental over time. Likewise, augmenting contractility in a ventricle with substantial scarring often yields little additional output and may not offset the rise in afterload from arteriolar vasoconstriction.

If the failing heart is unable to compensate for the increase in sympathetic activity, this becomes a self-reinforcing cycle, further amplified over time by neurohormonal systems such as RAAS [118]. Consequently, manifest heart failure is characterized by elevated sympathetic activity at rest and exaggerated autonomic responses to exercise.

This sustained sympathetic drive increases afterload and myocardial oxygen demand, raises the risk of arrhythmias, and promotes fibrotic remodeling. In parallel, neurohormonal activation increases salt and water retention via the kidneys, leading to congestion [116]. Left unchecked, this sustained sympathetic state is linked to higher hospitalization rates and mortality [119].

1.3.1 Classification and Staging

Several consensus criteria currently exist to classify and stage heart failure, based on underlying cardiac dysfunction, disease progression, or the patient's symptoms and limitations of physical activity.

Historically, classification of heart failure has followed the systolic/diastolic dichotomy, using cutoff values based on ejection fraction. Today, these are split into heart failure with reduced (HFrEF), mildly reduced (HFmrEF), and preserved (HFpEF) ejection fractions. The criteria for diagnosis, as per the European Society of Cardiology, are presented in Table 1.1 [98].

Table 1.1: Heart failure categories and diagnostic criteria. *Adapted from the 2021 ESC Guidelines for the diagnosis and treatment of acute and chronic heart failure* [98].

Type of heart failure	Criteria 1	Criteria 2	Criteria 3
HFrEF	Signs and symptoms of heart failure.	Ejection fraction: $\leq 40\%$	–
HFmrEF	Signs and symptoms of heart failure.	Ejection fraction: 41–49%	–
HFpEF	Signs and symptoms of heart failure.	Ejection fraction: $\geq 50\%$	Evidence of structural/functional abnormalities indicating diastolic dysfunction or increased filling pressures, including biomarkers (natriuretic peptides).

HFrEF = heart failure with reduced ejection fraction; HFmrEF = heart failure with mildly reduced ejection fraction; HFpEF = heart failure with preserved ejection fraction.

While ejection fraction does not fully capture the complexity of heart failure, this categorization has historically been used in clinical trials for treatment evaluation and outcome assessment. Thus, much of the evidence base underlying today's pharmacological and interventional guidelines is based on these classifications.

The American College of Cardiology and American Heart Association (ACC/AHA) provide guidelines that include stages emphasizing the development and progression of heart failure, rather than categorization based on dysfunction [97]. The stages range from A to D, increasing in severity as seen in Table 1.2. This system aims to facilitate prevention and early treatment of manifest heart failure by addressing risk factors already at an early stage.

Furthermore, the New York Heart Association (NYHA) Functional Classification of heart failure is a scale that emphasizes the patient's daily life rather than measurable findings [120].

Table 1.2: Condensed table of heart failure stages A–D and corresponding criteria. *Adapted from the 2022 AHA/ACC/HFSA Guideline for the Management of Heart Failure* [97].

Stage	**Definition / Criteria**
Stage A: At risk for heart failure	Presence of risk factors for heart failure (such as hypertension, atherosclerosis, diabetes, obesity), but no symptoms/signs of heart failure or structural heart disease.
Stage B: Pre-heart failure	No symptoms/signs of heart failure, but one of: • Presence of structural heart disease • Evidence of increased filling pressures • Risk factors and presence of heart failure biomarkers
Stage C: Symptomatic heart failure	Current or past symptoms of heart failure together with established structural heart disease
Stage D: Advanced heart failure	Severe heart failure symptoms that interfere with daily life and which require recurring hospitalizations

The NYHA classification focuses on the subjective experience of patients with manifest disease and is often used by clinicians to assess quality of life, symptom trajectory, and treatment response. The scale ranges from class I, indicating no limitation of physical activity, to class IV, indicating symptoms of heart failure even at rest. The criteria are summarized in Table 1.3.

Table 1.3: NYHA functional classification and typical symptoms [120].

NYHA Class	**Symptoms**
I	No limitation of physical activity. Ordinary physical activity does not cause undue fatigue or shortness of breath.
II	Slight limitation of physical activity, but comfortable at rest. Ordinary physical activity results in fatigue or shortness of breath.
III	Marked limitation of physical activity, but comfortable at rest. Less than ordinary physical activity results in fatigue or shortness of breath.
IV	Severe limitation of physical activity with symptoms of heart failure already at rest. No physical activity can be undertaken without increased discomfort.

Finally, heart failure can also be classified as chronic or acute. Chronic heart failure refers to the established diagnosis of heart failure (such as HFrEF or HFpEF) but does not necessarily imply the presence of symptoms at a given time. Acute heart failure denotes current symptoms severe enough to require urgent medical attention, for example following a myocardial infarction. While heart failure may debut this way, acute heart failure can also present on top of chronic heart failure.

1.3.2 Diagnosis and Treatment

Cardiac imaging is essential for diagnosing heart failure, either to measure ejection fraction or to assess structural cardiac abnormalities [97, 98]. Echocardiography, an ultrasound-based imaging technique, is a cost-effective and widely used method for this purpose. Among biomarkers, natriuretic peptides are the most commonly used to assess the presence and progression of heart failure. These hormones are released from the myocardium in response to increased stretch, serving as a proxy for elevated filling pressures. When signs of heart failure or structural disease are absent, as can occur in HFpEF, invasive measurement of filling pressures at rest or during exercise may be required to establish the diagnosis [121].

As mentioned, the recommended treatment of heart failure is traditionally guided by both the type of dysfunction (systolic or diastolic) and the severity of the disease. Most pharmacological therapies aim to reduce mortality and morbidity by decreasing the myocardial workload of the failing heart, while others are primarily intended to relieve symptoms such as fatigue and swelling. With modern treatment strategies and early intervention, many patients with structural evidence of heart failure are classified as NYHA class I and may even consider themselves free of disease.

Notably, there is one treatment that not only reduces mortality but also alleviates symptoms and improves health-related quality of life: physical exercise [122–125].

1.3.3 Exercise and Heart Failure

Given the underlying pathophysiology of heart failure, it is unsurprising that the cardinal symptom is exercise intolerance [103]. Indeed, as mentioned, with contemporary early intervention and medical therapy, patients may be completely free of symptoms at rest. In such cases, the only symptoms reported may be increased fatigue or dyspnea during exertion.

Thus, considering the previously described benefits of exercise, it follows that regular physical activity can alleviate exercise intolerance. Indeed, numerous studies show both the benefit and safety of exercise in heart failure, demonstrated by increases in peak oxygen uptake and improvements in health-related quality of life [123, 125, 126].

The precise mechanisms by which exercise training leads to these improvements, however, are likely multiple and not yet fully understood [103, 127]. For example, in systolic heart failure, exercise training does not consistently improve resting systolic function as evaluated by ejection fraction. Nevertheless, HFrEF patients who complete exercise interventions show improvements in exercise capacity and quality of life. The uncertainty of the underlying mechanisms likely reflects differences between studies regarding training protocols, the diversity of heart failure as a syndrome, and differences in outcome measures.

Some identified or proposed mechanisms of improvement include a reduction in sympathetic activity at rest, improved endothelial function in peripheral vessels, improved mitochondrial function in skeletal muscles, and improved ventilatory efficiency or better diffusion capacity in the lungs during exercise [128–132]. Given the wide range of adaptations involved, it is understandable that studies have struggled to isolate a single definitive mechanism of improvement.

Finally, it may simply be that improvements in cardiac function from exercise are not apparent at rest, but only manifest during exercise. Yet, most cardiovascular imaging is performed under resting conditions. Therefore, to understand what improves with training, we may need to evaluate the heart during actual ongoing exercise.

1.4 Cardiovascular Imaging

This finally brings us to cardiovascular imaging, an exciting and rapidly evolving field encompassing several fundamentally different modalities. As mentioned previously, cardiovascular imaging has been central to advancing our understanding of physiology, correcting misconceptions derived from early vivisections and surgical observations, and improving diagnosis and prognosis of cardiovascular disease.

To note, several of the modalities described below can be applied to a wide range of purposes, including angiography (imaging of blood vessels), ischemia assessment, risk stratification, and tissue characterization. Because the primary focus of this thesis is on cardiac pump mechanics, the descriptions will focus primarily on functional and anatomical imaging.

1.4.1 A Brief History of Cardiovascular Functional Imaging

After Röntgen's discovery of X-rays in the late 19th century, chest radiographs (chest X-rays) quickly became a staple of clinical practice in the early 20th century [133]. Although not ideal for detailed cardiac assessment, it nonetheless delineates the cardiac silhouette and pulmonary vessels, allowing for a rough estimate of heart size and for checking for signs of congestion [97].

Building on X-ray technology, the 1950s saw the emergence of the first truly functional cardiac imaging technique: invasive left ventriculography [134]. This involved injecting a contrast agent directly into the ventricle during continuous X-ray imaging, allowing real-time visualization of ventricular contraction and blood ejection. It would take until the 1970s for the next major cardiac imaging modalities, radionuclide imaging and echocardiography, to gain widespread clinical adoption.

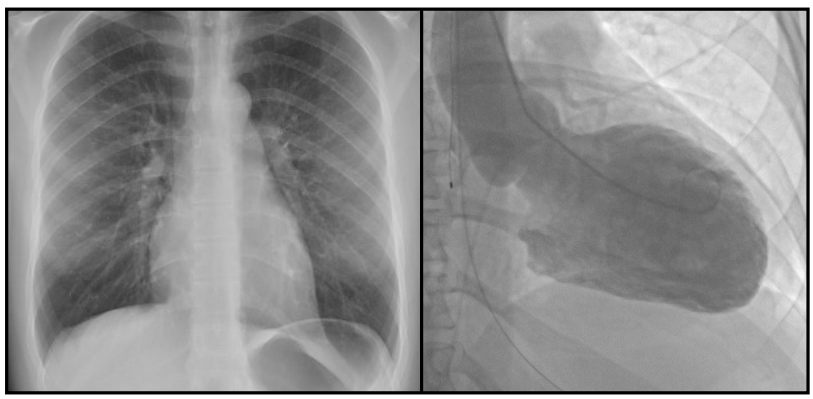

Figure 1.12: Examples of a chest X-ray (left) and a still image from ventriculography (right).
X-ray: Wikimedia Commons, licensed CC0 1.0 (public domain).
Ventriculography: Still image cropped from (https://www.wikidoc.org/index.php/File:011-0436-1.gif), WikiDoc, licensed CC BY-SA 3.0 (https://creativecommons.org/licenses/by-sa/3.0/)

Radionuclide imaging is a technique that detects emissions from radioactive isotopes administered to the patient using a nuclear medicine scanner [135]. By using different tissue-specific tracers, imaging of the myocardial wall and myocardial perfusion becomes possible. Today, the main cardiac application of radionuclide imaging is single-photon emission computed tomography (SPECT) [136]. While SPECT is primarily used for diagnosing myocardial ischemia, it can also quantify ejection fraction and ventricular volumes in addition to assessing myocardial perfusion [137].

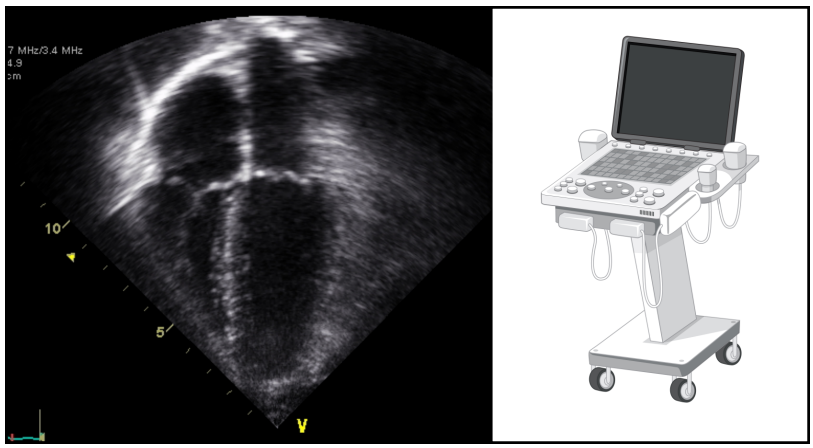

Figure 1.13: Example of an echocardiogram of the heart (left) and an illustration of an ultrasound machine (right). *Echocardiogram: Cropped image from Wikimedia Commons, licensed public domain. Ultrasound machine: Image by brgfx on Freepik [138], Freepik Free license (attribution required).*

Pioneered by experiments by Inge Edler and Hellmuth Hertz in Lund in the 1950s, echocardiography utilizes ultrasound technology to examine the heart [139]. However, it was not until the 1970s that ultrasound devices capable of producing two-dimensional images of the heart became commercially available. The introduction of color Doppler for measuring motion and blood flow transformed echocardiography into a versatile hemodynamic tool for assessing cardiac volumes and function. Today, echocardiography is a cost-effective and portable modality used in cardiac diagnostics worldwide.

Finally, two additional modalities entered clinical practice in the 1980s: cardiac computed tomography (CT) and cardiovascular magnetic resonance (CMR) imaging [140, 141]. Cardiac CT uses a rotating X-ray source with computer-based reconstruction to generate three-dimensional images of the heart. When paired with an ECG signal, the acquisition can be ECG-gated to reconstruct images spanning the entire cardiac cycle, called cine images. Although ECG-gated cine reconstructions allow for functional assessment, cardiac CT is predominantly used for coronary angiography and calcium scoring (for coronary artery disease risk assessment).

Cardiovascular magnetic resonance uses strong magnetic fields and radio waves to image the heart, without ionizing radiation [142]. The underlying principle of CMR, nuclear

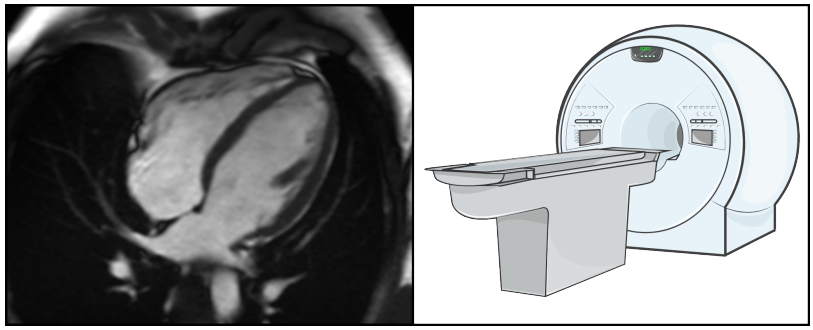

Figure 1.14: Example of a CMR image of the heart in the four-chamber view (left) and an illustration of an MR scanner (right). *Illustration of MR scanner from Servier Medical Art by Servier. Licensed CC BY 4.0 (https://creativecommons.org/licenses/by/4.0/)*

magnetic resonance, was first demonstrated in the 1930s and 1940s, but it was not until the 1970s that magnetic resonance imaging (MRI) was developed [143]. Finally, in 1984 Higgins and colleagues demonstrated the first gated CMR images in humans, enabling sharp visualization of the heart in end-diastole and end-systole [144].

Today, CMR is a versatile modality and an established part of clinical routine worldwide. It is the gold-standard method for assessing cardiac volumes and function and can be complemented by late gadolinium enhancement to visualize fibrosis or infarction, first-pass perfusion for ischemia assessment, and parametric mapping for tissue characterization [145, 146].

Of the modalities described above, echocardiography and CMR are the two most widely used non-ionizing techniques for evaluating cardiac function. Echocardiography is portable and affordable, whereas CMR is the reference standard for volumetric assessment and enables tissue characterization, among other applications. Therefore, since the focus of this thesis is on cardiac pump mechanics, echocardiography and CMR are described in greater detail below.

1.4.2 Echocardiography

Although echocardiography has undergone numerous technical advances since its inception, the fundamental principles of pulse transmission and echo detection remain the same today.

Fundamental Principles of Ultrasound

A transducer is placed on the skin and directed toward the region of interest (e.g., the heart). It emits short bursts (pulses) of high-frequency sound into the body while simultaneously detecting the returning echoes [147]. Echoes arise when the ultrasound beam travels across bordering tissues or structures with different acoustic properties (acoustic impedance), such

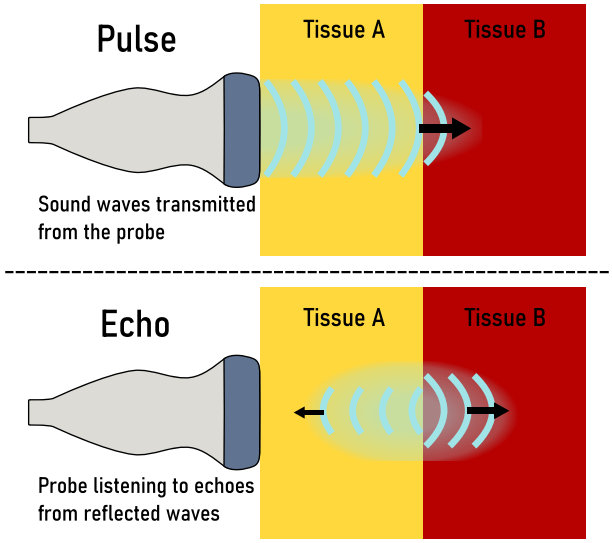

Figure 1.15: Illustration of how sound waves are transmitted, reflected and picked up again by an ultrasound probe. The reflection, or echo, is created when the sound waves travel across bordering tissues with different acoustic properties (such as Tissues A and B in this illustration).

as between blood and myocardium. The greater the difference in acoustic impedance between tissues, the stronger the resulting echo. The echocardiography system then analyzes the timing and amplitude of the returning echoes to construct an image.

The transmitted ultrasound frequency can be adjusted, with higher frequencies providing better spatial resolution but reduced penetration, and lower frequencies offering the opposite trade-off. The ultrasound beam can also be widened or focused. A more focused beam yields sharper detail but limits the field of view.

Transducer Modes and Cardiac Applications

Furthermore, different transducers can be set to different scan modes [148]. The most commonly used and widely available mode in echocardiography is B-mode, which generates a two-dimensional, fan-shaped image originating from the transducer. This mode is well suited for visualizing anatomical structures and for measuring cardiac volumes.

Another mode frequently used for cardiac applications is the M-mode. This mode provides a one-dimensional line over time and is useful for visualizing or measuring the motion and timing of specific structures, such as cardiac valves. For example, M-mode can be used to measure mitral annular plane systolic excursion (MAPSE), a measure of longitudinal pumping comparable to atrioventricular plane displacement in CMR. Modern echocardiography systems may also include 3D or even 4D modes, in which multiple 2D scans are combined into a static (3D) or time-resolved (4D) volumetric dataset.

Doppler Ultrasound

Another important application of ultrasound is Doppler imaging [149]. This technique exploits the Doppler effect, whereby motion of tissues or blood under the transducer causes a frequency shift in the returning echo. Based on this frequency shift, the system calculates both velocity and direction of motion. Color Doppler can be used to visualize jets caused by valvular stenosis or regurgitation, while continuous-wave Doppler can be used to measure peak velocity [150]. Tissue Doppler can also be used to measure myocardial motion, for example in assessing ventricular dyssynchrony.

Strengths and Limitations

The major strength of echocardiography lies in its accessibility. Ultrasound systems capable of standard workhorse modes, including Doppler, are cost-effective and portable, allowing bedside examinations when necessary. Ultrasound is also a very safe modality, with no known direct risks when used within safe exposure limits and no ionizing radiation. Echocardiography is also highly versatile and offers excellent temporal resolution, enabling precise assessment of timings.

One of the major drawbacks of echocardiography is that it is a very operator-dependent modality. Learning the modality takes extensive practice when it comes to both probe handling and navigating the machine. Further, several measurements, such as asynchronous wall-motion or valve grading, are only semi-quantitative measures and thus prone to the subjectivity of the operator. Volumetric calculations based on two-dimensional images also make certain assumptions of the shape of the chambers, which do not always reflect reality [151].

However, some of these limitations can be mitigated by operator experience, standardized acquisition protocols, or 3D/4D acquisitions of volumes instead of relying on two-dimensional images and geometrical assumptions. Standardized acquisition specifically is important when comparing measurements between different examinations or operators.

Another limitation is how dependent the acoustic window is on the anatomy and bodily constitution of the person being examined. The acoustic window is, in the context of echocardiography, a spot on the chest or abdomen where ultrasound can pass between ribs and lungs to reach the heart with minimal signal loss. In some individuals, the heart is simply situated in such a way that it is very difficult to get a clean ultrasound image with minimal interfering tissues causing signal loss such as bone, air from the lungs or excessive adipose tissue.

1.4.3 Cardiovascular Magnetic Resonance Imaging

Basic Magnetic Resonance Imaging Physics

Magnetic resonance imaging exploits the intrinsic quantum trait of certain atomic nuclei to spin, giving rise to a magnetic moment, which can be excited to produce a detectable signal [152–154]. For CMR, and other clinical MRI scans in general, hydrogen is the most important nucleus in this context. The hydrogen nucleus consists of a single proton, and is abundant in water and fat, two major constituents of the body.

Spin in the context of MRI does not signify literal rotation but intrinsic angular momentum. Still, as a simplification, we can think of each hydrogen proton as spinning around its own axis and generating a magnetic moment, causing it to act as a miniature bar magnet with a north and a south pole.

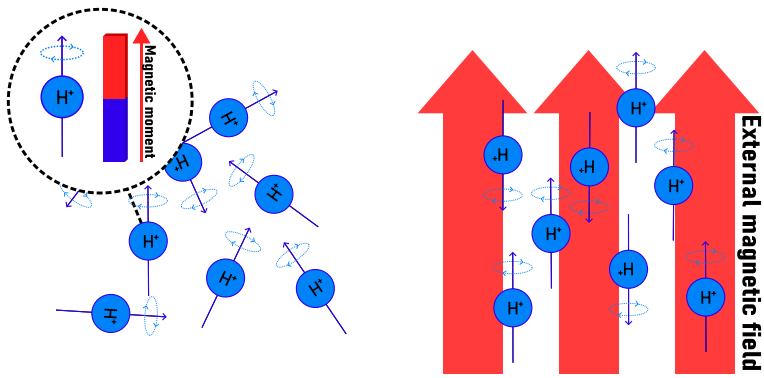

Figure 1.16: Hydrogen protons have innate spin, giving rise to a magnetic moment. These align parallel when placed in a strong external magnetic field (B_0).

Normally, the magnetic moments of these protons are randomly oriented in space. However, when placed in a strong external static magnetic field, a small excess of the protons aligns parallel to the static magnetic field. In MRI, the strong external static magnetic field provided by the scanner is referred to as B_0, with the most common scanners for CMR at field strengths of 1.5T or 3T. For reference, the magnetic field of a 1.5T scanner is 30 000 to 60 0000 times stronger than that of our planet's at surface level. By convention, B_0 defines the z-axis, or the longitudinal direction.

Furthermore, the magnetic moments precess about the direction of B_0, analogous to a spinning top, which both spins along its own axis and rotates in relation to the underlying surface at the same time.

The protons precessing around B_0 do so at the same frequency, but their phases are randomly distributed. Transverse (x-y) components of the magnetization thus cancel, leaving a net magnetization along the z-axis, parallel to B_0.

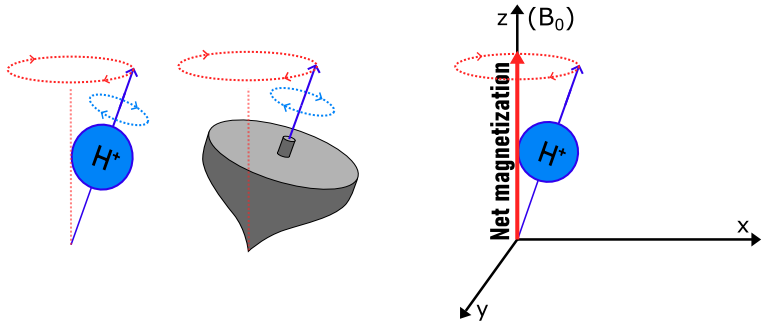

Figure 1.17: Hydrogen protons precess, likened to spinning tops, around B_0, giving rise to a net magnetization in the longitudinal direction

The frequency at which the protons precess around B_0 is called the Larmor frequency (ω_0), which is specific to each nucleus based on its gyromagnetic ratio (γ) and the external magnetic field strength (B_0). This can be calculated using the Larmor equation [155]:

$$\omega_0 = B_0$$

The Larmor frequency is of vital importance in MRI, as it defines the frequency of the radiofrequency (RF) pulse used to excite protons in the body. Each RF pulse is a short burst of oscillating electromagnetic waves at the Larmor frequency, transmitted by the scanner to the body.

An RF pulse applied on resonance (ω_0) generates a small magnetic field (B_1) which is perpendicular to B_0. The RF pulse excites the protons into a higher energy state and tips the net magnetization away from B_0 by a specified flip angle, determined by the duration and amplitude of the RF pulse.

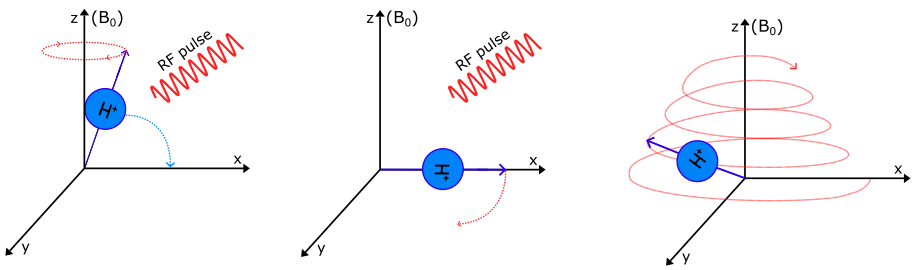

Figure 1.18: The effects of a radiofrequency (RF) pulse on precessing hydrogen protons, showing the initial tipping of the net magnetization away from B_0 and the ensuing recovery after the pulse.

Further, the RF pulse phase-aligns many of the precessing protons, creating a net magnetization in the transverse (x-y) plane. This transverse precession induces an alternating voltage in nearby receiver coils, which is the MR signal picked up by the MR scanner.

In the example illustrated in Figure 1.18, a 90° pulse rotates, or flips, the magnetization fully from the longitudinal direction into the transverse plane. After the pulse, magnetization relaxes towards equilibrium over time, which can be measured. The recovery of magnetization along B_0 is referred to as longitudinal relaxation, and transverse relaxation refers to the magnetization decay along x-y caused by the precessing protons dephasing again after excitation.

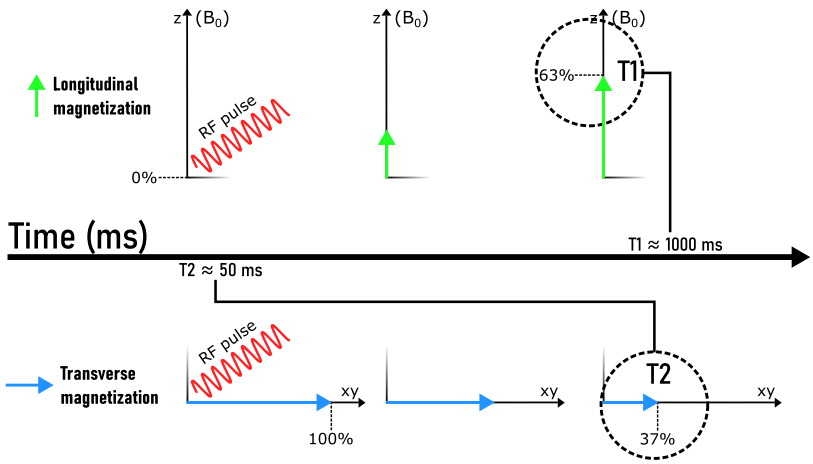

Figure 1.19: Illustration of how T1 and T2 values are measured in time after a radiofrequency (RF) pulse.

Longitudinal relaxation is measured as T1, defined as when 63% of the original magnetization has recovered. T2 instead is a measure of the transverse relaxation, defined as the time when the transverse component has decayed to 37% its initial value immediately after the RF pulse. While these values vary depending on settings on the MRI machine (sequence parameters), magnetic field strength, tissue type and different scanner vendors, T2 is typically much shorter than T1. The example illustrated above is based on healthy myocardium using a 1.5T scanner.

From MR Signal to Image

Having described how the MR signal is generated and evolves over time with T1 and T2, the next step towards generating an image is to encode spatial positioning to the signal. That is, we need to be able to localize from where the acquired signal originates in the body. This can be done using magnetic-field gradients, generated by gradient coils in the MR scanner.

Gradients are small, rapidly switchable additions to B_0 that affect the magnetic field. This can be done in the x, y or z directions by using the so-called frequency, phase and slice encoding gradients, causing the Larmor frequency to be slightly different in different parts of the body [155]. This enables the scanner to send an RF pulse which is specific to the

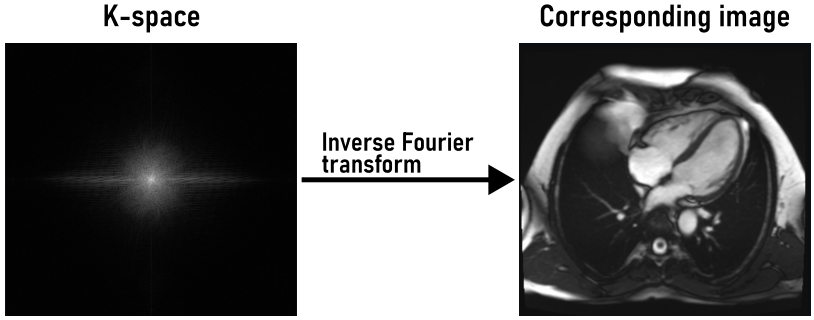

Figure 1.20: Example of k-space (left) and the corresponding reconstructed image (right) from a CMR acquisition. *The illustration of k-space was generated using the open source software K-Space Explorer (https://github.com/birogeri/kspace-explorer)*

spins in a certain slice of the body. Thus, by applying gradients, the scanner can spatially encode the signals acquired.

The acquired signals are then stored in k-space, the spatial-frequency domain of MRI. K-space is a grid of signal samples, where each point encodes how rapidly intensity varies (frequency) across space (spatial). It is not an image, but contains information about the pixels of an image. By using the inverse Fourier transform, a mathematical formula, an image can be generated from k-space.

Thus, the resulting image is dependent on the acquired signals. By modifying the RF pulse, usage of gradients and other MR sequence parameters, different parts of the body or tissue types can be targeted to provide strong signals.

Applications of CMR

The standard, or maybe most basic, cardiac application of CMR could be considered anatomical and functional images of the heart. Cine images spanning the whole cardiac cycle used in clinical routine are made possible through ECG-gating [145]. In principle, this means acquiring an ECG signal at the same time as acquiring images and prospectively or retrospectively synchronizing these. Instead of acquiring the entire cardiac cycle in one go, images at specific timepoints of the cardiac cycle are acquired from several cardiac cycles. These are then combined into one, high-resolution cine of the cardiac cycle, as an average from multiple cardiac cycles. Typically, cine images of the left ventricle are acquired in a sequential stack of short-axis (SAX) images and three long-axis views — four-, three-, and two-chamber (4ch, 3ch, 2ch) (Figure 1.21).

Aside from the standard cine images, there are numerous more applications of CMR [145, 146, 156]. One of the earliest, and still most often used, applications is phase-contrast

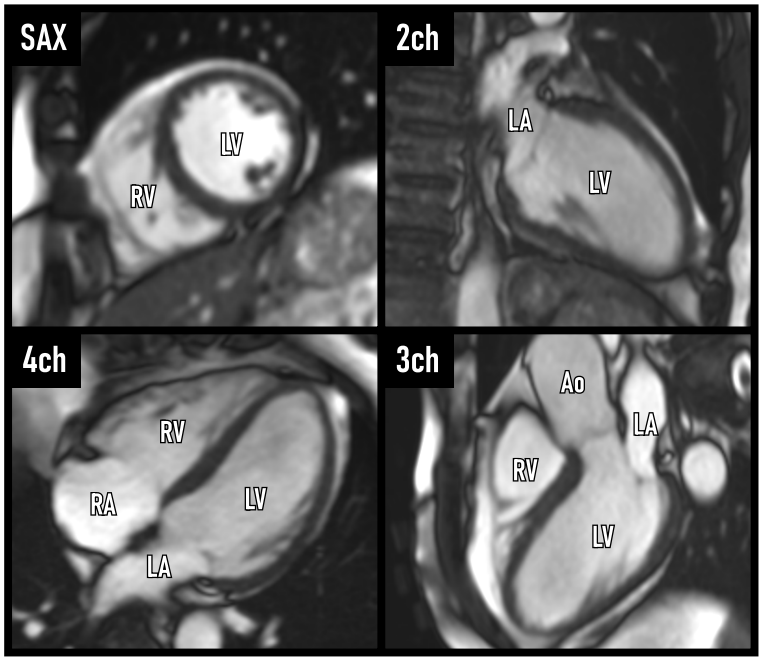

Figure 1.21: Collage of standard cine CMR planes, one short-axis (SAX) and three long-axis views (2ch, 3ch, 4ch), illustrating the left and right ventricles (LV, RV), atria (LA, RA), and aorta (Ao).

imaging. This enables quantification of blood flow, and is used in quantifying valve insufficiencies and shunts. Tissue characterization detecting, for example, myocardial inflammation or fibrosis, can be done by T1 and T2 mapping. By adding an MR contrast agent, late gadolinium enhancement (more commonly known as LGE) can further help tissue characterization or detection of infarction, as well as quantification of extracellular volume. First-pass perfusion, and with modern techniques even quantitative perfusion, allows for diagnosis of myocardial ischemia. A currently hot research topic in CMR is 4D flow, which gathers flow and functional data simultaneously in 3D. This can be used for measuring kinetic energy, hemodynamic forces, and visualizing vortex patterns.

Strengths and Limitations of CMR

CMR is the gold-standard method for quantifying ventricular volumes, mass, ejection fraction, and flow for measuring valve regurgitation or shunt ratio. Cine CMR yields highly reproducible results, even between different operators, which generally allows for smaller sample-sized studies compared to other modalities [157, 158].

One other major strength of CMR is the versatility of the modality. While some of the most common cardiac applications are discussed above, it is far from a comprehensive list. As examples, CMR can also be used in tumor diagnosis, or in the evaluation of iron depositing and fatty infiltration.

Similarly to echocardiography, CMR does not come with any ionizing radiation, making it ideal for repeat examinations or examinations of younger individuals. MRI in general also has no known direct health risks associated with it when conducted according to standard clinical protocols, aside from short-term benign side effects on the level of feeling lightheaded when entering or leaving the MR bore.

Admittedly, there are several limitations of CMR that bear mentioning. In contrast to echocardiography, the access, cost and logistics associated with CMR limit the availability of the modality. The equipment is expensive, requires a specially built room and the exam times are lengthy.

For standard cine imaging, requiring a regular ECG signal can be a limitation in patients with arrhythmia as an irregular rhythm results in blurry images of potentially non-diagnostic quality. Similarly, image acquisition must be performed during breath hold, as to not have the heart moving in and out of the imaged slice with the breathing motion, to avoid blurring. This can make it difficult to perform cine in patients with dyspnea severe enough to be symptomatic already at rest.

CMR also entails a risk in the form of the strong, static magnetic field around the scanner. The magnetic field is strong enough to potentially create dangerous projectiles of heavy ferromagnetic objects if accidentally brought into the scanner room, such as an oxygen tank [159]. The strong magnetic field also has to be taken into consideration in patients with implants or foreign objects with ferromagnetic properties. While modern cardiac devices can be MR-conditional or MR-safe, they tend to cause image artifacts which can obscure parts of the heart in acquired images. This can be limiting for patients with pacemakers or other implanted cardiac devices.

1.4.4 Stress Imaging

Thus far, we have only described methods of imaging the heart during rest. Yet, some patients with cardiovascular disease are asymptomatic at rest and only experience symptoms during exertion. Thus, it may be necessary to investigate the heart during ongoing stress, whether provoked by pharmacological agents or by physical exercise.

Pharmacological Stress

The most common way of stressing the heart is through pharmacological means, as this allows the patient to be stationary during the examination. In general, there are two principally different methods of stressing the heart that are used in clinical practice, regardless of imaging modality. The first of these are vasodilators, agents that dilate the coronary arteries, the vessels supplying the myocardium with blood [160]. Vasodilators can be used to assess myocardial ischemia, either through detecting persisting stenosis after dilation or through

measuring perfusion before and after dilation. The most commonly used vasodilators are adenosine via infusion, or regadenoson injected as a bolus.

The second group comprises pharmacological agents that induce both inotropic (increased contractility) and chronotropic (increased heart rate) stress, most commonly using dobutamine [161]. While this can also be used to assess inducible ischemia, this approach is generally more suitable for assessment of myocardial viability or contractile reserve, for example in patients with heart failure.

If all pharmacological agents are contraindicated, then a third alternative is to induce stress through actual physical exercise.

Physical Exercise

While pharmacological agents can artificially stress the heart, none can replicate the effects on the entire cardiovascular system that actual physical exercise produces. The main challenge with physical exercise, though, is the difficulty of imaging the heart during ongoing exertion.

Historically, echocardiography (stress echocardiography) has been the modality of choice for imaging during physical exercise, owing to its relatively simple logistics compared with other imaging techniques [162]. Exercise protocols typically involve use of a treadmill or bicycle ergometer, with immediate post-exercise imaging. This approach provides higher-quality images, as the patient can remain still during image acquisition, but it does not fully reflect the physiological effects of ongoing exercise.

An alternative is to use a supine or semi-supine bicycle ergometer, allowing imaging during actual ongoing exercise. This approach, however, is technically challenging for the operator, as it is difficult to maintain a stable probe position and an adequate acoustic window due to the combination of heavy breathing, perspiration, and body motion during exercise.

Exercise CMR

One potential way to overcome these challenges is through the use of CMR. This approach, though promising, introduces its own technical limitations. Similar to echocardiography, studies have been performed with exercise followed by imaging immediately post-exercise [163]. In CMR, this can be particularly difficult because image acquisition typically requires breath-holding for at least 10–15 seconds, which is challenging immediately after exercise cessation.

Recent developments in CMR now enable free-breathing, non-ECG-gated imaging with sufficient image quality to quantify cardiac volumes and mass [67, 164, 165]. These advances also allow imaging during actual ongoing exercise within the MR bore, and one such method is described in the Methods section.

To understand exertional breathlessness,
you have to exert the breathless.

— Prof. André La Gerche

2. Rationale

Heart failure is currently one of the largest global health burdens, projected to increase in tandem with our aging population. Earlier detection or better understanding of the underlying pathophysiology could help reduce mortality and morbidity associated with heart failure. To use heart failure with preserved ejection fraction as an example, this category of patients can be difficult to detect at an early stage due to the absence of obvious structural cardiac defects and a by definition preserved ejection fraction.

One avenue to help earlier detection could be to investigate the heart during ongoing exercise — the state in which heart failure patients are most likely to actually experience symptoms. Another would be to find new or new ways of investigating cardiovascular parameters to be used in diagnosis, prognosis, or as endpoints in studies.

Further, we already know that exercise is an effective form of treatment for cardiac disease, but it is woefully underutilized [166]. By deepening our understanding of exercise physiology and pinpointing the mechanisms leading to better health, we could contribute to the evidence needed for exercise to be considered a legitimate treatment for heart failure, on par with pharmacological treatment.

This thesis hopes to contribute to the above-mentioned goals by using state-of-the-art CMR techniques to investigate both cardiac parameters previously requiring invasive measurements (pressure-volume analysis) and novel parameters (hydraulic force), at rest and during ongoing exercise.

The answers you get from literature depend on the questions you pose.

— Margaret Atwood

3. Aims

The overall aim of this thesis was to utilize CMR to assess novel aspects of cardiac mechanics both at rest and during exercise in the healthy, the trained, and the failing heart.

The specific aims for the four included studies were:

Study I: To evaluate inter- and intraobserver variability of CMR-derived, noninvasive pressure-volume analysis parameters across healthy controls, patients with subclinical diastolic dysfunction, and heart failure patients, and to evaluate a new method designed to greatly accelerate the workflow of said pressure-volume analysis.

Study II: To develop a post-processing algorithm for respiratory sorting of images acquired during free-breathing CMR, to determine the image acquisition time required for said algorithm to function, and to validate the accuracy of the algorithm for measuring volume and mass, first at rest and then during exercise.

Study III: To investigate whether the atrioventricular area difference, a proxy for hydraulic forces, changes when going from rest to moderate and vigorous exercise in sedentary controls and endurance athletes, as measured by exercise CMR.

Study IV: To investigate whether hydraulic forces impair or augment diastolic filling in heart failure patients during exercise by measuring atrioventricular area difference using exercise CMR.

Once you've got a task to do,
it's better to do it than live with the fear of it.

— Joe Abercrombie

4. Material and Methods

4.1 Study Population and Design

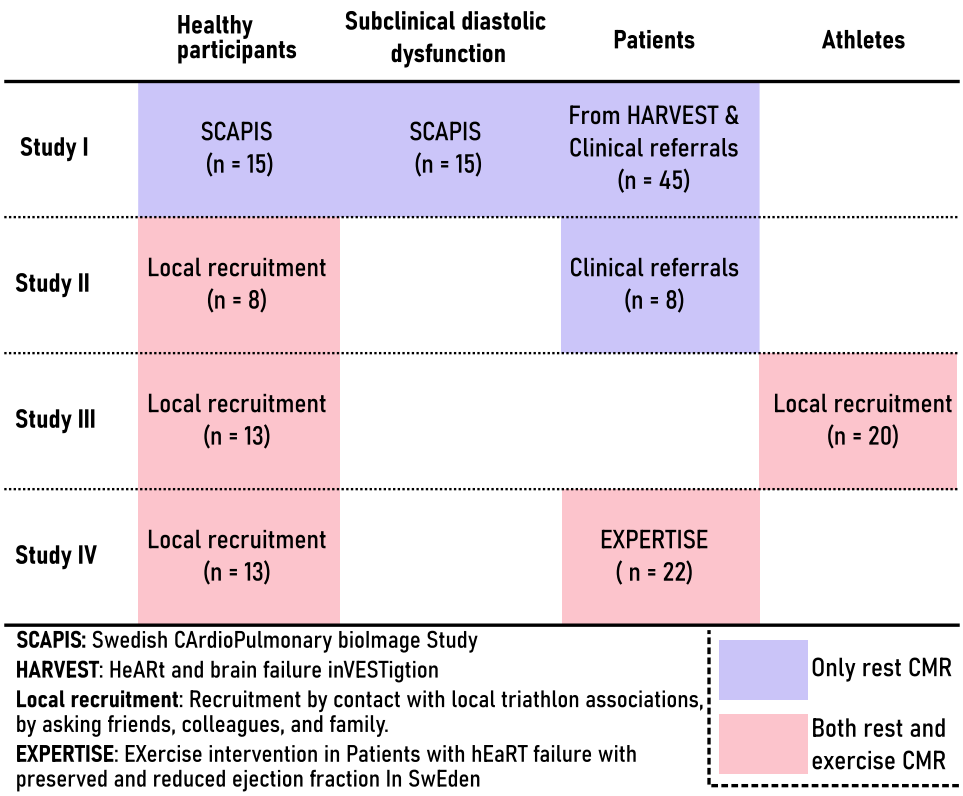

Figure 4.1: Overview of the study populations and methods used for the four studies in this thesis.

An overview of the study populations and the use of exercise CMR across the four studies is presented in Figure 4.1. More detailed descriptions of each study's population and design are provided in the following sections.

Ethical Approval

Written informed consent was obtained from all participants, and all four studies followed the Declaration of Helsinki [167]. All studies were approved by the regional ethics committee in Lund, Sweden, and Study IV was also approved by the Swedish Ethical Review Authority.

Study I

Study I included 75 participants who were prospectively recruited into five evenly split categories (Figure 4.1). Healthy controls and participants with subclinical diastolic dysfunction were included from the population-based Swedish CArdioPulmonary bioImage Study (SCAPIS) [168]. Heart failure patients were included from clinical referrals to the local clinic and from the prospective HeARt and brain failure investigation (HARVEST) study of hospitalized patients with heart failure [169].

Healthy controls had no history of cardiovascular disease, were non-smokers and had blood pressure <140/90 mmHg. Participants with subclinical diastolic dysfunction were non-smokers, had blood pressure <140/90 mmHg and no abnormal cardiac findings on CMR or coronary computed tomography angiography. However, on echocardiography, they fulfilled 1–2 of the 4 echocardiographic criteria clinically used to diagnose diastolic dysfunction, but did not exceed the >50% threshold required for a definitive diagnosis [170]. Heart failure patients all had a clinical diagnosis of heart failure made by a cardiologist and were divided into subgroups depending on ejection fraction as determined from CMR. HFpEF was defined as ejection fraction ≥50%, HFmrEF as ejection fraction 41–49%, HFrEF as ejection fraction ≤40% [98].

As part of Study I, all participants underwent CMR at rest, with brachial cuff blood pressure measurements taken in conjunction with CMR image acquisition.

This was primarily a methodological study, evaluating the inter- and intraobserver variability of PV loops computed using standard cine CMR images [23, 25]. A method for greatly accelerating said analysis was also successfully validated in the study.

Study II

Eight healthy volunteers were recruited by asking friends, colleagues, and family. Eight patients from the clinical workflow were also recruited, with the only inclusion criterion being sinus rhythm during acquisition. Healthy volunteers underwent CMR both at rest and during exercise, whereas the patients underwent CMR only at rest.

This study can be divided into two distinct parts: the development of an algorithm to sort already acquired images based on respiratory state, and the validation of said algorithm for measuring LV mass and volumes. The development was performed using CMR images

acquired at rest, whereas validation was performed on CMR images acquired both at rest and during exercise.

Study III

Twenty athletes and thirteen sedentary controls were recruited through contact with a local triathlon association, through digital and physical advertisements, and by asking friends, colleagues, and family. Sedentary controls were age- and sex-matched to the athletes, had no history of cardiovascular disease, and exercised less than 150 minutes of moderate intensity aerobic exercise per week, which is below the minimum recommended physical activity level by the World Health Organization [94].

All participants underwent CMR both at rest and during exercise to first evaluate the feasibility of measuring the atrioventricular area difference, a proxy for hydraulic force, during exercise using the method developed in Study II.

Study IV

The first 30 participants invited to the EXPERTISE trial were included in Study IV. In short, patients with a clinical diagnosis of heart failure in their medical records between 2011 and 2021 in the region of Scania, Sweden, were screened and invited to participate in EXPERTISE, a randomized controlled trial evaluating exercise as an intervention for heart failure. In the end, 22 of the 30 invited participants completed all baseline examinations necessary for analysis in this study.

The same thirteen healthy volunteers (no longer age- or sex-matched to this cohort) from Study III were included in the analysis of Study IV to contrast the findings from the heart failure group with those from the healthy heart.

4.2 Methods

4.2.1 CMR Image Acquisition

Central to all four studies was CMR. The same MR scanner was used in all four studies: a 1.5 T Siemens Aera (Siemens Healthineers, Forchheim, Germany).

For images acquired at rest in all studies, standard ECG-gated balanced steady-state free precession (bSSFP) sequences during breath-hold were used with the following typical sequence parameters: echo time 1.1 ms, repetition time 2.2 ms, flip angle 67°, acquired in-plane spatial resolution 1.0 × 1.0 mm, slice thickness 8 mm with no slice gap and reconstructed temporal resolution to fit 25 time-frames per cardiac cycle (typically 40 ms).

For imaging during exercise in Studies II, III, and IV, as well as for rest in Study II, a Siemens product real-time bSSFP sequence with free breathing and no ECG gating was

used. Typical sequence parameters were: echo time 1.1 ms, repetition time 2.2 ms, flip angle 60°, acquired in-plane spatial resolution 1.9 × 2.8 mm, slice thickness 10 mm with no slice gap. Parallel imaging (GRAPPA with reduction factor 3) and Partial Fourier (factor 5/8) acceleration were used to enable an acquired temporal resolution of 28–37 ms. For both rest and exercise, cine SAX images covering the whole heart as well as long-axis images in the 2ch, 3ch, and 4ch views were acquired.

Total acquisition time for real-time images varied across studies, determined by the number of time-frames gathered per slice multiplied by number of slices (typically 14–17 slices). For Studies II and III, 800–1000 time-frames were acquired (34s/slice). For Study IV, this was instead 250 time-frames (8.5s/slice).

4.2.2 Exercise CMR

Exercise CMR was used for Studies II, III and IV. Images were acquired during ongoing exercise using an MR-compatible cycle ergometer (Lode BV, Gronigen, The Netherlands) (Figure 4.2). Muscle activity from performing exercise disrupted the ECG-signal which, combined with the difficulty of performing breath-hold during exercise, necessitated the use of real-time, ungated CMR sequences. Heart rate could still be monitored during exercise via peripheral pulse oximetry, measured from one or two fingers.

Figure 4.2: The exercise CMR setup used at the local clinic. The MR-compatible ergometer is attached to the table, allowing for exercise while inside the bore. *Photograph used with permission from author Katarina Steding-Ehrenborg.*

Exercise Protocols

The exercise protocols used during image acquisition differed slightly depending on the study population but followed the same general principle: exercise started at a fixed resistance, was manually ramped up until the desired exertion intensity was reached, and was then held at a steady state for the duration of image acquisition. See Figure 4.3 for an overview of the two protocols.

What differed was the target exercise intensity. For the healthy volunteers and athletes, this was based on heart rate. Moderate intensity was defined as 60% of the age-predicted maximum heart rate, calculated using the formula (220 - age in years) beats per minute, and vigorous intensity was defined as 80% [171].

For the heart failure patients, target exercise intensity was instead determined by ergometer resistance. All patients had performed cardiopulmonary exercise testing prior to the CMR examination as part of the EXPERTISE trial. The target intensity was set to 30% of the maximum load achieved during the exercise test, guided by previous studies and experience in converting upright to supine exercise [164].

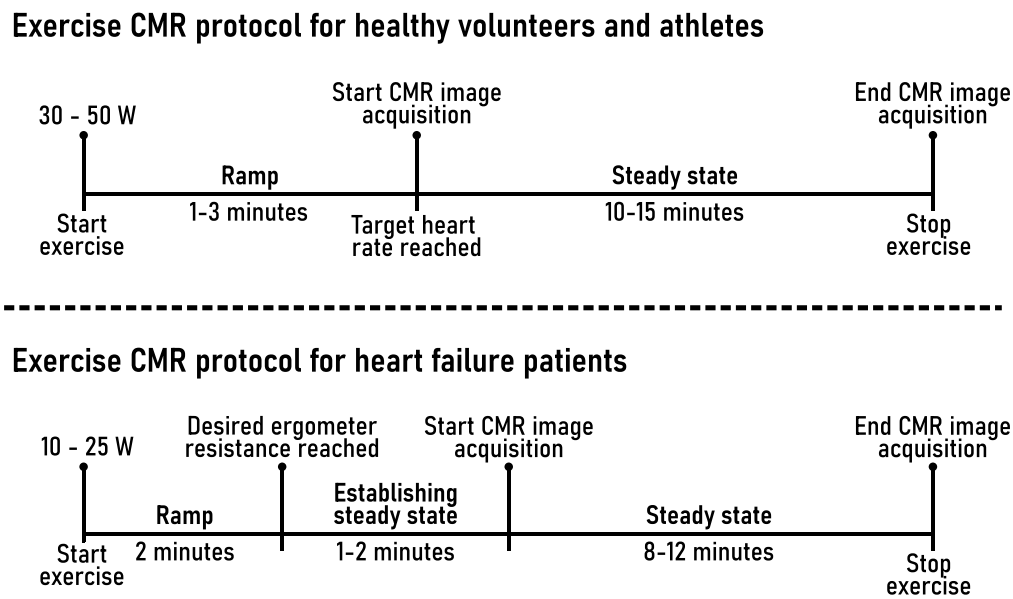

Figure 4.3: Overview of the two different exercise protocols used during exercise CMR image acquisitions.

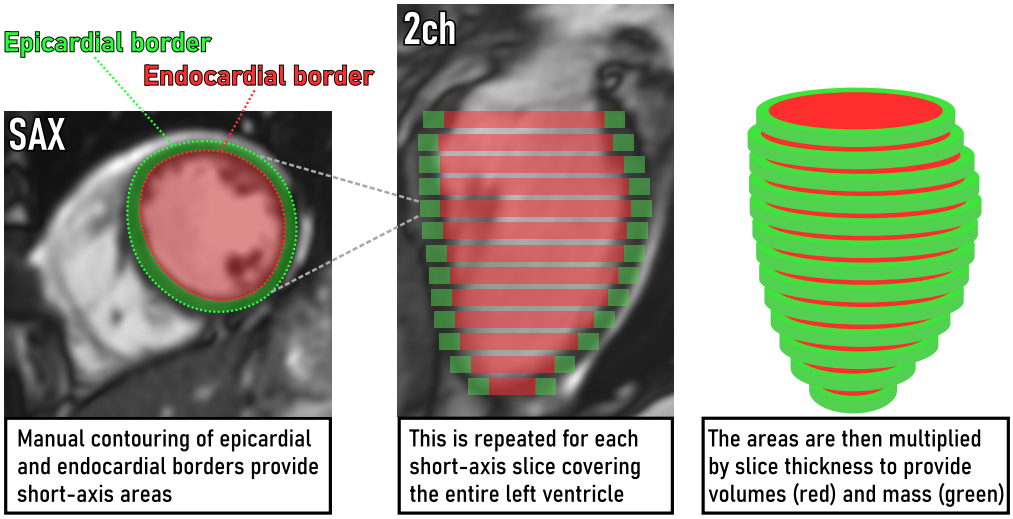

Figure 4.4: Illustration of the workflow for manual contouring of endocardial and epicardial borders on short-axis images. Slice areas are multiplied by slice thickness and summed across the stack to calculate ventricular volumes and mass.

4.2.3 CMR Image Analysis

All CMR image analysis was performed using the freely available software Segment (Medviso, Lund, Sweden) [172]. In all studies, cardiac volumes and mass were calculated from SAX images in end-diastole (ED) and end-systole (ES) using planimetry. In short, volumes were obtained by manually segmenting (contouring) the endocardial and epicardial borders in each slice comprising the ventricle. The areas were then summed and multiplied by the slice thickness to get a volume (volume = area × height). Left ventricular (LV) mass (LVM), end-diastolic volume (EDV), and end-systolic volume (ESV) were derived from these contours across all slices spanning the ventricle.

Papillary muscles and trabeculations were treated as part of the blood pool and thus excluded from myocardial mass, in accordance with international recommendations [173]. LVM was computed as myocardial volume (the difference between epicardial and endocardial contours) multiplied by the myocardial density of 1.05 g/cm^3. Further, contouring of the left atrial (LA) endocardial border was used in Studies III and IV to calculate LA volumes in ventricular ED and ES.

4.2.4 Respiratory Sorting of Images from Exercise CMR

One challenge regarding exercise CMR lies in the analysis of images after acquisition. First, without ECG gating, time-frames containing ED and ES must be visually identified and selected on a slice-by-slice basis. Second, acquiring images during free breathing introduces a risk of acquiring the same cardiac imaging slice multiple times due to the heart moving up and down through the imaging plane with each breath (illustrated in Figure 4.5). Thus, analysis should ideally be performed in the same respiratory state across the entire ventricle.

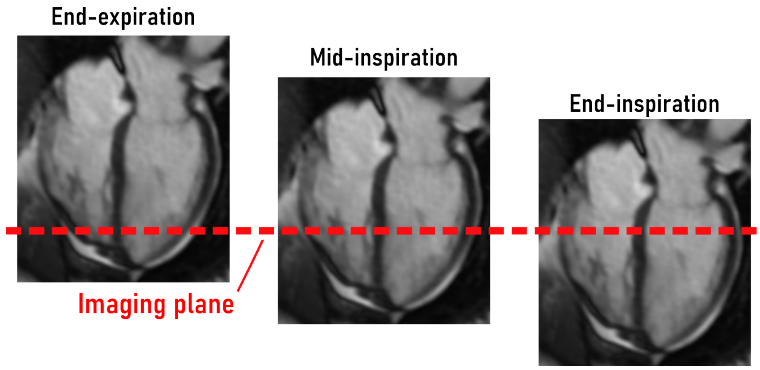

Figure 4.5: An exaggerated example of how the heart moves through the MR imaging plane when acquiring images during free-breathing.

A potential solution to this is to sort the acquired images by respiratory state during the post-processing stage. A semi-automatic algorithm for this purpose was developed and validated in Study II and then used in the image analysis of Studies III and IV. An overview of how this method works is shown in Figure 4.6.

In brief, the algorithm uses structures outside the heart, mainly the diaphragm, to create a curve displaying the respiratory state of each time-frame. Next, manual selection of ED and ES within the desired respiratory state is performed and repeated for each slice comprising the ventricle (and/or atrium). The result is a SAX stack with two time-frames, ED and ES, in a fixed respiratory state which is ready for analysis. Images in Studies II, III, and IV were sorted to end-expiration to align with standard practice in conventional cine CMR, where end-expiration breath-holds are used [145].

Additionally, this method has been further developed and now allows for cine images in fixed respiratory states, not only single time-frames [174]. This updated method was used in part for Study IV to generate SAX image stacks for time-resolved analysis.

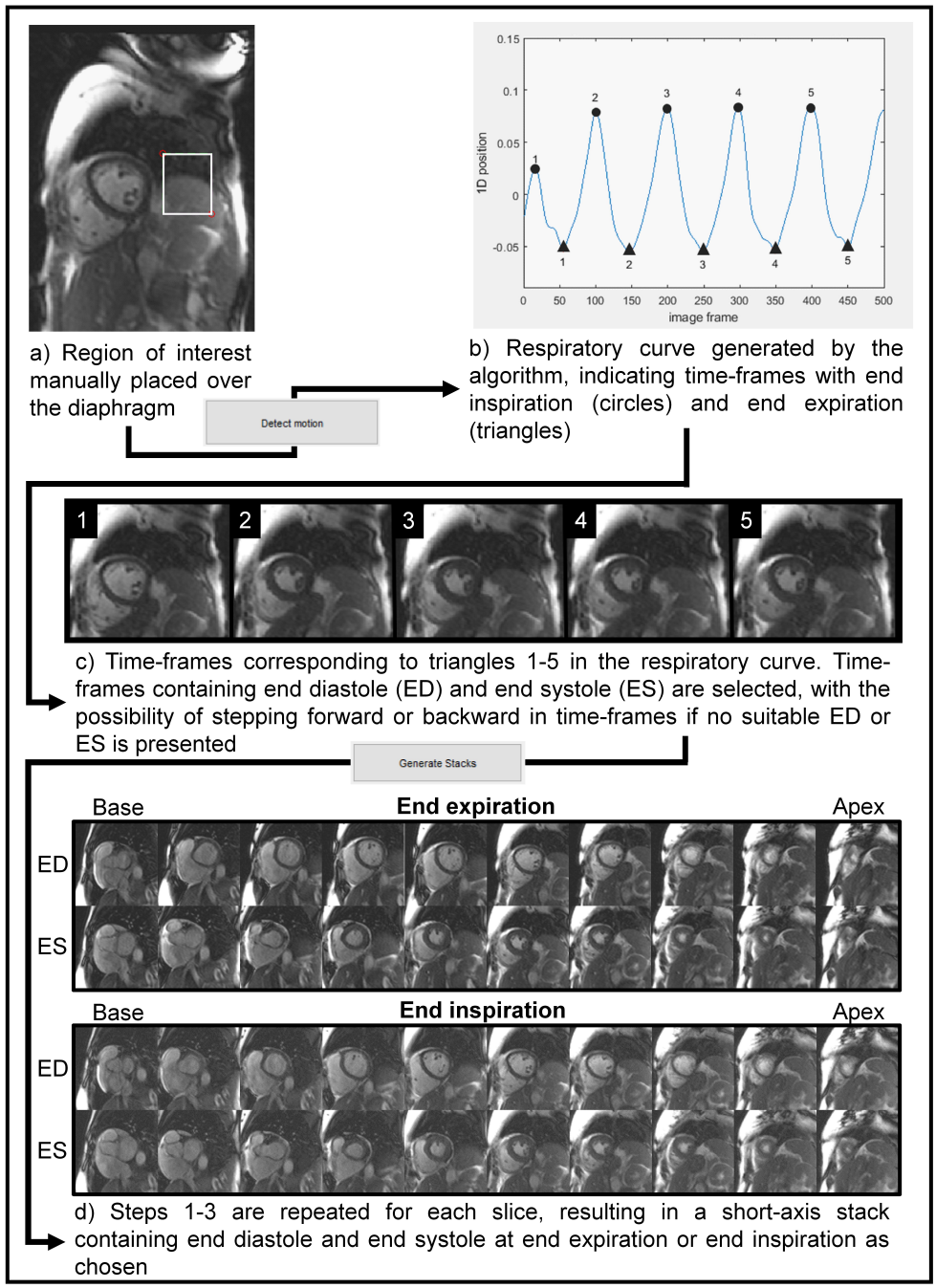

Figure 4.6: Overview of the algorithm developed for respiratory sorting of non-ECG-gated real-time CMR images acquired in free breathing.

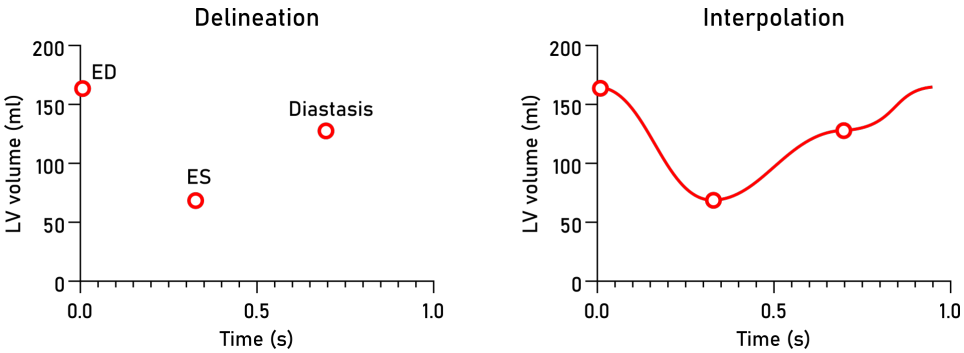

Figure 4.7: Graphs showcasing spline interpolation. The left graph shows the three manually contoured time-frames, end-diastole (ED), end-systole (ES), and diastasis. The right shows the resulting volume curve after spline interpolation, filling the missing time-frames.

4.2.5 Spline Interpolation for Left Ventricular Segmentation

Some analyses require measuring LV volume across the entire cardiac cycle, not only at ED and ES. When using the manual method of contouring, this greatly increases analysis time as there are typically 25 time-frames instead of just two to measure.

One potential way of circumventing this is by utilizing a spline interpolation approach, which was evaluated and validated in Study I. In short, this entails manual contouring of ED, ES, and diastasis (when applicable), followed by spline interpolation to fill in the contours of the missing time-frames. This is done on a slice-by-slice basis, allowing for manual correction where needed.

4.2.6 Pressure-Volume Loop Analysis

For Study I, noninvasive PV loops were computed using an in-house developed and experimentally validated method by Seeman et al. [23, 25]. In brief, the model uses heart rate and time-resolved volumetric data from CMR images as well as brachial blood pressure as input. The brachial blood pressure was used to estimate the peak systolic LV pressure using the following formula [175]:

$$\text{Peak LV pressure} = (0.83 \times \text{systolic blood pressure}) + (0.15 \times \text{diastolic blood pressure})$$

These data are then used to scale a time-varying elastance model to calculate ventricular pressure over the cardiac cycle which, combined with volumetric data from CMR, computes the PV relationship over one cardiac cycle, one loop (Figure 4.8. Note that in this model, V0, the theoretical ventricular volume when pressure is zero, is assumed to be zero.

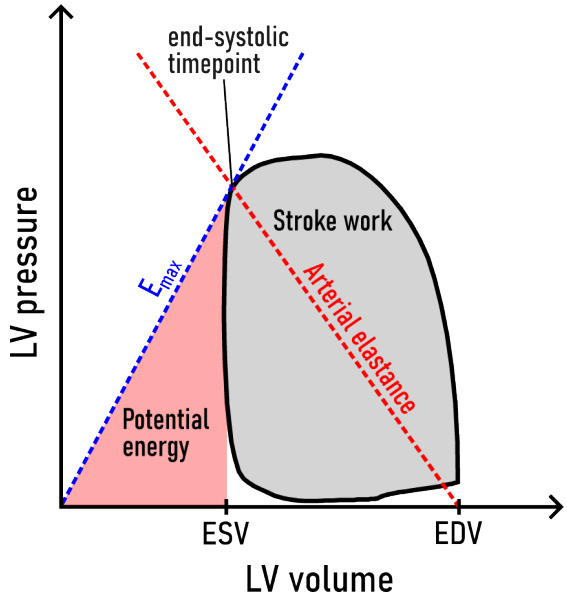

Figure 4.8: Illustration of a pressure-volume loop derived from CMR images with parameters denoted in the image.

Parameters derived from PV relationship analysis were the following:

E_{max} (mmHg/ml) — the maximal ventricular elastance, calculated as the slope intersecting the origin (V0) and the end-systolic timepoint. This is a load-independent measure of contractility.

Arterial elastance (mmHg/ml) — calculated as the slope intersecting the end-systolic timepoint and the point for EDV on the x-axis. This characterizes the load in the arterial system.

Ventricular-arterial coupling (ratio) — calculated as the ratio between arterial elastance and Emax. This represents the interaction between myocardial contractile capacity and afterload.

Stroke work (J) — calculated as the area of the PV loop. This represents the external work the myocardium performs to pump blood in each cardiac cycle.

Potential energy (J) — calculated as the triangular area to the left of the PV loop with corners defined by V0, the point for ESV on the x-axis and the end-systolic timepoint. This represents the internal energy the heart needs to uphold to maintain a certain pressure.

Pressure-volume area (J) — calculated as stroke work plus potential energy. This represents the total energy expenditure of one cardiac cycle, proportional to myocardial oxygen consumption [176].

Ventricular efficiency (%) — calculated as the ratio between stroke work and PV area. Analogous to ejection fraction for volumes.

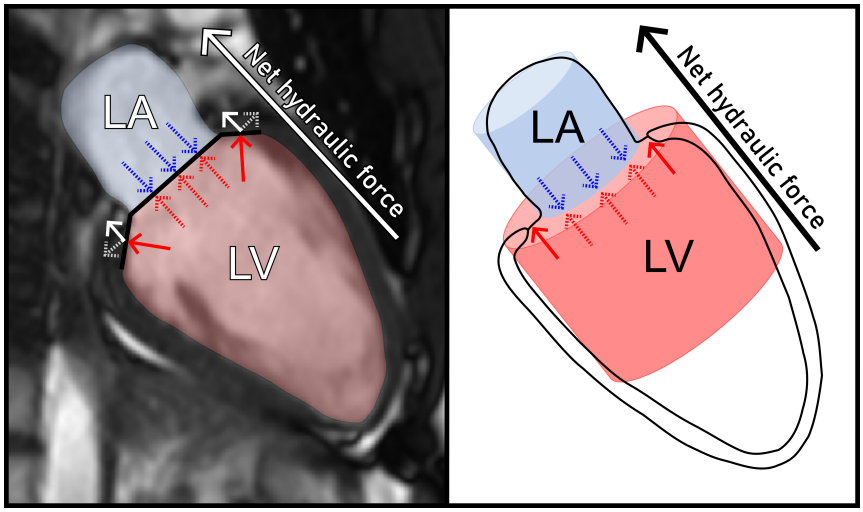

Figure 4.9: Illustrations showcasing net hydraulic force aiding left ventricular filling by pushing the atrioventricular plane toward the base. Left panel: cardiovascular magnetic resonance 2-chamber view of the left atrium (shaded in blue) and ventricle (shaded in red), separated by the atrioventricular plane (black line). Hydraulic force is exerted by the blood on the atrioventricular plane both from the atrium (blue arrows) and the ventricle (red arrows), canceling out where the two chambers overlap (dashed red and blue arrows). The hydraulic force exerted where the chambers do not overlap (solid red arrows) can be divided into radial (dashed white arrow) and longitudinal (white arrow) components of the hydraulic force. The radial component is counteracted by the stiff pericardium, while the longitudinal component contributes to pushing the atrioventricular plane in the basal direction. Right panel: Stylized 2-chamber view with the two chambers represented as two connected cylinders. Here it becomes more apparent that a larger short-axis area leads to a larger hydraulic force, which is proportional to the difference in surface area between the two cylinders. This is the atrioventricular area difference.

4.2.7 Hydraulic Forces and Atrioventricular Area Difference

Studies III and IV introduce the concept of atrioventricular area difference (AVAD). This is a proxy for hydraulic force, a novel mechanic shown to be important for ventricular filling (Figure 4.9). To summarize, a hydraulic force can be described as the pressure a fluid exerts on a given area (force = pressure × area). In the context of the heart, the fluid is blood and the area it exerts on is the endocardium of the ventricle and atrium. The atrioventricular plane, separating the ventricle and atrium, is constantly exerted upon by hydraulic forces. When the mitral valve is open, the pressure difference between the two chambers can be considered negligible. Thus, in diastole, the net hydraulic force affecting the atrioventricular plane is directly proportional to the difference in SAX area between the two chambers — the atrioventricular area difference.

A more intuitive way of conceptualizing AVAD is imagining the atrium and ventricle as two connected cylinders with different diameters (Figure 4.9, right panel). Whichever cylinder is larger in diameter confers the larger force in the direction of the other cylinder. Note that this only shows the net direction of the hydraulic force. Calculating the magnitude of the hydraulic force would require the addition of measuring invasive pressures.

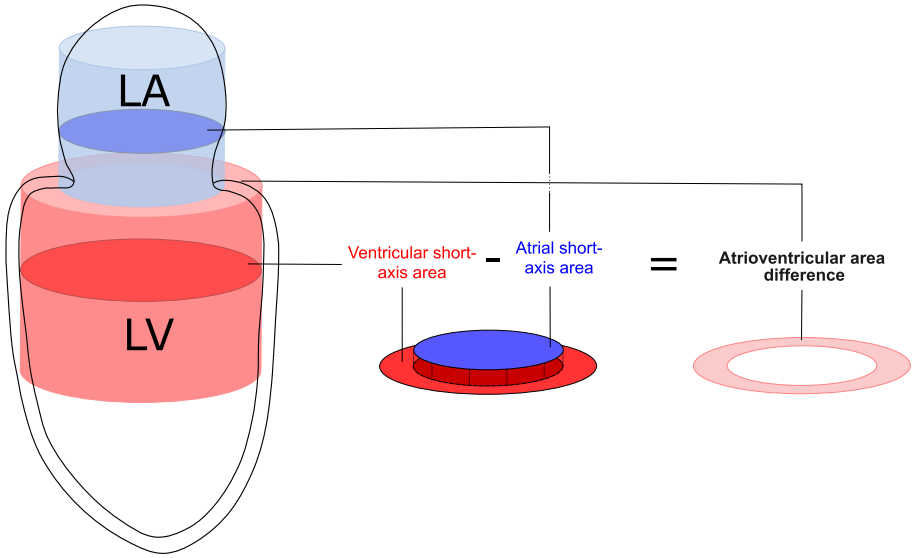

Figure 4.10: Schematic illustration of how the atrioventricular area difference is calculated from ventricular and atrial short-axis areas.

The AVAD was calculated from SAX areas measured by manual contouring of the endocardial borders in CMR SAX images covering both LV and LA using the following equation:

$$\text{AVAD } (\text{cm}^2) = \text{ventricular SAX area } (\text{cm}^2) - \text{atrial SAX area } (\text{cm}^2)$$

Atrioventricular area difference was measured at ED and ES for both Studies III and IV. Additionally for Study IV, complete time-resolved analysis of SAX areas and AVAD was performed in two datasets. In the two time-resolved datasets, a mixture of spline interpolation (used for LV) and manual (used for LA) contouring was used to speed up the process.

4.3 Statistical Analysis and Figures

Software used for statistical analysis were SPSS (versions 26–27; IBM Corp, Armonk, New York, USA), GraphPad Prism (versions 8.4.1–10; GraphPad Software, Boston, Massachusetts, USA) and R using the Tidyverse [177] package ecosystem (version 4.4.3; R Core Team 2025, https://www.r-project.org/).

Normality was assessed using Shapiro-Wilk tests or visually using histograms. Continuous data were presented as mean and standard deviation (SD) or as median and interquartile range [IQR] as appropriate. A p-value of < 0.05 was considered statistically significant in

all studies. Interobserver and intraobserver variability was evaluated using Bland-Altman analysis in all studies [178, 179].

Study I evaluated intergroup differences using Kruskal-Wallis H test with Dunn's post hoc test. Intraobserver and interobserver correlation was tested using Pearson correlation coefficients.

Study II calculated intraclass correlation coefficient (ICC) with 95% confidence intervals using a two-way mixed model to assess the reliability of measurements, and coefficient of variation to assess precision. Bland-Altman analysis was further used to compare differences in measurements between methods, and Pearson or Spearman's rank correlation as appropriate for calculating correlations.

Study III used a two-way repeated measures ANOVA with Bonferroni correction to test for between-group differences and interaction. Within-group differences were tested for by repeated measures ANOVA with Tukey's multiple comparisons. Unpaired Student's t-test was used to compare cardiac parameters between groups.

Study IV used paired t-tests to compare within-group differences going from rest to exercise.

Graphs visualizing data were created using GraphPad Prism. The open-source graphics editor Inkscape (Inkscape.org) was used in creating figures, illustrations and modifying graphs.

I am among those who think that science has great beauty.

— Marie Skłodowska-Curie

5. Results and Comments

This section summarizes and provides an overview of the most important findings from Studies I–IV with some added commentary. The complete results are presented in the respective studies located at the end of this thesis in Part II.

5.1 Study I

Noninvasive Assessment of Left Ventricular Pressure-Volume Relations: Inter- and Intraobserver Variability and Assessment Across Heart Failure Subtypes

This study evaluated a new method for accelerating the workflow of computing PV loops through spline interpolation. This method was then used to assess inter- and intraobserver variability of noninvasive PV loops in healthy controls, participants with subclinical diastolic dysfunction, and three categories of heart failure.

Inter- and intraobserver evaluation

Figure 5.1 summarizes the inter- and intraobserver evaluation when comparing manual LV segmentation and spline interpolation for PV-loop-derived parameters. Bias was low, limits of agreement narrow and correlation high for all parameters. Further, bias was lower and limits of agreement narrower when comparing manual to interpolated measurements compared to the interobserver evaluation.

Pressure-volume Loop Assessment

Pressure-volume loops were successfully computed in all participants using spline interpolation. Comparison of the different PV-loop-derived parameters between groups are presented in Figure 5.2 and Figure 5.3. In general, the largest differences were found between HFrEF and HFmrEF compared to healthy controls, subclinical diastolic dysfunction and HFpEF. No differences were found between healthy controls and subclinical dysfunction or HFpEF.

Summary

The results from this study show spline interpolation to be a reliable method for accelerating time-resolved CMR LV analysis for noninvasive assessment of PV loops, with results comparable to manual segmentation. Parameters derived from PV-loop analysis in heart failure patients and healthy controls were consistent with previous studies using invasive data.

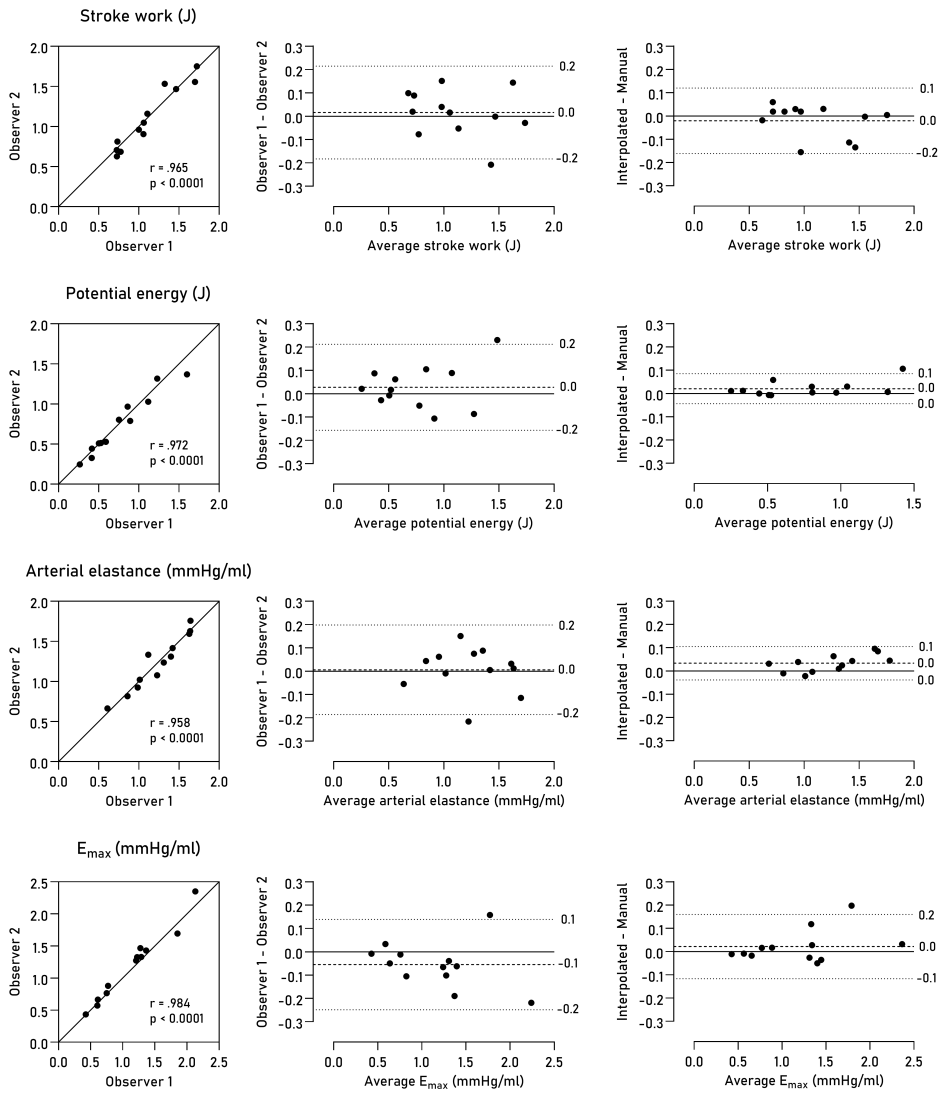

Figure 5.1: Inter- and intraobserver variability in pressure-volume-loop-derived parameters computed from manual and interpolated left ventricular segmentation. In the scatter plots, the solid line is a line of identity. In the Bland-Altman plots (center and right columns), the dashed line denotes the bias and the dotted lines the limits of agreement (defined as bias±1.96 SD).

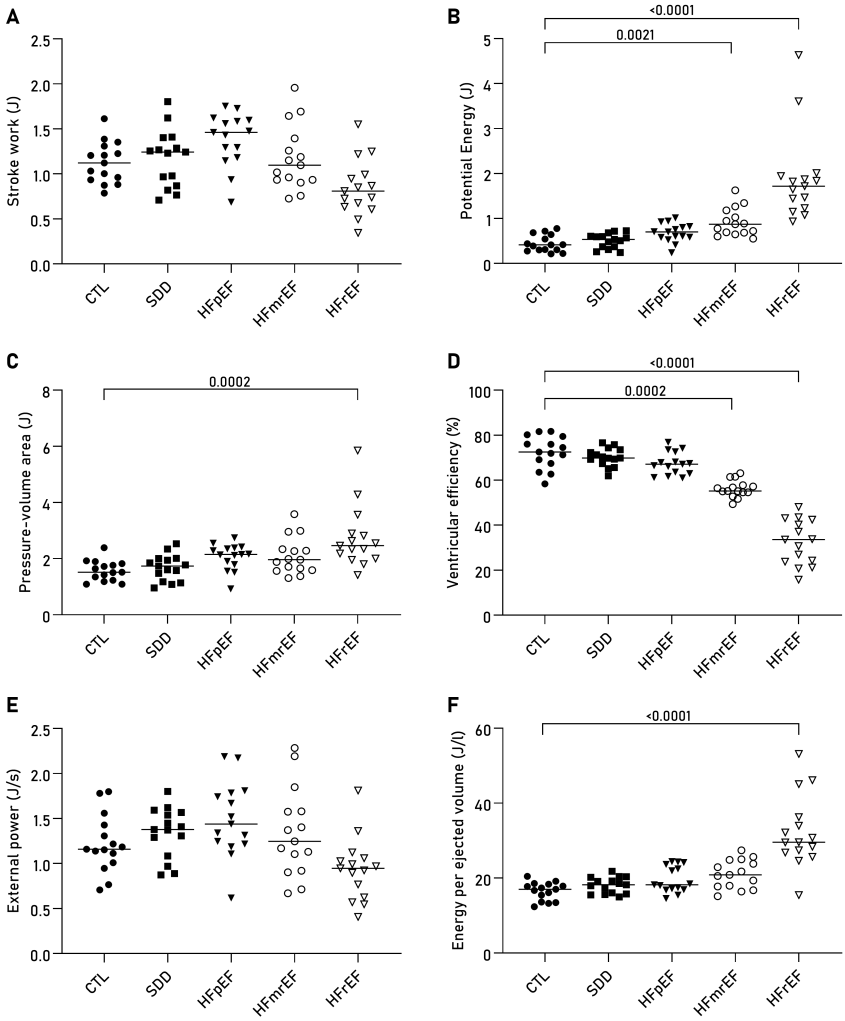

Figure 5.2: Results from pressure-volume-loop-derived parameters related to cardiac energetics and work. CTL = healthy controls; SDD = subclinical diastolic dysfunction; HFpEF = heart failure with preserved ejection fraction; HFmrEF = heart failure with mildly reduced ejection fraction; HFrEF = heart failure with reduced ejection fraction.

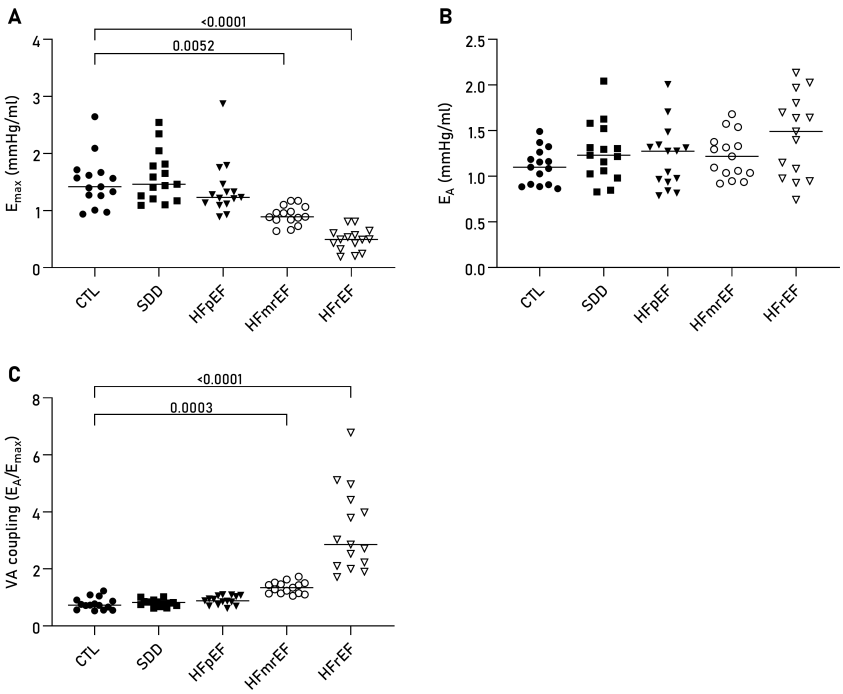

Figure 5.3: Results from pressure-volume-loop-derived parameters related to contractility (E_{max}) and arterial elastance (E_A), and their coupling. CTL = healthy controls; SDD = subclinical diastolic dysfunction; HFpEF = heart failure with preserved ejection fraction; HFmrEF = heart failure with mildly reduced ejection fraction; HFrEF = heart failure with reduced ejection fraction.

5.2 Study II

Validation and quantification of left ventricular function during exercise and free breathing from real-time cardiac magnetic resonance images

In this study, we developed and validated a semi-automatic algorithm for sorting real-time CMR images based on respiratory state, enabling measurement of LV mass and volumes during exercise. The length of CMR image acquisition required for the algorithm to function was also evaluated.

The Respiratory Module and Necessary Acquisition Time

In short, the developed algorithm worked purely on an image basis from real-time, ungated CMR SAX images and allowed the user to place a region of interest over a structure which correlates with breathing (such as the diaphragm). This structure was then tracked over in all time-frames for the selected slice, providing a curve over the respiratory motion.

This algorithm was implemented as the "respiratory module" in the software Segment (Medviso, Lund, Sweden) [172]. The resulting module allowed for semi-automatic respiratory sorting with manual selection of ED and ES. An overview of the algorithm in action is presented previously under methods.

The module successfully sorted images in images with acquisition times of 34, 17 and 8 seconds (1000, 500, and 250 time-frames respectively) per SAX slice. This allowed for the construction of new SAX image stacks consisting of two time-frames, ED and ES, in a fixed respiratory state. The algorithm was unsuccessful in slices with 4 seconds (100 time-frames) acquisition time.

Agreement of Real-time Images Versus ECG-gated Images at Rest in Healthy Volunteers and Patients

The bias for LVM, EDV and ESV for real-time images at rest at end expiration compared to ECG-gated images measured in both healthy volunteers and patients at rest was 0±5 g, 3±15 ml, and -3±12 ml, respectively (Figure 5.4).

Agreement of LV mass from ECG-gated images at rest compared to RT images at end expiration and inspiration during exercise Bias for LVM from real-time images during exercise compared to ECG-gated images at rest in healthy volunteers was for end expiration 0±7 g and end inspiration -1±8 g (Figure 5.5).

Summary

The results from this study demonstrated the utility of a semi-automatic algorithm for respiratory sorting of real-time exercise CMR images. The method was validated for LV mass and volume measurements against conventional ECG-gated CMR imaging.

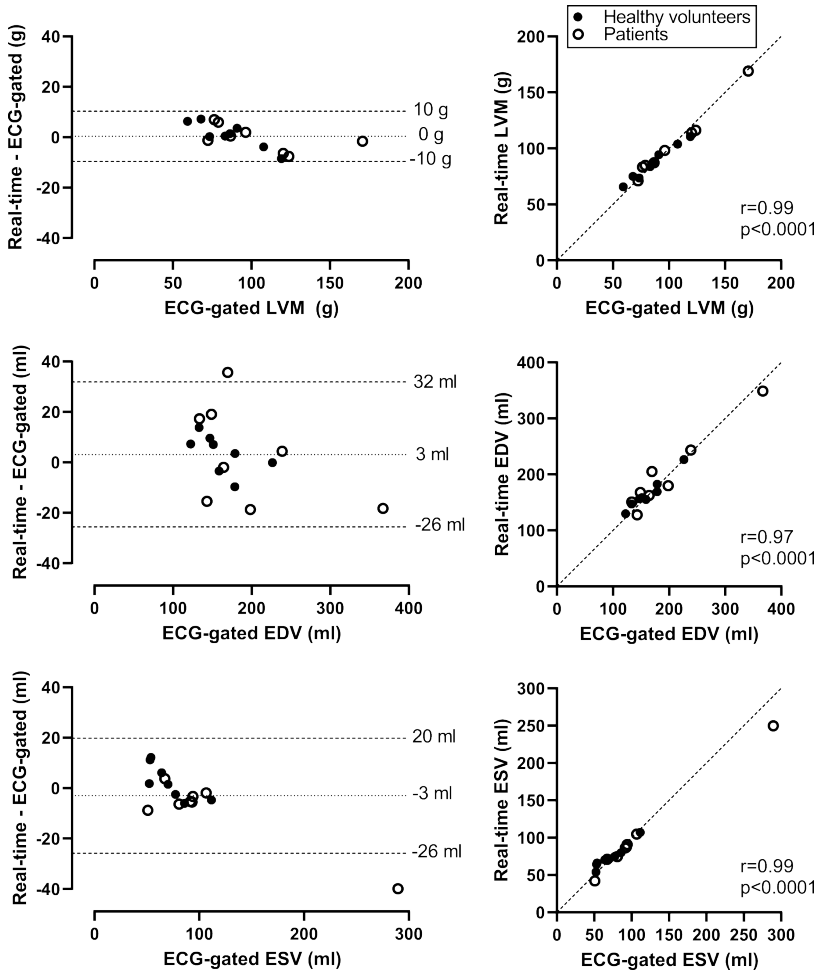

Figure 5.4: Bland-Altman plots showing the bias and limits of agreement when comparing left ventricular mass (LVM), end-diastolic volume (EDV) and end-systolic volume (ESV) between ungated real-time CMR images and ECG-gated CMR images, both acquired at rest.

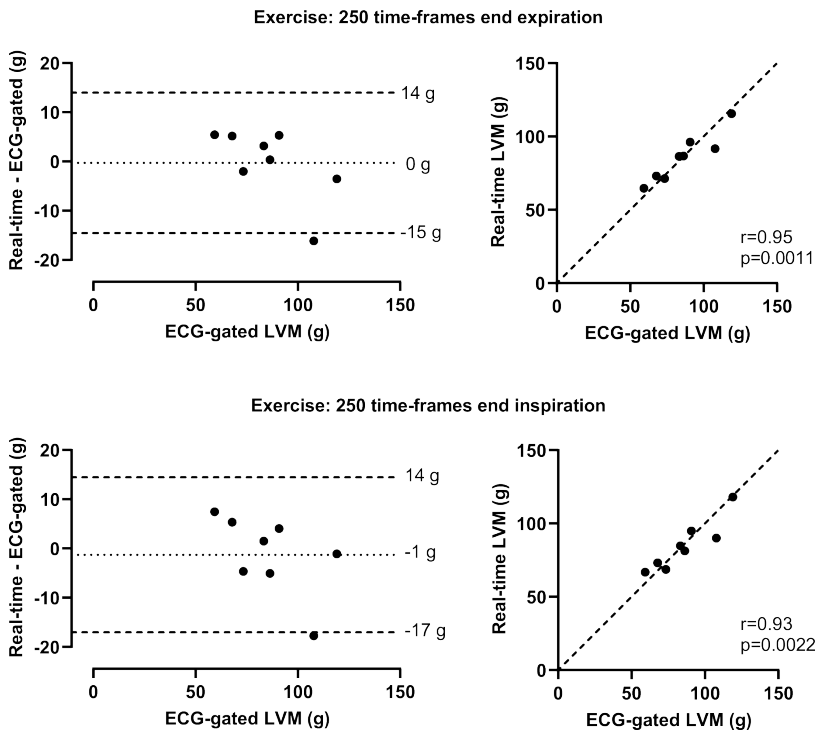

Figure 5.5: Bland-Altman plots showing the bias and limits of agreement when comparing left ventricular mass (LVM) measured from ungated real-time CMR images during exercise and from ECG-gated CMR images at rest.

5.3 Study III

Exercise cardiovascular magnetic resonance shows improved diastolic filling by atrioventricular area difference in athletes and controls

This study used exercise CMR to measure AVAD at ED and ES at rest and during exercise in sedentary controls and athletes. Exercise was performed at moderate and vigorous levels.

Atrioventricular Area Difference at ED and ES in Sedentary Controls and Athletes

At ED, AVAD increased when going from rest to moderate exercise for sedentary controls and remained unchanged when going from moderate to vigorous exercise. Similarly, AVAD at ED also increased for athletes when going from rest to moderate exercise, but not from moderate to vigorous exercise. AVAD at ES decreased when going from rest to moderate exercise but did not differ from moderate to vigorous exercise in sedentary controls. AVAD at ES for athletes did not differ between rest, moderate, or vigorous exercise. AVAD did not differ between the groups, except for at ES at rest, where athletes had significantly lower AVAD than controls.

Cardiac parameters and SAX areas, including AVAD values, are presented in Table 5.1 and Table 5.2, respectively.

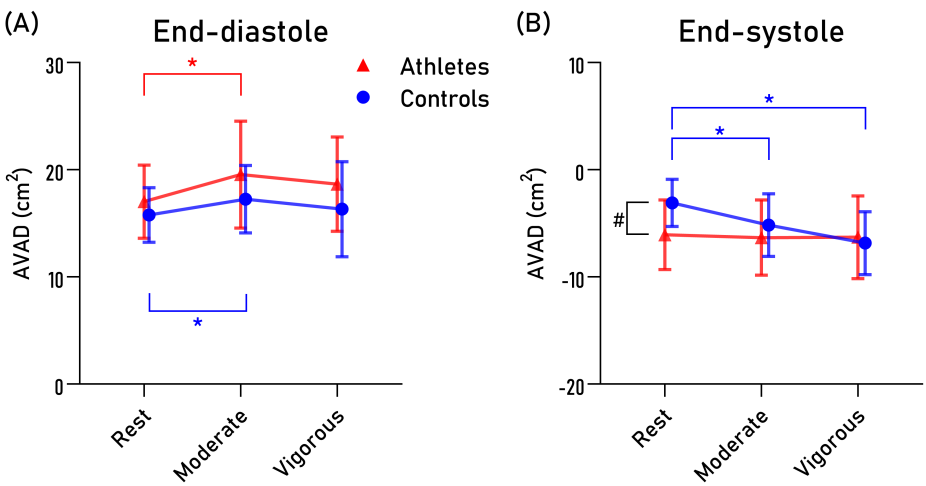

Figure 5.6: Atrioventricular area difference (AVAD) measured at rest and during moderate and vigorous exercise in athletes and sedentary controls at end-diastole and end-systole.

Table 5.1: Cardiac volumes and cardiac output at rest, moderate, and vigorous exercise in sedentary controls and athletes.

	Rest	Moderate exercise	Vigorous exercise
Sedentary controls (n=13)			
Heart rate (beats/min)	60±6	122±12	151±10
Cardiac output (l/min)	6.0±0.9	13.2±2.5	15.3±4.3
LV EDV (ml)	170±31	176±34	155±32
LV ESV (ml)	69±19	67±19	55±14
LA volume at ventricular ES (ml)	76±15	92±20	85±19
LA volume at ventricular ED (ml)	30±7	31±9	29±11
Athletes (n=20)			
Heart rate (beats/min)	50±7	128±14	152±17
Cardiac output (l/min)	6.3±1.3	17.6±3.6	19.9±2.7
LV EDV (ml)	215±39	215±37	199±30
LV ESV (ml)	88±21	79±21	67±19
LA volume at ventricular ES (ml)	102±21	111±27	102±24
LA volume at ventricular ED (ml)	46±13	43±17	36±13

Values are means ± SD. LV = left ventricular; EDV = end-diastolic volume; ESV = end-systolic volume; LA = left atrial; ES = end-systole; ED = end-diastole

Table 5.2: Short-axis areas and atrioventricular area difference.

	Rest	Moderate exercise	Vigorous exercise
Sedentary controls (n=13)			
LV short-axis area, ventricular ED (cm^2)	24.9±3.5	26.5±3.8*	24.6±3.8†
LA short-axis area, ventricular ED (cm^2)	9.1±1.6	9.2±2.3	8.2±2.8
AVAD, ventricular ED (cm^2)	15.8±2.6	17.3±3.1*	16.3±4.4
LV short-axis area, ventricular ES (cm^2)	13.4±2.4	13.3±2.4	11.1±2.1#†
LA short-axis area, ventricular ES (cm^2)	16.5±2.7	18.5±3.2*	17.9±2.6#
AVAD, ventricular ES (cm^2)	−3.1 ± 2.2	−5.2 ± 2.9*	−6.8 ± 2.9#
Athletes (n=20)			
LV short-axis area, ventricular ED (cm^2)	30.0±4.4	31.2±4.8*	29.5±4.4†
LA short-axis area, ventricular ED (cm^2)	13.0±2.9	11.7±3.8	10.8±3.2#
AVAD, ventricular ED (cm^2)	17.0±3.4	19.6±5.0*	18.7±4.4
LV short-axis area, ventricular ES (cm^2)	15.6±2.9	15.8±2.9	14.7±4.0
LA short-axis area, ventricular ES (cm^2)	21.7±3.6	22.1±4.1	21.0±4.1
AVAD, ventricular ES (cm^2)	−6.0 ± 3.2	−6.3 ± 3.5	−6.3 ± 3.9

Values are means ± SD. LV = left ventricular; ED = end-diastole; LA = left atrial; AVAD = atrioventricular area difference; ES = end-systole. * $p<0.05$ for rest vs moderate exercise, # $p<0.05$ for rest vs vigorous exercise, † $p<0.05$ for moderate vs vigorous exercise.

Intraobserver and Interobserver Variability

Intraobserver variability was excellent with low bias for AVAD both at ED (-0.3±1.1 cm^2) and at ES (0.1±0.7 cm^2). Interobserver variability was also excellent with low bias for AVAD at ED (0.2±0.7 cm^2) and at ES (-0.4±1.7 cm^2).

Summary

Both sedentary controls and athletes saw an initial increase in AVAD measured at ED during exercise. This increase indicates that the net hydraulic force aids LV diastolic filling to a greater extent during moderate exercise compared to rest, irrespective of training status.

5.4 Study IV

Atrioventricular area difference assessed by exercise cardiovascular magnetic resonance shows impaired diastolic filling in heart failure patients

This study built upon Study III by measuring AVAD at ED and ES, both at rest and during exercise, in heart failure patients and comparing these with the sedentary controls (here referred to as healthy volunteers) from Study III. Exercise was performed at a moderate intensity. Additionally, SAX areas were measured throughout the cardiac cycle in two selected cases to illustrate different patterns of how AVAD shifts from inhibiting to augmenting ventricular filling during different parts of diastole.

Table 5.3: Cardiac parameters, short-axis areas and AVAD for heart failure patients at rest and during exercise.

Heart failure patients (n=22)	Rest	Exercise	p-value
Heart rate (beats/min)	67 ± 11	102 ± 9	< 0.001
LVM (g)	92 ± 24	92 ± 24	ns
LV EDV (ml)	191 ± 43	219 ± 55	< 0.001
LV ESV (ml)	106 ± 32	113 ± 40	0.034
LV SV (ml)	85 ± 19	107 ± 24	< 0.001
LV EF (%)	45 ± 9	50 ± 9	< 0.001
Cardiac output (l/min)	5.55 ± 0.91	10.80 ± 2.08	< 0.001
LA volume at ventricular ED (ml)	45 ± 14	64 ± 21	< 0.001
LA volume at ventricular ES (ml)	91 ± 20	124 ± 26	< 0.001
LV short-axis area, ventricular ED (cm^2)	29 ± 6	32 ± 7	< 0.001
LA short-axis area, ventricular ED (cm^2)	13 ± 3	17 ± 4	< 0.001
AVAD, ventricular ED (cm^2)	17 ± 5	15 ± 6	0.006
LV short-axis area, ventricular ES (cm^2)	19 ± 5	19 ± 6	ns
LA short-axis area, ventricular ES (cm^2)	21 ± 4	27 ± 5	< 0.001
AVAD, ventricular ES (cm^2)	-2 ± 5	-8 ± 5	< 0.001

Values are means $\pm$ SD. LV = left ventricular; LVM = left ventricular mass; EDV = end-diastolic volume; ESV = end-systolic volume; LA = left atrial; ES = end-systole; ED = end-diastole; AVAD = atrioventricular area difference.

Atrioventricular Area Difference at ED and ES in Heart Failure Patients and Healthy Volunteers

For heart failure patients, both AVAD at ED and ES decreased during exercise (Figure 5.7). In contrast, AVAD at ED increased for the healthy volunteers going from rest to exercise, although AVAD at ES decreased.

Values regarding cardiac parameters, AVAD and SAX areas for the heart failure patients are presented in Table 5.3. Values for the healthy volunteers are presented under Study III (see "rest" and "moderate" values for sedentary controls in Tables 5.1 and 5.2).

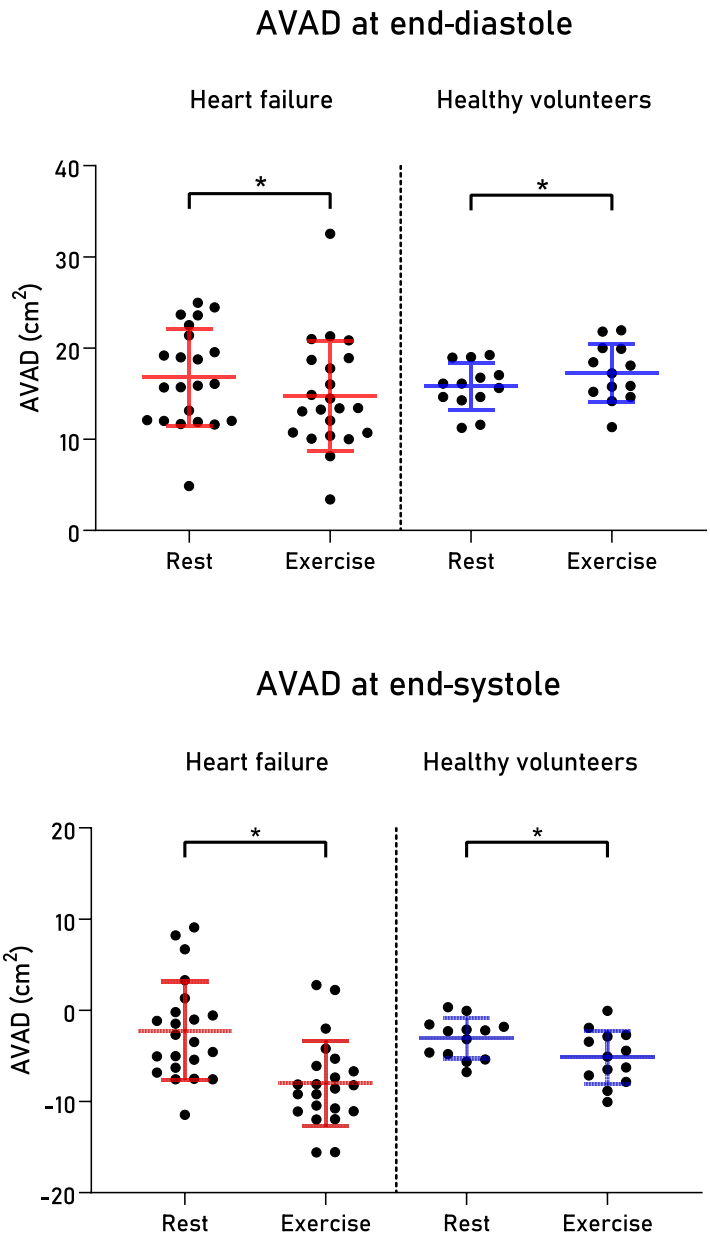

Figure 5.7: Atrioventricular area difference measured at rest and during exercise in heart failure patients and healthy volunteers at end-diastole and end-systole.

Intraobserver and Interobserver Variability

Intraobserver variability was excellent with low bias for AVAD at both ED (0.2 ± 0.9 cm^2) and ES (0.1 ± 0.6 cm^2), and interobserver variability was also excellent with low bias for AVAD at ED (0.0 ± 1.6 cm^2) and ES (1.3 ± 1.7 cm^2).

Short-axis Areas Over the Cardiac Cycle

Figure 5.8 illustrates the LA and LV SAX areas, plotted over the cardiac cycle at rest and during exercise, in two select cases. These were included to showcase the different patterns of AVAD in one patient with suspected systolic dysfunction and one with diastolic dysfunction.

Summary

The main finding of this study was that AVAD at ED decreased during exercise in heart failure, whereas it increased in the healthy individuals. This suggests that the contribution of hydraulic force to ventricular filling decreased during exercise in heart failure.

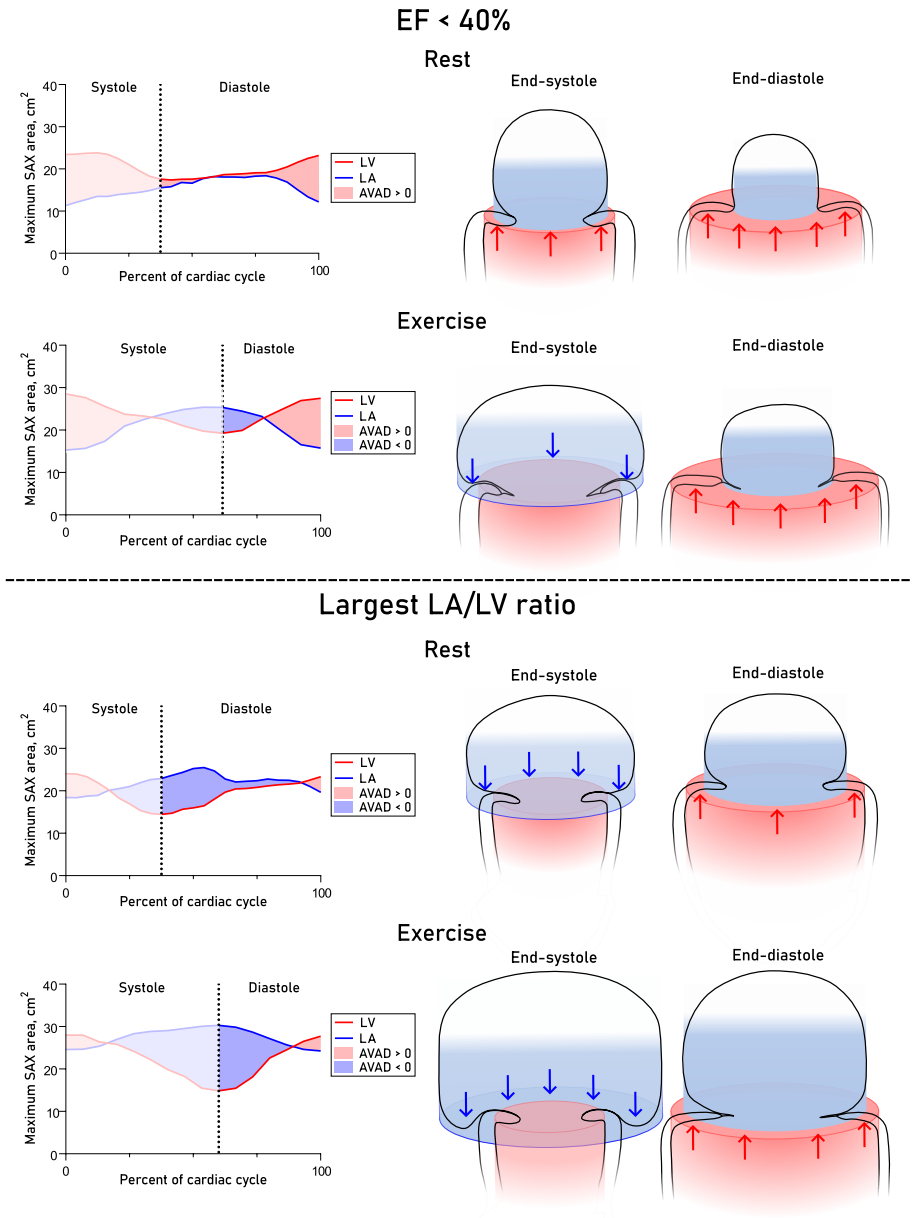

Figure 5.8: Maximum left ventricular (LV, red lines) and atrial (LA, blue lines) short-axis (SAX) areas and the resulting AVAD (shaded red > 0, shaded blue < 0) across the cardiac cycle in two selected cases from the heart failure group. Note that AVAD is only proportional to the hydraulic forces during diastole, when the mitral valve is open. The top half of the figure shows a patient with reduced ejection fraction (EF < 40%). At rest, AVAD is positive from the start of diastole, indicating a net positive effect of hydraulic force contributing to ventricular filling throughout diastole. During exercise, however, AVAD becomes negative at the onset of diastole, suggesting that hydraulic force does not aid ventricular filling until roughly halfway through diastole. The bottom half of the figure shows a patient with the largest atrial-to-ventricular volume ratio, suggestive of elevated atrial pressure and diastolic dysfunction. In this case, AVAD remains negative until atrial contraction at the end of diastole. This indicates a net negative effect of hydraulic force on ventricular filling both at rest and during exercise.

The purpose of a storyteller is not to tell you how to think,
but to give you questions to think upon.

— Brandon Sanderson

6. Discussion

The works presented in this thesis set out to explore novel aspects of cardiac mechanics by using and further developing advanced CMR methods, both at rest and during ongoing exercise. This section discusses the most important findings from the studies and places them in a broader context.

6.1 Pressure-volume Loop Analysis and Spline Interpolation

The first study in this thesis was primarily methodological, focusing on assessing the robustness and reliability of a novel method of computing noninvasive PV loops. To this end, it presented the first experience with noninvasive PV-loop analysis across healthy controls, participants with subclinical diastolic dysfunction, and three different heart failure subtypes. Furthermore, inter- and intraobserver comparisons showed low bias and narrow limits of agreement for all hemodynamic parameters, including those derived from LV segmentation based on spline interpolation.

The PV-loop-derived parameters in heart failure patients were largely consistent with previous studies using invasive data [23, 180–182]. Although diverging results might have been more striking, the similarities in results between methods strengthen confidence in the noninvasive PV-loop approach.

Equally important was evaluating spline interpolation to generate time-resolved LV segmentation from only a few time-frames. Figure 6.1 displays the LV volume curves from two manual segmentations and one interpolation of the same dataset, and the resulting PV-loops. In this case, no time-frame in diastasis was used for the interpolation. Note how visually similar the blue and black loops are, which is reflected in the derived hemodynamic parameters presented earlier.

Thus, using only ED and ES (and diastasis if needed), time-resolved LV segmentation can be derived for noninvasive PV-loop analysis with high agreement to fully manual approaches. Because ED and ES contouring is already routine in clinical CMR, this workflow brings CMR-derived noninvasive PV loops closer to clinical implementation.

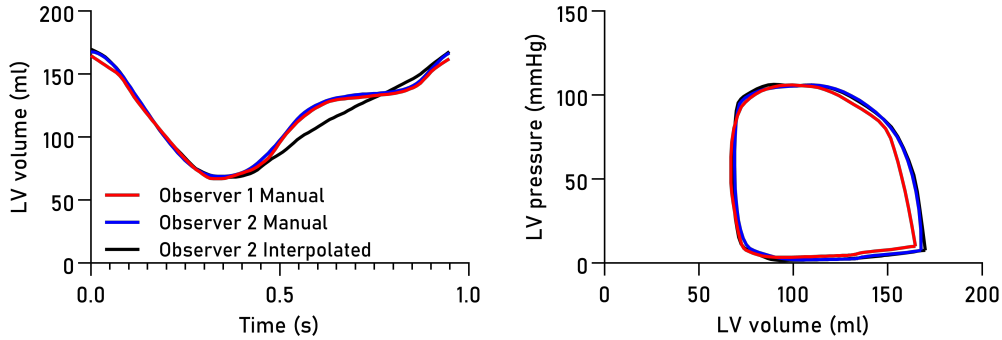

Figure 6.1: Three different left ventricular (LV) segmentations, two manual and one utilizing spline interpolation, and the resulting pressure-volume loops.

6.2 Validation of Exercise CMR for LV Volumes and Mass

Continuing the methodological theme, the second study of this thesis developed and validated a new semi-automatic algorithm for respiratory sorting of non-ECG-gated, free-breathing, real-time CMR to obtain accurate LV volumes and mass at rest and during exercise.

While this was not the first method to extract respiratory curves from MR images, the novelty of our approach lies in its single, integrated package [183–185]: (a) respiratory-curve extraction from image data alone, (b) construction of stacks at specified cardiac and respiratory phases, and (c) subsequent analysis. Furthermore, as noted earlier, the module has recently been extended to support full cine imaging, not just ED and ES [174]. This enables time-resolved LV segmentation during exercise, which was utilized in Study IV.

Exercise CMR is a growing field, with an increasing number of centers implementing the method [163]. Several studies have demonstrated good agreement between exercise real-time images and ECG-gated cine when using a respiratory plethysmograph to maintain a consistent respiratory phase during acquisition [164, 186]. Others have used brief exercise cessation, breath-hold, or both to obtain high-quality gated images [165, 187–190]. While convenient, these approaches may not fully reflect the physiology of ongoing exercise.

In contrast, our method requires no additional physiological signals and works during free breathing, relying only on a vendor product bSSFP real-time sequence (Siemens, in our case). We hope this lowers the barrier for researchers and clinicians to adopt exercise CMR as a practical and accessible method.

6.3 Hydraulic Forces and the Atrioventricular Area Difference

The role of hydraulic forces in LV diastolic function is a relatively recent concept [38]. Most studies to date have characterized this mechanism across different cohorts using CMR. These include heart failure subtypes, patients before and after repaired tetralogy of Fallot, before and after atrial septal defect closure, and post-heart transplantation [40–42, 191].

These studies have helped establish that hydraulic forces can either augment or impede ventricular filling depending on the geometrical relationship between the atrium and ventricle, as measured by AVAD. However, all were conducted at rest. Physical exercise alters loading conditions, and consequently atrial and ventricular volumes, meaning that exercise may potentially modify AVAD [59, 164, 186].

Accordingly, Studies III and IV first established the feasibility of, and then assessed, AVAD measured by CMR as a surrogate for hydraulic forces during exercise in sedentary controls, athletes, and heart failure patients. The primary results, AVAD at ED, from both studies are summarized in Figure 6.2.

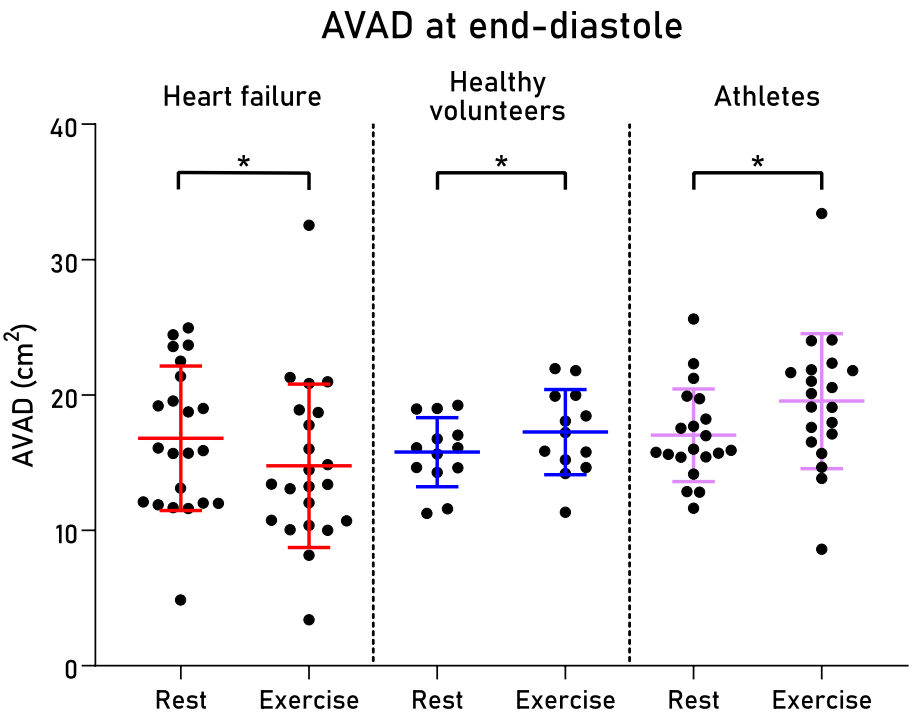

Figure 6.2: Atrioventricular area difference at end-diastole at rest and exercise in heart failure, healthy controls and athletes.

Study III showed that AVAD at ED increases during exercise, both in athletes and sedentary controls, indicating this to be a mechanism augmenting ventricular diastolic filling during exercise. Study IV, in contrast, found that heart failure patients show a decrease in AVAD at

ED during exercise, suggesting a reduced contribution from hydraulic forces to ventricular filling.

Together, these findings support a role for hydraulic forces in both the increased diastolic function of athletes during exercise, and the diminished exercise tolerance of heart failure patients. Further, the gradual improvement in AVAD from heart failure patients to healthy volunteers to athletes, raises the hypothesis that favorable hydraulic forces for diastolic filling may be trainable.

Finally, it bears repeating that AVAD and hydraulic forces are not synonymous. Other studies, using echocardiography or CMR with feature tracking on long-axis images, also report measuring LV hydraulic force [192, 193]. These measures likely capture different aspects of the hydraulic forces, and preliminary results from Clausen et al. suggest that results may not be directly comparable across modalities [194]. To avoid confusion, it may be safer to name the specific measurement and modality (such as AVAD by CMR) when discussing these mechanisms.

We look up at the same stars and see such different things.

— George R.R. Martin

7. Conclusions

The overall aim of this thesis was to utilize CMR to assess novel aspects of cardiac mechanics both at rest and during exercise in the healthy, the trained, and the failing heart.

First, we validated a method that greatly accelerates time-resolved LV segmentation for use in computing noninvasive, CMR-derived PV loops. This method was then used to assess PV-loop-derived parameters across healthy volunteers, participants with subclinical diastolic dysfunction, and heart failure patients. Second, we developed and validated an algorithm and workflow that allow analysis of free-breathing, non-ECG-gated, real-time CMR images acquired during exercise.

Using these tools, AVAD, a surrogate for hydraulic forces, was assessed during exercise for the first time in sedentary controls, athletes, and heart failure patients. Results indicate that hydraulic forces augment diastolic function during exercise in the healthy and trained heart, whereas it appears reduced in heart failure patients compared with rest.

Collectively, these findings further our understanding of the role of diastolic hydraulic forces during exercise and advance CMR-derived, noninvasive PV-loop analysis and exercise CMR toward clinical adoption and broader research application.

The specific conclusions for each study in the thesis were:

Study I: This study was the first to conduct noninvasive, CMR-derived PV-loop analysis across healthy controls, participants with subclinical diastolic dysfunction, and heart failure patients with preserved or impaired systolic function. Bias was low, and inter- and intraobserver limits of agreement were narrow for all hemodynamic parameters. A spline-based interpolation applied to clinically standard manual LV contours greatly accelerated PV-loop analysis, helping bridge clinical and research workflows.

Study II: This study presented a semi-automatic algorithm with retrospective respiratory sorting for reconstructing image stacks to assess LV mass, volumes, and function from free-breathing, non-ECG-gated real-time CMR at rest and during exercise. The algorithm requires no ECG or additional physiological signals during acquisition. It was successful

in all cases when using an image acquisition of 17 seconds per slice, with a total post-processing time typically 20–40 minutes. Validation showed good agreement and high correlation between measurements at rest and during exercise.

Study III: AVAD at ED increased during exercise in both sedentary controls and athletes. This is consistent with a net hydraulic force that augments diastolic filling during moderate exercise compared with rest, regardless of training status, providing new insight into how diastolic function increases with exercise. AVAD at ES was negative at rest and during exercise in both groups. While this indicates that hydraulic forces may impede ventricular filling at the very start of diastole, this effect is likely counteracted by elastic recoil in the healthy heart.

Study IV: In heart failure patients, AVAD at ED decreased during exercise, suggesting reduced contribution of hydraulic forces to diastolic filling compared with rest. In contrast, healthy volunteers showed increased AVAD and thus an augmented contribution. AVAD at ES decreased during exercise more in heart failure patients than in healthy volunteers, further diminishing the potential for hydraulic forces to assist early diastole. These results provide mechanistic insight that may partly explain exercise intolerance in heart failure.

The future can ever promise but one thing and one thing only: surprises.

— Steven Erikson

8. Future Perspectives

While this thesis advances select areas of CMR, much remains to be done. For noninvasive, PV-loop-derived parameters, there is still a need for studies demonstrating their utility in diagnosis, prognosis, and as surrogate endpoints in clinical trials [195]. However, the method was first described in 2019, so a large evidence base is not yet expected.

Notably, one study has shown that ventricular efficiency derived from noninvasive PV loops is associated with major adverse cardiac events in HFrEF [196]. Beyond HFrEF, another study demonstrated promise in Duchenne muscular dystrophy associated cardiomyopathy, where PV-loop-derived parameters were proposed as a longitudinal diagnostic endpoint [197]. These studies are encouraging, and more studies will hopefully further establish the clinical utility of noninvasive PV-loop analysis.

Exercise CMR has substantial potential for both clinical and research applications. For example, stress imaging modalities are core tools for evaluating suspected ischemia and for prognostic assessment [198, 199]. Here, stress CMR stands out thanks to advances enabling quantitative perfusion, previously largely exclusive to radionuclide techniques [200].

In clinical practice, stress CMR is typically performed with pharmacological stressors [160]. While the feasibility of exercise CMR perfusion has been demonstrated in a few studies, these used post-exercise imaging with first-pass perfusion [201–204]. Thus, absolute quantitative perfusion, or any perfusion, during ongoing exercise remains, to our knowledge, largely unexplored. Further development of exercise CMR could enable stress testing in patients who do not tolerate pharmacological stressors and, by reflecting the physiological state of ongoing exercise, may better expose pathology.

Looking beyond perfusion, exercise CMR for prognosis, diagnosis and functional assessment in studies and trials is gaining traction [202, 205–207]. For example, one study highlights exercise CMR as a noninvasive diagnostic alternative to LV catheterization for identifying HFpEF [205].

It would also be valuable to combine the methods of this thesis, using exercise CMR to compute noninvasive PV loops during exercise. This has been explored in athletes with immediate post-exercise scanning, but not yet in patients [189]. From a physiological

standpoint, applying PV loops during ongoing exercise across heart failure subtypes could provide new hemodynamic insights into the mechanisms underlying exercise intolerance.

Overall, it is encouraging to see continued progress in both the use and development of exercise CMR. As noted earlier, one desired outcome of this thesis is to lower the barrier to entry so more centers can adopt this modality.

The future of AVAD and diastolic hydraulic forces is promising and exciting. As noted in the discussion, there is a need to reach consensus on definitions and reporting, clarifying what is meant by "hydraulic forces" across modalities and measurement methods to avoid confusion and improve comparability between studies.

Similar to noninvasive PV-loop analysis, hydraulic forces are a recently described mechanism, so current studies are understandably limited in scope and largely descriptive or exploratory. Elevating hydraulic forces and AVAD from physiological mechanisms to clinically useful parameters will require studies that define their role across additional contexts, followed by larger trials testing diagnostic and prognostic utility.

Finally, building on Studies III and IV, it would be valuable to test the hypothesis that favorable hydraulic forces are trainable, for example, through exercise interventions, and to assess whether training-induced changes in AVAD during exercise relate to improvements in exercise tolerance in heart failure.

It is good to have an end to journey toward;
but it is the journey that matters, in the end.

— Ursula K. Le Guin

Acknowledgments

First, thank you, and congratulations, on having made it to the end of my thesis summary (or at least for opening the book to this chapter). It's impossible to list everyone who, in one way or another, has contributed to this thesis being written, but I'll do my best to mention at least a few. If your name is missing, please blame the weeks, or rather, months, of sleep deprivation preceding the writing of this final chapter.

Katarina and Håkan, thank you for supervising me through this endeavor — Katarina, for your guidance, understanding, and the mutual growth this journey has entailed; and Håkan, for being the bedrock of this group, an endless source of reflective thought, and for creating the unique culture that is the Lund Cardiac MR Group.

Thank you, Henrik, Erik, Anthony A, Ellen, Einar, Johannes, Barbro, and Ashwin, for your leadership and subject expertise, and for tirelessly maintaining the open and welcoming work environment I've come to take for granted. Tony, Tina, Jane, Karin L, and the entire Medviso team — thank you for always helping out with a smile, no matter the time or place, whether the issue was technical, organizational, or of any other kind. Shahnaz, Mariam, Per, Fredrik, Robert, David, Pia, Alessandro, and Mattias — thank you for thoughtful discussions, fruitful collaborations, and for contributing to such a great work environment.

I would also like to thank my past and present fellow PhD students and research colleagues — Elsa, Kristian, Martin, Tania, Theodor, Marjolein, Anna Sz, Julius, Romeissa, Mathias, Fanny, Karin P, Petter, Jonas, Anthony L, Jonathan B, and Daniel — for sharing my journey, and for letting me share yours, into research, including tears of both frustration and happiness. Björn, thank you for our collaborations, for teaching me the ways of exercise CMR, and for our enjoyable discussions on physiology. Axel, for taking up the exercise CMR mantle, for your enthusiasm for learning, and for simply being fun to work with. Anders, for always being willing to help out, regardless of the time you actually have.

Thank you, Anna S and Annmarie, for your tireless work — both behind the scenes and hands-on — for our great teamwork, and for being able to discuss everything between heaven and earth. Ann-Helen, Johanna, Charlotte, Reza, and all other clinical colleagues at the Department of Physiology — thank you for making it possible to conduct the research

we do, all while making the difficult seem easy. A special thanks to Axel, Tania, Sam, and Susanna for helping out with the thesis summary.

Thank you to all my friends and family, both near and far, offline and online, for cheering me on and helping me stay sane after all these years. Thank you, mamma and pappa, for your unconditional love and support. Thank you, Henrietta and Philip (and little Tyra), for always being there and for all the fun we have. Finally, thank you, Hanna, for your patience, love, and understanding throughout.

...but for my own part, if a book is well written, I always find it too short.

— Jane Austen

Bibliography

[1] A. M. Metwaly, M. M. Ghoneim, I. H. Eissa, I. A. Elsehemy, A. E. Mostafa, M. M. Hegazy, W. M. Afifi, and D. Dou. Traditional ancient egyptian medicine: A review. *Saudi J Biol Sci*, 28(10):5823–5832, 2021.

[2] F. Zampieri, G. Thiene, and A. Zanatta. Cardiocentrism in ancient medicines. *Int J Cardiol Heart Vasc*, 48:101261, 2023.

[3] M. Loukas, P. Youssef, J. Gielecki, J. Walocha, K. Natsis, and R. S. Tubbs. History of cardiac anatomy: A comprehensive review from the egyptians to today. *Clinical Anatomy*, 29(3):270–284, 2016.

[4] M. M. Shoja, R. S. Tubbs, M. Loukas, and M. R. Ardalan. The aristotelian account of "heart and veins". *International Journal of Cardiology*, 125(3):304–310, 2008.

[5] W. C. Aird. Discovery of the cardiovascular system: from galen to william harvey. *Journal of Thrombosis and Haemostasis*, 9:118–129, 2011.

[6] S. Standring. A brief history of topographical anatomy. *J Anat*, 229(1):32–62, 2016.

[7] J. B. West. Ibn al-nafis, the pulmonary circulation, and the islamic golden age. *J Appl Physiol (1985)*, 105(6):1877–80, 2008.

[8] D. Ribatti. William harvey and the discovery of the circulation of the blood. *J Angiogenes Res*, 1:3, 2009.

[9] J. B. West. Marcello malpighi and the discovery of the pulmonary capillaries and alveoli. *American Journal of Physiology-Lung Cellular and Molecular Physiology*, 304 (6):L383–L390, 2013.

[10] E. A. Tansey, L. E. A. Montgomery, J. G. Quinn, S. M. Roe, and C. D. Johnson. Understanding basic vein physiology and venous blood pressure through simple physical assessments. *Advances in Physiology Education*, 43(3):423–429, 2019.

[11] J. Sanz, D. Sánchez-Quintana, E. Bossone, H. J. Bogaard, and R. Naeije. Anatomy, function, and dysfunction of the right ventricle: Jacc state-of-the-art review. *J Am Coll Cardiol*, 73(12):1463–1482, 2019.

[12] J. R. Mitchell and J. J. Wang. Expanding application of the wiggers diagram to teach cardiovascular physiology. *Adv Physiol Educ*, 38(2):170–5, 2014.

[13] C. J. Wiggers. *Modern aspects of the circulation in health and disease*. Lea & Febiger, 1923.

[14] J. E. Hall. *Guyton and Hall Textbook of Medical Physiology*. ClinicalKey Student Foundation Medicine English Language Complete. Elsevier Health Sciences, 2025. ISBN 9780443111013 9780443113499.

[15] D. G. Allen and J. C. Kentish. The cellular basis of the length-tension relation in cardiac muscle. *J Mol Cell Cardiol*, 17(9):821–40, 1985.

[16] O. Frank. *Zur Dynamik des Herzmuskels*. Druck v. R. Oldenbourg, 1895.

[17] E. H. Starling. *The Linacre lecture on the law of the heart*. Longmans, Green, & Company, 1918.

[18] K. Sagawa, R. K. Lie, and J. Schaefer. Translation of otto frank's paper" die grundform des arteriellen pulses" zeitschrift für biologie 37: 483-526 (1899). *Journal of molecular and cellular cardiology*, 22(3):253–254, 1990.

[19] H. Suga. Total mechanical energy of a ventricle model and cardiac oxygen consumption. *American Journal of Physiology-Heart and Circulatory Physiology*, 236(3): H498–H505, 1979.

[20] H. Suga. Ventricular energetics. *Physiol Rev*, 70(2):247–77, 1990.

[21] K. Sunagawa, W. L. Maughan, D. Burkhoff, and K. Sagawa. Left ventricular interaction with arterial load studied in isolated canine ventricle. *American Journal of Physiology-Heart and Circulatory Physiology*, 245(5):H773–H780, 1983.

[22] J. Baan, E. T. van der Velde, H. G. de Bruin, G. J. Smeenk, J. Koops, A. D. van Dijk, D. Temmerman, J. Senden, and B. Buis. Continuous measurement of left ventricular volume in animals and humans by conductance catheter. *Circulation*, 70 (5):812–23, 1984.

[23] F. Seemann, P. Arvidsson, D. Nordlund, S. Kopic, M. Carlsson, H. Arheden, and E. Heiberg. Noninvasive quantification of pressure-volume loops from brachial pressure and cardiovascular magnetic resonance. *Circ Cardiovasc Imaging*, 12(1): e008493, 2019.

[24] F. Seemann, E. Heiberg, C. G. Bruce, J. M. Khan, A. Potersnak, R. Ramasawmy, M. Carlsson, H. Arheden, R. J. Lederman, and A. E. Campbell-Washburn. Non-invasive pressure-volume loops using the elastance model and cmr: a porcine validation at transient pre-loads. *Eur Heart J Imaging Methods Pract*, 2(1):qyae016, 2024.

[25] P. Sjöberg, F. Seemann, H. Arheden, and E. Heiberg. Non-invasive quantification of pressure-volume loops from cardiovascular magnetic resonance at rest and during dobutamine stress. *Clinical Physiology and Functional Imaging*, 41(5):467–470, 2021.

[26] A. W. Bowman and S. J. Kovacs. Assessment and consequences of the constant-volume attribute of the four-chambered heart. *American Journal of Physiology-Heart and Circulatory Physiology*, 285(5):H2027–H2033, 2003.

[27] M. Carlsson, P. Cain, C. Holmqvist, F. Stahlberg, S. Lundback, and H. Arheden. Total heart volume variation throughout the cardiac cycle in humans. *American Journal of Physiology-Heart and Circulatory Physiology*, 287(1):H243–H250, 2004.

[28] M. Carlsson, M. Ugander, E. Heiberg, and H. Arheden. The quantitative relationship between longitudinal and radial function in left, right, and total heart pumping in humans. *American Journal of Physiology-Heart and Circulatory Physiology*, 293(1): H636–H644, 2007.

[29] M. Carlsson, M. Ugander, H. Mosén, T. Buhre, and H. Arheden. Atrioventricular plane displacement is the major contributor to left ventricular pumping in healthy adults, athletes, and patients with dilated cardiomyopathy. *American Journal of Physiology-Heart and Circulatory Physiology*, 292(3):H1452–H1459, 2007.

[30] K. Steding-Ehrenborg, R. C. Boushel, J. A. Calbet, P. Åkeson, and S. P. Mortensen. Left ventricular atrioventricular plane displacement is preserved with lifelong endurance training and is the main determinant of maximal cardiac output. *J Physiol*, 593(23):5157–66, 2015.

[31] C. S. Chung, L. Shmuylovich, and S. J. Kovács. What global diastolic function is, what it is not, and how to measure it. *American Journal of Physiology-Heart and Circulatory Physiology*, 309(9):H1392–H1406, 2015.

[32] A. Opdahl, E. W. Remme, T. Helle-Valle, E. Lyseggen, T. Vartdal, E. Pettersen, T. Edvardsen, and O. A. Smiseth. Determinants of left ventricular early-diastolic lengthening velocity: independent contributions from left ventricular relaxation, restoring forces, and lengthening load. *Circulation*, 119(19):2578–2586, 2009.

[33] E. W. Remme, A. Opdahl, and O. A. Smiseth. Mechanics of left ventricular relaxation, early diastolic lengthening, and suction investigated in a mathematical model. *American Journal of Physiology-Heart and Circulatory Physiology*, 300(5): H1678–H1687, 2011.

[34] T. F. Robinson, S. M. Factor, and E. H. Sonnenblick. The heart as a suction pump. *Scientific American*, 254(6):84–91, 1986.

[35] S. Lundbäck. Cardiac pumping and function of the ventricular septum. *Acta physiologica scandinavica. Supplementum*, 550:1–101, 1986.

[36] P. P. Lunkenheimer. The hydraulic function of intramyocardial fluids subject to the erectile properties of the ventricular wall of mammalian hearts. *Zentralblatt für Veterinärmedizin Reihe A*, 22(8):632–644, 1975.

[37] E. Maksuti, A. Bjällmark, and M. Broomé. Modelling the heart with the atrioventricular plane as a piston unit. *Medical engineering & physics*, 37(1):87–92, 2015.

[38] E. Maksuti, M. Carlsson, H. Arheden, S. J. Kovács, M. Broomé, and M. Ugander. Hydraulic forces contribute to left ventricular diastolic filling. *Scientific reports*, 7(1): 1–10, 2017.

[39] J. Edlund, B. Östenson, E. Heiberg, H. Arheden, and K. Steding-Ehrenborg. Exercise cardiovascular magnetic resonance shows improved diastolic filling by atrioventricular area difference in athletes and controls. *Journal of Applied Physiology*, 137(6):1554–1562, 2024.

[40] M. Johansson, E. Hedström, K. Steding-Ehrenborg, M. Bhat, P. Liuba, H. Arheden, and P. Sjöberg. Atrioventricular area difference aids diastolic filling in patients with repaired tetralogy of fallot. *Pediatr Cardiol*, 2024.

[41] P. Sjöberg, H. Clausen, H. Arheden, K. Steding-Ehrenborg, P. Liuba, and E. Hedström. Left ventricular diastolic function in children with atrial septal defects improves after closure by means of increased hydraulic force. *Pediatr Cardiol*, Accepted May 22, 2024.

[42] K. Steding-Ehrenborg, E. Hedström, M. Carlsson, E. Maksuti, M. Broomé, M. Ugander, M. Magnusson, J. G. Smith, and H. Arheden. Hydraulic force is a novel mechanism of diastolic function that may contribute to decreased diastolic filling in hfpef and facilitate filling in hfref. *J Appl Physiol (1985)*, 130(4):993–1000, 2021.

[43] B. Pascal. *Traites de l'equilibre des liqueurs, et de la pesanteur de la masse de l'air*. Savreux, 1956.

[44] E. A. Wehrwein, H. S. Orer, and S. M. Barman. Overview of the anatomy, physiology, and pharmacology of the autonomic nervous system. *Compr Physiol*, 6(3): 1239–78, 2016.

[45] R. Gordan, J. K. Gwathmey, and L. H. Xie. Autonomic and endocrine control of cardiovascular function. *World J Cardiol*, 7(4):204–14, 2015.

[46] M. W. Chapleau. *Chapter 33 - Baroreceptor Reflexes*, pages 161–165. Academic Press, San Diego, 2012. ISBN 978-0-12-386525-0.

[47] J. P. Fisher, C. N. Young, and P. J. Fadel. Autonomic adjustments to exercise in humans. *Compr Physiol*, 5(2):475–512, 2015.

[48] H. Triebel and H. Castrop. The renin angiotensin aldosterone system. *Pflügers Archiv - European Journal of Physiology*, 476(5):705–713, 2024.

[49] T. L. Brazile, B. D. Levine, and K. M. Shafer. Physiological principles of exercise. *NEJM Evidence*, 4(1), 2025.

[50] B. Saltin and J. A. L. Calbet. Point: In health and in a normoxic environment, v⊠2 max is limited primarily by cardiac output and locomotor muscle blood flow. *Journal of Applied Physiology*, 100(2):744–748, 2006.

[51] R. Callister, A. V. Ng, and D. R. Seals. Arm muscle sympathetic nerve activity during preparation for and initiation of leg-cycling exercise in humans. *Journal of Applied Physiology*, 77(3):1403–1410, 1994.

[52] T. Miyamoto, D. Sotobayashi, G. Ito, E. Kawai, H. Nakahara, S. Ueda, T. Toyama, K. Saku, Y. Nakanishi, and H. Kinoshita. Physiological role of anticipatory cardiorespiratory responses to exercise. *Physiol Rep*, 10(5):e15210, 2022.

[53] J. W. Williamson, R. McColl, D. Mathews, J. H. Mitchell, P. B. Raven, and W. P. Morgan. Brain activation by central command during actual and imagined handgrip under hypnosis. *Journal of Applied Physiology*, 92(3):1317–1324, 2002.

[54] M. J. Joyner and D. P. Casey. Regulation of increased blood flow (hyperemia) to muscles during exercise: a hierarchy of competing physiological needs. *Physiol Rev*, 95(2):549–601, 2015.

[55] Y. Alimi, P. Barthelemy, and C. Juhan. Venous pump of the calf: a study of venous and muscular pressures. *Journal of vascular surgery*, 20(5):728–735, 1994.

[56] F. Lurie, R. L. Kistner, and B. Eklof. The mechanism of venous valve closure in normal physiologic conditions. *Journal of Vascular Surgery*, 35(4):713–717, 2002.

[57] P. Agostoni, C. Vignati, P. Gentile, C. Boiti, S. Farina, E. Salvioni, M. Mapelli, D. Magrì, S. Paolillo, and N. Corrieri. Reference values for peak exercise cardiac output in healthy individuals. *Chest*, 151(6):1329–1337, 2017.

[58] P.-O. Åstrand, T. E. Cuddy, B. Saltin, and J. Stenberg. Cardiac output during submaximal and maximal work. *Journal of Applied Physiology*, 19(2):268–274, 1964.

[59] V. Froelicher and J. Myers. *Exercise and the Heart*, book section 1, pages 1–10. Saunders, fifth edition edition, 2006. ISBN 9781416003113.

[60] C. A. Vella and R. A. Robergs. A review of the stroke volume response to upright exercise in healthy subjects. *British Journal of Sports Medicine*, 39(4):190–195, 2005.

[61] S. S. Vieira, B. Lemes, P. d. T. de Carvalho, R. N. de Lima, D. S. Bocalini, J. A. Junior, G. Arsa, C. A. Casarin, E. L. Andrade, and A. J. Serra. Does stroke volume increase during an incremental exercise? a systematic review. *The Open Cardiovascular Medicine Journal*, 10:57, 2016.

[62] C. S. Chung, M. Karamanoglu, and S. J. Kovács. Duration of diastole and its phases as a function of heart rate during supine bicycle exercise. *Am J Physiol Heart Circ Physiol*, 287(5):H2003–8, 2004.

[63] W. S. Harris, C. D. Schoenfeld, and A. M. Weissler. Effects of adrenergic receptor activation and blockade on the systolic preejection period, heart rate, and arterial pressure in man. *J Clin Invest*, 46(11):1704–14, 1967.

[64] T. L. Whitsett and J. Naughton. The effect of exercise on systolic time intervals in sedentary and active individuals and rehabilitated patients with heart disease. *American Journal of Cardiology*, 27(4):352–358, 1971.

[65] R. G. Fritzsche, T. W. Switzer, B. J. Hodgkinson, and E. F. Coyle. Stroke volume decline during prolonged exercise is influenced by the increase in heart rate. *Journal of Applied Physiology*, 86(3):799–805, 1999.

[66] M. B. Higginbotham, K. G. Morris, R. S. Williams, P. A. McHale, R. E. Coleman, and F. R. Cobb. Regulation of stroke volume during submaximal and maximal upright exercise in normal man. *Circulation Research*, 58(2):281–291, 1986.

[67] K. Steding-Ehrenborg, R. Jablonowski, P. M. Arvidsson, M. Carlsson, B. Saltin, and H. Arheden. Moderate intensity supine exercise causes decreased cardiac volumes and increased outer volume variations: a cardiovascular magnetic resonance study. *Journal of Cardiovascular Magnetic Resonance*, 15(1):96, 2013.

[68] J. González-Alonso. Point: Stroke volume does/does not decline during exercise at maximal effort in healthy individuals. *J Appl Physiol (1985)*, 104(1):275–6; discussion 279–80, 2008.

[69] B. Ekblom and L. Hermansen. Cardiac output in athletes. *Journal of Applied Physiology*, 25(5):619–625, 1968.

[70] H. Tanaka, K. D. Monahan, and D. R. Seals. Age-predicted maximal heart rate revisited. *JACC*, 37(1):153–156, 2001.

[71] N. Gledhill, D. Cox, and R. Jamnik. Endurance athletes' stroke volume does not plateau: major advantage is diastolic function. *Medicine and science in sports and exercise*, 26(9):1116–1121, 1994.

[72] B. J. Rubal, J. M. Moody, S. Damore, S. R. Bunker, and N. M. Diaz. Left ventricular performance of the athletic heart during upright exercise: a heart rate-controlled study. *Medicine and science in sports and exercise*, 18(1):134–140, 1986.

[73] V. A. CONVERTINO. Blood volume: its adaptation to endurance training. *Medicine & Science in Sports & Exercise*, 23(12):1338–1348, 1991.

[74] N. Fellmann. Hormonal and plasma volume alterations following endurance exercise. a brief review. *Sports Med*, 13(1):37–49, 1992.

[75] C. M. Gillen, R. Lee, G. W. Mack, C. M. Tomaselli, T. Nishiyasu, and E. R. Nadel. Plasma volume expansion in humans after a single intense exercise protocol. *J Appl Physiol (1985)*, 71(5):1914–20, 1991.

[76] A. L. Baggish, F. Wang, R. B. Weiner, J. M. Elinoff, F. Tournoux, A. Boland, M. H. Picard, J. Adolph M. Hutter, and M. J. Wood. Training-specific changes in cardiac structure and function: a prospective and longitudinal assessment of competitive athletes. *Journal of Applied Physiology*, 104(4):1121–1128, 2008.

[77] S. Sharma, A. Merghani, and L. Mont. Exercise and the heart: the good, the bad, and the ugly. *European Heart Journal*, 36(23):1445–1453, 2015.

[78] K. Steding, H. Engblom, T. Buhre, M. Carlsson, H. Mosén, B. Wohlfart, and H. Arheden. Relation between cardiac dimensions and peak oxygen uptake. *Journal of Cardiovascular Magnetic Resonance*, 12(1):8, 2010.

[79] A. L. Gerche, M. M. Wasfy, M. J. Brosnan, G. Claessen, D. Fatkin, H. Heidbuchel, A. L. Baggish, and J. C. Kovacic. The athlete's heart—challenges and controversies. *JACC*, 80(14):1346–1362, 2022.

[80] A. Apor, B. Merkely, T. Morrell, S. Zhu, E. Ghosh, H. Vágó, P. Andrássy, and S. J. Kovács. Diastolic function in olympic athletes versus controls: Stiffness-based and relaxation-based echocardiographic comparisons. *Journal of Exercise Science & Fitness*, 11(1):29–34, 2013.

[81] A. Arbab-Zadeh, E. Dijk, A. Prasad, Q. Fu, P. Torres, R. Zhang, J. D. Thomas, D. Palmer, and B. D. Levine. Effect of aging and physical activity on left ventricular compliance. *Circulation*, 110(13):1799–1805, 2004.

[82] J. B. Carter, E. W. Banister, and A. P. Blaber. Effect of endurance exercise on autonomic control of heart rate. *Sports Med*, 33(1):33–46, 2003.

[83] S. E. Meyer, M. Kimber, L. E. Maier, B. Matenchuk, R. Moldenhauer, S. de Waal, A. Sivak, M. H. Davenport, and C. D. Steinback. The impact of exercise training on muscle sympathetic nerve activity: a systematic review and meta-analysis. *Journal of Applied Physiology*, 137(2):429–444, 2024.

[84] V. L. Aengevaeren, A. Mosterd, T. L. Braber, N. H. Prakken, P. A. Doevendans, D. E. Grobbee, P. D. Thompson, T. M. Eijsvogels, and B. K. Velthuis. Relationship between lifelong exercise volume and coronary atherosclerosis in athletes. *Circulation*, 136(2):138–148, 2017.

[85] G. Claessen, T. M. H. Eijsvogels, C. M. Albert, A. L. Baggish, B. D. Levine, E. Marijon, E. D. Michos, and A. La Gerche. Coronary atherosclerosis in athletes: emerging concepts and preventive strategies. *European Heart Journal*, 46(10): 890–903, 2025.

[86] B. Domenech-Ximenos, M. Sanz-de la Garza, S. Prat-González, A. Sepúlveda-Martínez, F. Crispi, K. Duran-Fernandez, R. J. Perea, B. Bijnens, and M. Sitges. Prevalence and pattern of cardiovascular magnetic resonance late gadolinium enhancement in highly trained endurance athletes. *Journal of Cardiovascular Magnetic Resonance*, 22(1), 2020.

[87] A. D. Elliott, D. Linz, R. Mishima, K. Kadhim, C. Gallagher, M. E. Middeldorp, C. V. Verdicchio, J. M. Hendriks, D. H. Lau, and A. La Gerche. Association between physical activity and risk of incident arrhythmias in 402 406 individuals: evidence from the uk biobank cohort. *European heart journal*, 41(15):1479–1486, 2020.

[88] A. Merghani, V. Maestrini, S. Rosmini, A. T. Cox, H. Dhutia, R. Bastiaenan, S. David, T. J. Yeo, R. Narain, and A. Malhotra. Prevalence of subclinical coronary artery disease in masters endurance athletes with a low atherosclerotic risk profile. *Circulation*, 136(2):126–137, 2017.

[89] M. Wilson, R. O'Hanlon, S. Prasad, A. Deighan, P. Macmillan, D. Oxborough, R. Godfrey, G. Smith, A. Maceira, S. Sharma, K. George, and G. Whyte. Diverse patterns of myocardial fibrosis in lifelong, veteran endurance athletes. *J Appl Physiol (1985)*, 110(6):1622–6, 2011.

[90] A. W. Ashor, J. Lara, M. Siervo, C. Celis-Morales, C. Oggioni, D. G. Jakovljevic, and J. C. Mathers. Exercise modalities and endothelial function: a systematic review and dose-response meta-analysis of randomized controlled trials. *Sports Med*, 45(2): 279–96, 2015.

[91] D. J. Green, M. T. Hopman, J. Padilla, M. H. Laughlin, and D. H. Thijssen. Vascular adaptation to exercise in humans: Role of hemodynamic stimuli. *Physiol Rev*, 97(2):495–528, 2017.

[92] A. K. Meinild Lundby, R. A. Jacobs, S. Gehrig, J. de Leur, M. Hauser, T. C. Bonne, D. Flück, S. Dandanell, N. Kirk, A. Kaech, U. Ziegler, S. Larsen, and C. Lundby. Exercise training increases skeletal muscle mitochondrial volume density by enlargement of existing mitochondria and not de novo biogenesis. *Acta Physiol (Oxf)*, 222 (1), 2018.

[93] V. Tedjasaputra, M. M. Bouwsema, and M. K. Stickland. Effect of aerobic fitness on capillary blood volume and diffusing membrane capacity responses to exercise. *J Physiol*, 594(15):4359–70, 2016.

[94] F. C. Bull, S. S. Al-Ansari, S. Biddle, K. Borodulin, M. P. Buman, G. Cardon, C. Carty, J. P. Chaput, S. Chastin, R. Chou, P. C. Dempsey, L. DiPietro, U. Ekelund, J. Firth, C. M. Friedenreich, L. Garcia, M. Gichu, R. Jago, P. T. Katzmarzyk, E. Lambert, M. Leitzmann, K. Milton, F. B. Ortega, C. Ranasinghe, E. Stamatakis, A. Tiedemann, R. P. Troiano, H. P. van der Ploeg, V. Wari, and J. F. Willumsen. World health organization 2020 guidelines on physical activity and sedentary behaviour. *Br J Sports Med*, 54(24):1451–1462, 2020.

[95] P. Posadzki, D. Pieper, R. Bajpai, H. Makaruk, N. Könsgen, A. L. Neuhaus, and M. Semwal. Exercise/physical activity and health outcomes: an overview of cochrane systematic reviews. *BMC Public Health*, 20(1):1724, 2020.

[96] B. Singh, T. Olds, R. Curtis, D. Dumuid, R. Virgara, A. Watson, K. Szeto, E. O'Connor, T. Ferguson, E. Eglitis, A. Miatke, C. E. Simpson, and C. Maher. Effectiveness of physical activity interventions for improving depression, anxiety and distress: an overview of systematic reviews. *British Journal of Sports Medicine*, 57(18): 1203–1209, 2023.

[97] P. A. Heidenreich, B. Bozkurt, D. Aguilar, L. A. Allen, J. J. Byun, M. M. Colvin, A. Deswal, M. H. Drazner, S. M. Dunlay, L. R. Evers, J. C. Fang, S. E. Fedson, G. C. Fonarow, S. S. Hayek, A. F. Hernandez, P. Khazanie, M. M. Kittleson, C. S. Lee, M. S. Link, C. A. Milano, L. C. Nnacheta, A. T. Sandhu, L. W. Stevenson, O. Vardeny, A. R. Vest, and C. W. Yancy. 2022 aha/acc/hfsa guideline for the management of heart failure: A report of the american college of cardiology/american

heart association joint committee on clinical practice guidelines. *Circulation*, 145 (18):e895–e1032, 2022.

[98] T. A. McDonagh, M. Metra, M. Adamo, R. S. Gardner, A. Baumbach, M. Böhm, H. Burri, J. Butler, J. Čelutkienė, O. Chioncel, J. G. F. Cleland, A. J. S. Coats, M. G. Crespo-Leiro, D. Farmakis, M. Gilard, S. Heymans, A. W. Hoes, T. Jaarsma, E. A. Jankowska, M. Lainscak, C. S. P. Lam, A. R. Lyon, J. J. V. McMurray, A. Mebazaa, R. Mindham, C. Muneretto, M. Francesco Piepoli, S. Price, G. M. C. Rosano, F. Ruschitzka, A. Kathrine Skibelund, and E. S. D. Group. 2021 esc guidelines for the diagnosis and treatment of acute and chronic heart failure: Developed by the task force for the diagnosis and treatment of acute and chronic heart failure of the european society of cardiology (esc) with the special contribution of the heart failure association (hfa) of the esc. *European Heart Journal*, 42(36):3599–3726, 2021.

[99] S. L. James, D. Abate, K. H. Abate, S. M. Abay, C. Abbafati, N. Abbasi, H. Abbastabar, F. Abd-Allah, J. Abdela, A. Abdelalim, I. Abdollahpour, R. S. Abdulkader, Z. Abebe, S. F. Abera, O. Z. Abil, H. N. Abraha, L. J. Abu-Raddad, N. M. E. Abu-Rmeileh, M. M. K. Accrombessi, D. Acharya, P. Acharya, I. N. Ackerman, A. A. Adamu, O. M. Adebayo, V. Adekanmbi, O. O. Adetokunboh, M. G. Adib, J. C. Adsuar, K. A. Afanvi, M. Afarideh, A. Afshin, G. Agarwal, K. M. Agesa, R. Aggarwal, S. A. Aghayan, S. Agrawal, A. Ahmadi, M. Ahmadi, H. Ahmadieh, M. B. Ahmed, A. N. Aichour, I. Aichour, M. T. E. Aichour, T. Akinyemiju, N. Akseer, Z. Al-Aly, A. Al-Eyadhy, H. M. Al-Mekhlafi, R. M. Al-Raddadi, F. Alahdab, K. Alam, T. Alam, A. Alashi, S. M. Alavian, K. A. Alene, M. Alijanzadeh, R. Alizadeh-Navaei, S. M. Aljunid, A. Alkerwi, F. Alla, P. Allebeck, M. M. L. Alouani, K. Altirkawi, N. Alvis-Guzman, A. T. Amare, L. N. Aminde, W. Ammar, Y. A. Amoako, N. H. Anber, C. L. Andrei, S. Androudi, M. D. Animut, M. Anjomshoa, M. G. Ansha, C. A. T. Antonio, P. Anwari, J. Arabloo, A. Arauz, O. Aremu, F. Ariani, B. Armoon, J. Ärnlöv, A. Arora, A. Artaman, K. K. Aryal, H. Asayesh, R. J. Asghar, Z. Ataro, S. R. Atre, M. Ausloos, L. Avila-Burgos, E. F. G. A. Avokpaho, A. Awasthi, B. P. Ayala Quintanilla, R. Ayer, P. S. Azzopardi, A. Babazadeh, H. Badali, A. Badawi, A. G. Bali, et al. Global, regional, and national incidence, prevalence, and years lived with disability for 354 diseases and injuries for 195 countries and territories, 1990–2017: a systematic analysis for the global burden of disease study 2017. *The Lancet*, 392(10159):1789–1858, 2018.

[100] M. S. Khan, I. Shahid, A. Bennis, A. Rakisheva, M. Metra, and J. Butler. Global epidemiology of heart failure. *Nature Reviews Cardiology*, 21(10):717–734, 2024.

[101] E. E. van Riet, A. W. Hoes, K. P. Wagenaar, A. Limburg, M. A. Landman, and F. H. Rutten. Epidemiology of heart failure: the prevalence of heart failure and ventricular dysfunction in older adults over time. a systematic review. *European journal of heart failure*, 18(3):242–252, 2016.

[102] B. Shahim, C. J. Kapelios, G. Savarese, and L. H. Lund. Global public health burden of heart failure: An updated review. *Card Fail Rev*, 9:e11, 2023.

[103] M. G. D. Buono, R. Arena, B. A. Borlaug, S. Carbone, J. M. Canada, D. L. Kirkman, R. Garten, P. Rodriguez-Miguelez, M. Guazzi, C. J. Lavie, and A. Abbate. Exercise intolerance in patients with heart failure. *JACC*, 73(17):2209–2225, 2019.

[104] M. B. Bastos, D. Burkhoff, J. Maly, J. Daemen, C. A. den Uil, K. Ameloot, M. Lenzen, F. Mahfoud, F. Zijlstra, J. J. Schreuder, and N. M. Van Mieghem. Invasive left ventricle pressure–volume analysis: overview and practical clinical implications. *European Heart Journal*, 41(12):1286–1297, 2019.

[105] I. Protti, A. van den Enden, N. M. Van Mieghem, C. L. Meuwese, and P. Meani. Looking back, going forward: understanding cardiac pathophysiology from pressure–volume loops. *Biology*, 13(1):55, 2024.

[106] H.-P. Schultheiss, D. Fairweather, A. L. P. Caforio, F. Escher, R. E. Hershberger, S. E. Lipshultz, P. P. Liu, A. Matsumori, A. Mazzanti, J. McMurray, and S. G. Priori. Dilated cardiomyopathy. *Nature Reviews Disease Primers*, 5(1):32, 2019.

[107] M. Sekulic, M. Zacharias, and B. Medalion. Ischemic cardiomyopathy and heart failure. *Circulation: Heart Failure*, 12(6):e006006, 2019.

[108] A. B. Gevaert, J. R. A. Boen, V. F. Segers, and E. M. Van Craenenbroeck. Heart failure with preserved ejection fraction: A review of cardiac and noncardiac pathophysiology. *Front Physiol*, 10:638, 2019.

[109] C. Ma, H. Luo, L. Fan, X. Liu, and C. Gao. Heart failure with preserved ejection fraction: an update on pathophysiology, diagnosis, treatment, and prognosis. *Braz J Med Biol Res*, 53(7):e9646, 2020.

[110] T. van Loon, C. Knackstedt, R. Cornelussen, K. D. Reesink, H.-P. Brunner La Rocca, T. Delhaas, V. van Empel, and J. Lumens. Increased myocardial stiffness more than impaired relaxation function limits cardiac performance during exercise in heart failure with preserved ejection fraction: a virtual patient study. *European Heart Journal - Digital Health*, 1(1):40–50, 2020.

[111] W. J. Paulus and C. Tschöpe. A novel paradigm for heart failure with preserved ejection fraction: Comorbidities drive myocardial dysfunction and remodeling through coronary microvascular endothelial inflammation. *Journal of the American College of Cardiology*, 62(4):263–271, 2013.

[112] B. A. Borlaug, M. D. Jensen, D. W. Kitzman, C. S. P. Lam, M. Obokata, and O. J. Rider. Obesity and heart failure with preserved ejection fraction: new insights and pathophysiological targets. *Cardiovasc Res*, 118(18):3434–3450, 2023.

[113] D. Kotecha, C. S. Lam, D. J. Van Veldhuisen, I. C. Van Gelder, A. A. Voors, and M. Rienstra. Heart failure with preserved ejection fraction and atrial fibrillation: vicious twins. *Journal of the American College of Cardiology*, 68(20):2217–2228, 2016.

[114] A. Jasinska-Piadlo and P. Campbell. Management of patients with heart failure and preserved ejection fraction. *Heart*, 109(11):874–883, 2023.

[115] J. W. Chang and R. Ramchandra. The sympathetic nervous system in heart failure with preserved ejection fraction. *Heart Fail Rev*, 30(1):209–218, 2025.

[116] V. G. Florea and J. N. Cohn. The autonomic nervous system and heart failure. *Circulation Research*, 114(11):1815–1826, 2014.

[117] G. Grassi, F. Quarti-Trevano, and M. D. Esler. Sympathetic activation in congestive heart failure: an updated overview. *Heart Fail Rev*, 26(1):173–182, 2021.

[118] J. Hartupee and D. L. Mann. Neurohormonal activation in heart failure with reduced ejection fraction. *Nat Rev Cardiol*, 14(1):30–38, 2017.

[119] J. N. Cohn, T. B. Levine, M. T. Olivari, V. Garberg, D. Lura, G. S. Francis, A. B. Simon, and T. Rector. Plasma norepinephrine as a guide to prognosis in patients with chronic congestive heart failure. *N Engl J Med*, 311(13):819–23, 1984.

[120] M. Dolgin and N. Y. H. A. C. Committee. *Nomenclature and Criteria for Diagnosis of Diseases of the Heart and Great Vessels*. Little, Brown, 1994. ISBN 9780316605380.

[121] B. Pieske, C. Tschöpe, R. A. De Boer, A. G. Fraser, S. D. Anker, E. Donal, F. Edelmann, M. Fu, M. Guazzi, C. S. Lam, et al. How to diagnose heart failure with preserved ejection fraction: the hfa–peff diagnostic algorithm: a consensus recommendation from the heart failure association (hfa) of the european society of cardiology (esc). *European heart journal*, 40(40):3297–3317, 2019.

[122] Exercise training meta-analysis of trials in patients with chronic heart failure (extramatch). *BMJ*, 328(7433):189, 2004.

[123] C. Molloy, L. Long, I. R. Mordi, C. Bridges, V. A. Sagar, E. J. Davies, A. J. Coats, H. Dalal, K. Rees, S. J. Singh, and R. S. Taylor. Exercise-based cardiac rehabilitation for adults with heart failure. *Cochrane Database Syst Rev*, 3(3):Cd003331, 2024.

[124] V. A. Sagar, E. J. Davies, S. Briscoe, A. J. Coats, H. M. Dalal, F. Lough, K. Rees, S. Singh, and R. S. Taylor. Exercise-based rehabilitation for heart failure: systematic review and meta-analysis. *Open heart*, 2(1):e000163, 2015.

[125] C. M. O'Connor, D. J. Whellan, K. L. Lee, S. J. Keteyian, L. S. Cooper, S. J. Ellis, E. S. Leifer, W. E. Kraus, D. W. Kitzman, J. A. Blumenthal, D. S. Rendall, N. H. Miller, J. L. Fleg, K. A. Schulman, R. S. McKelvie, F. Zannad, and I. L. Piña. Efficacy and safety of exercise training in patients with chronic heart failure: Hf-action randomized controlled trial. *Jama*, 301(14):1439–50, 2009.

[126] J. J. Edwards and J. M. O'Driscoll. Exercise training in heart failure with preserved and reduced ejection fraction: A systematic review and meta-analysis. *Sports Med Open*, 8(1):76, 2022.

[127] M. Elahi, M. Mahmood, A. Shahbaz, N. Malick, J. Sajid, S. Asopa, and B. M. Matata. Current concepts underlying benefits of exercise training in congestive heart failure patients. *Curr Cardiol Rev*, 6(2):104–11, 2010.

[128] M. G. Gademan, C. A. Swenne, H. F. Verwey, A. van der Laarse, A. C. Maan, H. van de Vooren, J. van Pelt, H. J. van Exel, C. M. Lucas, G. V. Cleuren, S. Somer, M. J. Schalij, and E. E. van der Wall. Effect of exercise training on autonomic derangement and neurohumoral activation in chronic heart failure. *J Card Fail*, 13 (4):294–303, 2007.

[129] D. J. Green, A. Maiorana, G. O'Driscoll, and R. Taylor. Effect of exercise training on endothelium-derived nitric oxide function in humans. *J Physiol*, 561(Pt 1):1–25, 2004.

[130] A. Y. Lim, Y. C. Chen, C. C. Hsu, T. C. Fu, and J. S. Wang. The effects of exercise training on mitochondrial function in cardiovascular diseases: A systematic review and meta-analysis. *Int J Mol Sci*, 23(20), 2022.

[131] A. Pandey, A. Parashar, D. J. Kumbhani, S. Agarwal, J. Garg, D. Kitzman, B. D. Levine, M. Drazner, and J. D. Berry. Exercise training in patients with heart failure and preserved ejection fraction. *Circulation: Heart Failure*, 8(1):33–40, 2015.

[132] M. F. Piepoli. Exercise training in chronic heart failure: mechanisms and therapies. *Neth Heart J*, 21(2):85–90, 2013.

[133] R. F. Mould. The early history of x-ray diagnosis with emphasis on the contributions of physics 1895-1915. *Physics in Medicine & Biology*, 40(11):1741, 1995.

[134] J. Ross. Transseptal left heart catheterization: a 50-year odyssey. *Journal of the American College of Cardiology*, 51(22):2107–2115, 2008.

[135] D. E. Kuhl and R. Q. Edwards. Image separation radioisotope scanning. *Radiology*, 80(4):653–662, 1963.

[136] B. F. Hutton. The origins of spect and spect/ct. *European journal of nuclear medicine and molecular imaging*, 41(Suppl 1):3–16, 2014.

[137] H. J. Verberne, W. Acampa, C. Anagnostopoulos, J. Ballinger, F. Bengel, P. De Bondt, R. R. Buechel, A. Cuocolo, B. L. van Eck-Smit, A. Flotats, et al. Eanm procedural guidelines for radionuclide myocardial perfusion imaging with spect and spect/ct: 2015 revision. *European journal of nuclear medicine and molecular imaging*, 42(12):1929–1940, 2015.

[138] brgfx. Pregnancy ultrasound monitor on white background. https://www.freepik.com/free-vector/pregnancy-ultrasound-monitor-white-background_37013626.htm, 2025. Freepik Free license (attribution required). Accessed 23 Sep 2025.

[139] A. G. Fraser, M. J. Monaghan, A. F. van der Steen, and G. R. Sutherland. A concise history of echocardiography: timeline, pioneers, and landmark publications. *European Heart Journal-Cardiovascular Imaging*, 23(9):1130–1143, 2022.

[140] C. H. McCollough and P. S. Rajiah. Milestones in ct: past, present, and future. *Radiology*, 309(1):e230803, 2023.

[141] G. M. Pohost. The history of cardiovascular magnetic resonance. *JACC: Cardiovascular Imaging*, 1(5):672–678, 2008.

[142] D. J. Pennell. Cardiovascular magnetic resonance. *Circulation*, 121(5):692–705, 2010.

[143] T. Geva. Magnetic resonance imaging: historical perspective. *Journal of cardiovascular magnetic resonance*, 8(4):573–580, 2006.

[144] P. Lanzer, E. H. Botvinick, N. B. Schiller, L. E. Crooks, M. Arakawa, L. Kaufman, P. L. Davis, R. Herfkens, M. J. Lipton, and C. B. Higgins. Cardiac imaging using gated magnetic resonance. *Radiology*, 150(1):121–127, 1984.

[145] C. M. Kramer, J. Barkhausen, C. Bucciarelli-Ducci, S. D. Flamm, R. J. Kim, and E. Nagel. Standardized cardiovascular magnetic resonance imaging (cmr) protocols: 2020 update. *Journal of Cardiovascular Magnetic Resonance*, 22(1):17, 2020.

[146] J. Schulz-Menger, D. A. Bluemke, J. Bremerich, S. D. Flamm, M. A. Fogel, M. G. Friedrich, R. J. Kim, F. von Knobelsdorff-Brenkenhoff, C. M. Kramer, D. J. Pennell, S. Plein, and E. Nagel. Standardized image interpretation and post-processing in cardiovascular magnetic resonance - 2020 update. *Journal of Cardiovascular Magnetic Resonance*, 22(1):19, 2020.

[147] J. E. Aldrich. Basic physics of ultrasound imaging. *Critical care medicine*, 35(5): S131–S137, 2007.

[148] C. Mitchell, P. S. Rahko, L. A. Blauwet, B. Canaday, J. A. Finstuen, M. C. Foster, K. Horton, K. O. Ogunyankin, R. A. Palma, and E. J. Velazquez. Guidelines for performing a comprehensive transthoracic echocardiographic examination in adults: recommendations from the american society of echocardiography. *Journal of the American Society of Echocardiography*, 32(1):1–64, 2019.

[149] S. Satomura. Ultrasonic doppler method for the inspection of cardiac functions. *The Journal of the Acoustical Society of America*, 29(11):1181–1185, 1957.

[150] M. A. Quiñones, C. M. Otto, M. Stoddard, A. Waggoner, and W. A. Zoghbi. Recommendations for quantification of doppler echocardiography: a report from the doppler quantification task force of the nomenclature and standards committee of the american society of echocardiography. *Journal of the American Society of Echocardiography*, 15(2):167–184, 2002.

[151] R. M. Lang, M. Bierig, R. B. Devereux, F. A. Flachskampf, E. Foster, P. A. Pellikka, M. H. Picard, M. J. Roman, J. Seward, J. Shanewise, et al. Recommendations for chamber quantification. *European journal of echocardiography*, 7(2):79–108, 2006.

[152] D. W. McRobbie, E. A. Moore, M. J. Graves, and M. R. Prince, editors. *The basic stuff*, pages 9–10. Cambridge University Press, Cambridge, 2 edition, 2006. ISBN 9780511545405.

[153] F. Bloch. Nuclear induction. *Physical Review*, 70(7-8):460–474, 1946.

[154] P. C. Lauterbur. Image formation by induced local interactions: Examples employing nuclear magnetic resonance. *Nature*, 242(5394):190–191, 1973.

[155] J. P. Ridgway. Cardiovascular magnetic resonance physics for clinicians: part i. *Journal of Cardiovascular Magnetic Resonance*, 12(1):71, 2010.

[156] B. Herzog, J. Greenwood, S. Plein, P. Garg, P. Haaf, and S. Onciul. Cardiovascular magnetic resonance pocket guide. *Eur Soc Cardiol*, 2017.

[157] N. G. Bellenger, L. C. Davies, J. M. Francis, A. J. S. Coats, and D. J. Pennell. Reduction in sample size for studies of remodeling in heart failure by the use of cardiovascular magnetic resonance. *Journal of Cardiovascular Magnetic Resonance*, 2 (4):271–278, 2000.

[158] F. Grothues, G. C. Smith, J. C. Moon, N. G. Bellenger, P. Collins, H. U. Klein, and D. J. Pennell. Comparison of interstudy reproducibility of cardiovascular magnetic resonance with two-dimensional echocardiography in normal subjects and in patients with heart failure or left ventricular hypertrophy. *Am J Cardiol*, 90(1):29–34, 2002.

[159] L. P. Panych and B. Madore. The physics of mri safety. *Journal of Magnetic Resonance Imaging*, 47(1):28–43, 2018.

[160] A. R. Patel, M. Salerno, R. Y. Kwong, A. Singh, B. Heydari, and C. M. Kramer. Stress cardiac magnetic resonance myocardial perfusion imaging. *JACC*, 78(16): 1655–1668, 2021.

[161] P. A. Pellikka, V. L. Roger, J. K. Oh, F. A. Miller, J. B. Seward, and A. J. Tajik. Stress echocardiography. part ii. dobutamine stress echocardiography: techniques, implementation, clinical applications, and correlations. In *Mayo Clinic Proceedings*, volume 70, pages 16–27. Elsevier, 1995.

[162] P. A. Pellikka, A. Arruda-Olson, F. A. Chaudhry, M. H. Chen, J. E. Marshall, T. R. Porter, and S. G. Sawada. Guidelines for performance, interpretation, and application of stress echocardiography in ischemic heart disease: from the american society of echocardiography. *Journal of the American Society of Echocardiography*, 33(1):1–41, 2020.

[163] T. P. Craven, C. W. Tsao, A. La Gerche, O. P. Simonetti, and J. P. Greenwood. Exercise cardiovascular magnetic resonance: development, current utility and future applications. *Journal of Cardiovascular Magnetic Resonance*, 22(1):65, 2020.

[164] A. La Gerche, G. Claessen, A. Van de Bruaene, N. Pattyn, J. Van Cleemput, M. Gewillig, J. Bogaert, S. Dymarkowski, P. Claus, and H. Heidbuchel. Cardiac mri: a new gold standard for ventricular volume quantification during high-intensity exercise. *Circ Cardiovasc Imaging*, 6(2):329–38, 2013.

[165] T.-T. Le, J. A. Bryant, A. E. Ting, P. Y. Ho, B. Su, R. C. C. Teo, J. S.-J. Gan, Y.-C. Chung, D. P. O'Regan, S. A. Cook, and C. W.-L. Chin. Assessing exercise cardiac reserve using real-time cardiovascular magnetic resonance. *Journal of Cardiovascular Magnetic Resonance*, 19(1):7, 2017.

[166] 2015.

[167] World medical association declaration of helsinki: ethical principles for medical research involving human subjects. *Jama*, 310(20):2191–4, 2013.

[168] G. Bergström, M. Persson, M. Adiels, E. Björnson, C. Bonander, H. Ahlström, J. Alfredsson, O. Angerås, G. Berglund, A. Blomberg, J. Brandberg, M. Börjesson, K. Cederlund, U. de Faire, O. Duvernoy, ⊠. Ekblom, G. Engström, J. E. Engvall, E. Fagman, M. Eriksson, D. Erlinge, B. Fagerberg, A. Flinck, I. Gonçalves, E. Hagström, O. Hjelmgren, L. Lind, E. Lindberg, P. Lindqvist, J. Ljungberg, M. Magnusson, M. Mannila, H. Markstad, M. A. Mohammad, F. H. Nystrom, E. Ostenfeld, A. Persson, A. Rosengren, A. Sandström, A. Själander, M. C. Sköld,

J. Sundström, E. Swahn, S. Söderberg, K. Torén, C. J. Östgren, and T. Jernberg. Prevalence of subclinical coronary artery atherosclerosis in the general population. *Circulation*, 144(12):916–929, 2021.

[169] H. Holm, E. Bachus, A. Jujic, E. D. Nilsson, B. Wadström, J. Molvin, L. Minthon, A. Fedorowski, K. Nägga, and M. Magnusson. Cognitive test results are associated with mortality and rehospitalization in heart failure: Swedish prospective cohort study. *ESC Heart Fail*, 7(5):2948–2955, 2020.

[170] B. Pieske, C. Tschöpe, R. A. de Boer, A. G. Fraser, S. D. Anker, E. Donal, F. Edelmann, M. Fu, M. Guazzi, C. S. P. Lam, P. Lancellotti, V. Melenovsky, D. A. Morris, E. Nagel, E. Pieske-Kraigher, P. Ponikowski, S. D. Solomon, R. S. Vasan, F. H. Rutten, A. A. Voors, F. Ruschitzka, W. J. Paulus, P. Seferovic, and G. Filippatos. How to diagnose heart failure with preserved ejection fraction: the hfa–peff diagnostic algorithm: a consensus recommendation from the heart failure association (hfa) of the european society of cardiology (esc). *European Heart Journal*, 40(40):3297–3317, 2019.

[171] K. Norton, L. Norton, and D. Sadgrove. Position statement on physical activity and exercise intensity terminology. *Journal of science and medicine in sport*, 13(5): 496–502, 2010.

[172] E. Heiberg, J. Sjogren, M. Ugander, M. Carlsson, H. Engblom, and H. Arheden. Design and validation of segment–freely available software for cardiovascular image analysis. *BMC Med Imaging*, 10:1, 2010.

[173] J. Schulz-Menger, D. A. Bluemke, J. Bremerich, S. D. Flamm, M. A. Fogel, M. G. Friedrich, R. J. Kim, F. von Knobelsdorff-Brenkenhoff, C. M. Kramer, D. J. Pennell, S. Plein, and E. Nagel. Standardized image interpretation and post processing in cardiovascular magnetic resonance: Society for cardiovascular magnetic resonance (scmr) board of trustees task force on standardized post processing. *Journal of Cardiovascular Magnetic Resonance*, 15(1):35, 2013.

[174] J. Åkesson, J. Edlund, K. Steding-Ehrenborg, and E. Heiberg. Retrospectively synchronized time-resolved ventricular cine images from 2d real-time exercise cardiac magnetic resonance imaging. *Clinical Physiology and Functional Imaging*, 45(5): e70027, 2025.

[175] N. Westerhof, N. Stergiopulos, and M. I. Noble. *Snapshots of Hemodynamics: An Aid for Clinical Research and Graduate Education*. Springer Science & Business Media, 2010. ISBN 1441963634.

[176] H. Suga, T. Hayashi, and M. Shirahata. Ventricular systolic pressure-volume area as predictor of cardiac oxygen consumption. *American Journal of Physiology-Heart and Circulatory Physiology*, 240(1):H39–H44, 1981.

[177] H. Wickham, M. Averick, J. Bryan, W. Chang, L. D. McGowan, R. François, G. Grolemund, A. Hayes, L. Henry, and J. Hester. Welcome to the tidyverse. *Journal of open source software*, 4(43):1686, 2019.

[178] D. G. Altman and J. M. Bland. Measurement in medicine: The analysis of method comparison studies. *Journal of the Royal Statistical Society. Series D (The Statistician)*, 32(3):307–317, 1983.

[179] J. M. Bland and D. Altman. Statistical methods for assessing agreement between two methods of clinical measurement. *The lancet*, 327(8476):307–310, 1986.

[180] B. Ky, B. French, A. May Khan, T. Plappert, A. Wang, J. A. Chirinos, J. C. Fang, N. K. Sweitzer, B. A. Borlaug, D. A. Kass, M. St John Sutton, and T. P. Cappola. Ventricular-arterial coupling, remodeling, and prognosis in chronic heart failure. *J Am Coll Cardiol*, 62(13):1165–72, 2013.

[181] P. A. Majid, B. Sharma, and S. H. Taylor. Phentolamine for vasodilator treatment of severe heart-failure. *The Lancet*, 298(7727):719–724, 1971.

[182] J. ROSS and E. BRAUNWALD. The study of left ventricular function in man by increasing resistance to ventricular ejection with angiotensin. *Circulation*, 29(5): 739–749, 1964.

[183] F. Novillo, S. Van Eyndhoven, J. Moeyersons, J. Bogaert, G. Claessen, A. La Gerche, S. Van Huffel, and P. Claus. Unsupervised respiratory signal extraction from ungated cardiac magnetic resonance imaging at rest and during exercise. *Physics in Medicine & Biology*, 64(6):065001, 2019.

[184] M. Usman, G. Vaillant, D. Atkinson, T. Schaeffter, and C. Prieto. Compressive manifold learning: Estimating one-dimensional respiratory motion directly from undersampled k-space data. *Magnetic Resonance in Medicine*, 72(4):1130–1140, 2014.

[185] M. Yigitsoy, C. Wachinger, and N. Navab. *Manifold learning for image-based breathing gating in MRI*, volume 7962 of *SPIE Medical Imaging*. SPIE, 2011.

[186] G. Claessen, P. Claus, M. Delcroix, J. Bogaert, A. L. Gerche, and H. Heidbuchel. Interaction between respiration and right versus left ventricular volumes at rest and during exercise: a real-time cardiac magnetic resonance study. *American Journal of Physiology-Heart and Circulatory Physiology*, 306(6):H816–H824, 2014.

[187] S. Gusso, C. Salvador, P. Hofman, W. Cutfield, J. C. Baldi, A. Taberner, and P. Nielsen. Design and testing of an mri-compatible cycle ergometer for non-invasive cardiac assessments during exercise. *BioMedical Engineering OnLine*, 11 (1):13, 2012.

[188] P. Habert, Z. Bentatou, P. Aldebert, M. Finas, A. Bartoli, L. Bal, A. Lalande, S. Rapacchi, M. Guye, F. Kober, M. Bernard, and A. Jacquier. Exercise stress cmr reveals reduced aortic distensibility and impaired right-ventricular adaptation to exercise in patients with repaired tetralogy of fallot. *PloS one*, 13(12):e0208749–e0208749, 2018.

[189] B. Östenson, E. Ostenfeld, J. Edlund, E. Heiberg, H. Arheden, and K. Steding-Ehrenborg. Endurance-trained subjects and sedentary controls increase ventricular contractility and efficiency during exercise: Feasibility of hemodynamics assessed by non-invasive pressure-volume loops. *PLOS ONE*, 18(5):e0285592, 2023.

[190] S. Sampath, J. A. Derbyshire, M. J. Ledesma-Carbayo, and E. R. McVeigh. Imaging left ventricular tissue mechanics and hemodynamics during supine bicycle exercise using a combined tagging and phase-contrast mri pulse sequence. *Magnetic Resonance in Medicine*, 65(1):51–59, 2011.

[191] K. Steding-Ehrenborg, A. Nelsson, E. Hedström, H. Engblom, A. Ingvarsson, J. Nilsson, O. Braun, and H. Arheden. Diastolic filling in patients after heart transplantation is impaired due to an altered geometrical relationship between the left atrium and ventricle. *J Am Heart Assoc*, page e033672, 2024.

[192] M. Gueda Moussa, J. Lamy, V. Nguyen, P. Marsac, U. Gencer, E. Mousseaux, E. Bollache, and N. Kachenoura. Estimate of the hydraulic force in the aging heart: a cardiovascular magnetic resonance imaging study. *BMC Medical Imaging*, 24(1): 168, 2024.

[193] D. Soundappan, A. S. Y. Fung, D. E. Loewenstein, D. Playford, G. Strange, R. Kozor, J. Otton, and M. Ugander. Decreased diastolic hydraulic forces incrementally associate with survival beyond conventional measures of diastolic dysfunction. *Scientific Reports*, 13(1):16396, 2023.

[194] H. Clausen, E. Hedström, K. Steding-Ehrenborg, P. Liuba, and P. Sjöberg. Estimation of hydraulic forces that contribute to left ventricular filling assessed by echocardiography is not directly comparable to magnetic resonance imaging in children with atrial septal defects. *Journal of Cardiovascular Magnetic Resonance*, 27, 2025.

[195] K. Hanneman and G. S. Gulsin. Noninvasive pressure-volume loops: Can cardiac mri obviate the need for invasive catheter hemodynamic measurements? *JACC Adv*, 3(6):101000, 2024.

[196] P. M. Arvidsson, J. Berg, M. Carlsson, and H. Arheden. Noninvasive pressure-volume loops predict major adverse cardiac events in heart failure with reduced ejection fraction. *JACC Adv*, 3(6):100946, 2024.

[197] I. O. Ajiboye, S. M. Lang, M. D. Taylor, and R. K. Banerjee. Non-invasive pressure–volume loop derived temporal elastance, contractility, and efficiency indices for assessing duchenne muscular dystrophy patients. *Heart and Vessels*, 40(8):696–706, 2025.

[198] M. W. G. f. C. C. Disease, D. E. Winchester, D. J. Maron, R. Blankstein, I. C. Chang, A. J. Kirtane, R. Y. Kwong, P. A. Pellikka, J. M. Prutkin, and R. Russell. Acc/aha/ase/asnc/aspc/hfsa/hrs/scai/scct/scmr/sts 2023 multimodality appropriate use criteria for the detection and risk assessment of chronic coronary disease. *Journal of the American College of Cardiology*, 81(25):2445–2467, 2023.

[199] C. Vrints, F. Andreotti, K. C. Koskinas, X. Rossello, M. Adamo, J. Ainslie, A. P. Banning, A. Budaj, R. R. Buechel, and G. A. Chiariello. 2024 esc guidelines for the management of chronic coronary syndromes: developed by the task force for the management of chronic coronary syndromes of the european society of cardiology (esc) endorsed by the european association for cardio-thoracic surgery (eacts). *European heart journal*, 45(36):3415–3537, 2024.

[200] P. Kellman, M. S. Hansen, S. Nielles-Vallespin, J. Nickander, R. Themudo, M. Ugander, and H. Xue. Myocardial perfusion cardiovascular magnetic resonance: optimized dual sequence and reconstruction for quantification. *Journal of Cardiovascular Magnetic Resonance*, 19(1):43, 2016.

[201] M. Jekic, E. L. Foster, M. R. Ballinger, S. V. Raman, and O. P. Simonetti. Cardiac function and myocardial perfusion immediately following maximal treadmill exercise inside the mri room. *J Cardiovasc Magn Reson*, 10(1):3, 2008.

[202] T.-T. Le, B. W. Y. Ang, J. A. Bryant, C. Y. Chin, K. K. Yeo, P. E. H. Wong, K. W. Ho, J. W. C. Tan, P. T. Lee, C. W. L. Chin, and S. A. Cook. Multiparametric exercise stress cardiovascular magnetic resonance in the diagnosis of coronary artery disease: the empire trial. *Journal of Cardiovascular Magnetic Resonance*, 23(1):17, 2021.

[203] S. V. Raman, J. A. Dickerson, M. Jekic, E. L. Foster, M. L. Pennell, B. McCarthy, and O. P. Simonetti. Real-time cine and myocardial perfusion with treadmill exercise stress cardiovascular magnetic resonance in patients referred for stress spect. *J Cardiovasc Magn Reson*, 12(1):41, 2010.

[204] S. V. Raman, J. A. Dickerson, W. Mazur, T. C. Wong, E. B. Schelbert, J. K. Min, D. Scandling, C. Bartone, J. T. Craft, P. Thavendiranathan, E. L. Mazzaferri, J. W. Arnold, R. Gilkeson, and O. P. Simonetti. Diagnostic performance of treadmill exercise cardiac magnetic resonance: The prospective, multicenter exercise cmr's accuracy for cardiovascular stress testing (exact) trial. *Journal of the American Heart Association*, 5(8):e003811, 2016.

[205] S. J. Backhaus, T. Lange, E. F. George, K. Hellenkamp, R. J. Gertz, M. Billing, R. Wachter, M. Steinmetz, S. Kutty, U. Raaz, J. Lotz, T. Friede, M. Uecker, G. Hasenfuß, T. Seidler, and A. Schuster. Exercise stress real-time cardiac magnetic resonance imaging for noninvasive characterization of heart failure with preserved ejection fraction. *Circulation*, 143(15):1484–1498, 2021.

[206] J. T. Brown, R. Virsinskaite, T. Kotecha, J. A. Steeden, M. Fontana, N. Karia, B. E. Schreiber, V. H. Ong, C. P. Denton, J. G. Coghlan, V. Muthurangu, and D. S. Knight. Prognostic utility of exercise cardiovascular magnetic resonance in patients with systemic sclerosis-associated pulmonary arterial hypertension. *Eur Heart J Cardiovasc Imaging*, 25(12):1712–1720, 2024.

[207] P. Thavendiranathan, J. A. Dickerson, D. Scandling, V. Balasubramanian, M. L. Pennell, A. Hinton, S. V. Raman, and O. P. Simonetti. Comparison of treadmill exercise stress cardiac mri to stress echocardiography in healthy volunteers for adequacy of left ventricular endocardial wall visualization: A pilot study. *J Magn Reson Imaging*, 39(5):1146–52, 2014.

Part II

Research Studies

Author Contributions

	Study I	Study II	Study III	Study IV
Study design	0	0	0	1
Ethical application	0	0	0	3
Data acquisition	1	0	0	3
Data analysis	3	3	3	3
Statistical analysis	3	3	3	3
Figures and tables	3	3	3	3
Interpretation of results	3	3	3	3
Preparation of manuscript	3	3	3	3
Revision of manuscript	3	3	3	-
Reply to reviewers	3	3	3	-

Not yet applicable	-
No contribution	0
Limited contribution	1
Moderate contribution	2
Significant contribution	3

Printed by Media-Tryck, Lund 2025 NORDIC SWAN ECOLABEL 8041 0903

LUND UNIVERSITY

FACULTY OF MEDICINE

Lund Cardiac MR Group
Department of Clinical Physiology

Lund University, Faculty of Medicine
Doctoral Dissertation Series 2025:128
ISBN 978-91-8021-781-1
ISSN 1652-8220